

DEPARTMENT OF CIVIL ENGINEERING
UNIVERSITY OF MAINE

GAL: A 3-Dimensional
Numerical Model to Calculate Currents with
a Depth Varying Vertical Eddy Viscosity

by

Bryan Pearce
Cortis Cooper
Susan Nelson

CIRCULATING COPY
Sea Grant Depository

Prepared with the support of

Techniques Development Laboratory
National Weather Service
U.S. Department of Commerce
Washington, D.C.

and

Instituto Tecnológico Venezolano
Del Petróleo
Caracas, Venezuela

TR-MSG-78-1

November, 1978

ABSTRACT

GAL: A 3-D Numerical Model to Calculate
Currents with a Depth Varying Vertical Eddy Viscosity

A 3-D numerical model for simulating currents in coastal regions and lakes is presented. The model uses the Galerkin numerical method, allows for the vertical variation of the vertical eddy viscosity, and can simulate complicated bathymetry, density gradients and boundary conditions. The computer time and storage requirements are quite reasonable. These features make the model particularly attractive in the calculation of wind-induced drift or oil slick trajectory analysis.

Emphasis in this report is placed on the theoretical advantages of the model, the detailed formulation and comparisons of the model to various analytic solutions.

ACKNOWLEDGEMENTS

The research summarized in this paper was supported primarily by the National Weather Service of the National Oceanic and Atmospheric Administration. INTEVEP (Instituto Tecnológico del Petróleo Venezolano) is also acknowledged for its contribution to the research. Special thanks is extended to Dr. Celso Barrientos of the NWS and German Febres of INTEVEP.

CONTENTS

	<u>Page</u>
Abstract	i
Acknowledgements	ii
Table of Contents	iii
List of Figures	iv
Chapter 1. Introduction	1
1.1 Justification for Development of a Three-Dimensional Model	1
1.2 Discussion of the Eddy Viscosity Concept	2
1.3 Previous Efforts in Circulation Modeling	8
1.4 Initial Formulation of the Galerkin Solution	20
1.4.1 One Dimensional, Infinitely Long Channel with Constant N_v	21
1.4.2 One Dimensional, Closed-Ended Channel with Constant N_v	21
1.4.3 One Dimensional, Infinitely Long Channel with Linear Variation in N_v	25
1.4.4 Fourier Series Analysis	29
Chapter 2. Model Formulation	33
2.1 Governing Equations	33
2.2 Application of Galerkin Technique	39
2.3 Evaluation of the Galerkin Statement	46
2.3.1 Unsteady Term	46
2.3.2 Surface Slope Term	48
2.3.3 Horizontal Shear Stress Terms	48
2.3.4 Vertical Eddy Viscosity Term - Part One	53
2.3.5 Vertical Eddy Viscosity Term - Part Two	56
2.3.5 Coriolis Term	57
2.4 Continuity	59
2.5 Model Discretization Scheme	61
2.6 Special Considerations	65
Chapter 3. Model Verification	68
3.1 Test Case 1: Flow in an Infinite Channel	68
3.2 Test Case 2: Flow in a Closed-Ended Channel	72
3.3 Test Case 3: 3-D Analytical Model Comparison	77
3.4 Test Case 4: Flow in an Infinite Channel with a Multi-Linear Variation in the Eddy Viscosity.	86
Chapter 4. Summary and Conclusions	94
References	97
Appendix A Detailed Integration of the Terms of the Residual Equation	99
Appendix B Continuity Equation	110

LIST OF FIGURES AND TABLES

		<u>Page</u>
Table 1.1	Summary of Various Experiments Investigating the Effects of Wind on Surface Drift	14
Figure 1.1	One-Dimensional Velocity Profile	4
Figure 1.2	Mixing Length Concept	6
Figure 1.3	Typical Velocity Profile for Case of Wind-Induced Flow in a 1-D Channel of Finite Length	6
Figure 1.4	Vertical Structure of Pure Drift Current (Figure from Neumann (1968))	12
Figure 1.5	Hodograph Showing Development of a Pure Drift Current.	16
Figure 1.6	Physical Characteristics of the 1-D Channel Used in Model Verification	22
Figure 1.7	Grid Scheme Used for 1-D Channel	23
Figure 1.8	Comparison of Steady State Velocity Profile for the Case of a 1-D, Infinitely Long Channel with Constant N_v	24
Figure 1.9	Comparison of Galerkin Model to Analytic Solution for 1-D Closed-Ended Channel with a Constant Vertical Eddy Viscosity	26
Figure 1.10	Linear Vertical Eddy Viscosity Model	
Figure 1.11	Comparison of Velocity Profiles for $\alpha = -.04639$ ft/sec and $\beta = 1.5246$ ft ² /sec	28
Figure 1.12	Convergence of ϵ_2 Fourier Cosine Series for Case of $N_v = 1.5246$ ft ² /sec.	31
Figure 1.13	Convergence of Fourier Cosine Series for the Case of $\alpha = .04648$ and $\beta = .01$	31
Figure 2.1	Definition of Variables Used in the Model	34
Figure 2.2	Plot of Prescribed Functions, Ω_I vs. Depth	43
Figure 2.3	The Functional Form for the Vertical Variation of N_v Used in the Model	43
Figure 2.4	Horizontal Velocity Profile (at $z = \text{constant}$) Near a Coastline	51
Figure 2.5	Circulation Induced in a Bay Due to a Tangential Permanent Current	51
Figure 2.6	Discrete-Area Numerical Integration Scheme Used in the Model	54
Figure 2.7a	Finite Difference Discretization Scheme	63
Figure 2.7b	Location of Critical Parameters	63

Figure 3.1	Form of Eddy Viscosity Used in Test Cases 1, 2 and 3	69
Figure 3.2	Forces Acting on Fluid Section in 1-D Infinite Channel	69
Figure 3.3	Comparison of Steady State Velocity Profile from Model and Analytic Solution of 1-D Channel of Infinite Length with $\alpha = 0.04648$, $\beta = 0.01$, Bottom Friction Coefficient = 0.05 ft/sec.	73
Figure 3.4	Forces Acting on Section of Water in Closed Channel at Steady State	75
Figure 3.5	Comparison of Steady State Velocity Profile from Model and Analytic Solution of 1-D Channel of Finite Length with $\alpha = 0.04648$, $\beta = 0.01$ and Bottom Friction Coefficient = 0.05.	78
Figure 3.6	Comparison of 3-D Solution for Numerical and Analytical Models for Variable Eddy Viscosity	84
Figure 3.7	Comparison of 3-D Solution for Numerical and Analytical Models for Constant Eddy Viscosity	85
Figure 3.8	Variation of N_v used in Test Case 4	87
Figure 3.9	Comparison of the Model to the Analytic Solution for the Case of a Bilinear Variation in N_v ($N_I/N'_b \approx 1$)	91
Figure 3.10	Comparison of the Model to the Analytic Solution for the Case of a Bilinear Variation in N_v ($N_I/N'_b = 100$)	92

CHAPTER 1

1.1 Justification for Development of a Three-Dimensional Model*

A simple, efficient method to predict velocities which vary laterally and vertically in a water body has important implications for several areas of coastal engineering. In a practical sense, the model can play a role in environmental assessment, particularly in the development of offshore resources. For example, a three-dimensional velocity model could serve as the basis for predicting storm-induced current forces on offshore structures. As the water depth in which these structures are built increases (currently 250 meters but soon to be 330 meters) costs mushroom, and enhanced accuracy in predicting currents could mean substantial savings for even a single structure.

Another application of a three-dimensional circulation model is in the area of pollution control, specifically in predicting the trajectory of a surface pollutant such as oil. The state-of-the-art for predicting the advection of oil slicks is the "fixed wind factor" approach. This method consists of simply taking the center of mass movement to be a fixed percentage of the wind speed. When the factor is taken as 3%, as is commonly done, the procedure is known as the "3% rule." The effect of the earth's rotation on fluid motion, known as the Coriolis "force," is sometimes accounted for by deflecting the surface current a constant angle to the right of the direction of the

* A "three-dimensional model" is defined here as a model which yields the horizontal velocity variations in the vertical direction as well as in the horizontal. Vertical velocity is neglected.

wind (to the left in the Southern Hemisphere). This angle is commonly termed the deflection angle,

Oil spill modelers usually justify the fixed wind factor approach by referencing any number of previous field and laboratory studies investigating the wind factor. Stolzenbach et al. (1977) compiled the results of the most often quoted experiments, included here in Table 1.1. Note that the supposedly constant wind factor varies by a factor of five depending upon which investigator one chooses to believe. Even individual investigators found large variations in this wind factor as evidenced by the significant standard deviations. This should come as no surprise, as one would expect that the complex interaction of wind, waves, bathymetry, etc., could not be modeled for all cases by a single, constant parameter.

A three-dimensional modeling effort also has importance in a scientific sense. Such a model may be used as a tool to acquire greater understanding of the factors contributing to circulation in a water body. By comparing results from the model with field data or experimental results, it may be possible to determine some of the effects of parameters such as shear, density, or bathymetry on circulation.

1.2 Discussion of the Eddy Viscosity Concept

Since the eddy viscosity is considered an important addition to the formulation of this model, some discussion of the eddy viscosity concept is warranted. Central to the concept of friction in fluid motion is that shear stresses are produced when fluid layers slip.

For laminar flow, velocities near a solid boundary are smaller

than the velocities further from the boundary. This can be seen from a typical velocity profile for one-dimensional flow in an infinitely long channel shown in Figure 1.1. Shear occurs between the layers moving at different velocities. The expressions for shear stresses in the x-direction are:

$$\frac{\tau_{xx}}{\rho} = \nu \frac{\partial u}{\partial x}; \quad \frac{\tau_{xz}}{\rho} = \nu \frac{\partial u}{\partial z}; \quad \frac{\tau_{xy}}{\rho} = \nu \frac{\partial u}{\partial y} \quad (1.1)$$

τ_{ij} is the shear stress acting in the j-direction on a plane normal to the i-direction,

ρ is the fluid density

ν is the kinematic viscosity of the fluid

u is the velocity in the x direction

For the case of turbulent flow, rapid velocity fluctuations take place at all localities in the fluid. In this situation, the velocity can be characterized as the sum of two velocity components:

$$u = \bar{u} + u'; \quad v = \bar{v} + v'; \quad w = \bar{w} + w' \quad (1.2)$$

u, v, w are the velocities in the x, y, and z directions, respectively

$\bar{u}, \bar{v}, \bar{w}$ are the average velocities, taken over a long period of time, in the x, y, and z directions

u', v', w' are the turbulent components of the velocity in the x, y, and z directions. These turbulent components represent the deviation from average velocity in the three directions.

Owing to the nature of turbulent motion, fluid masses are

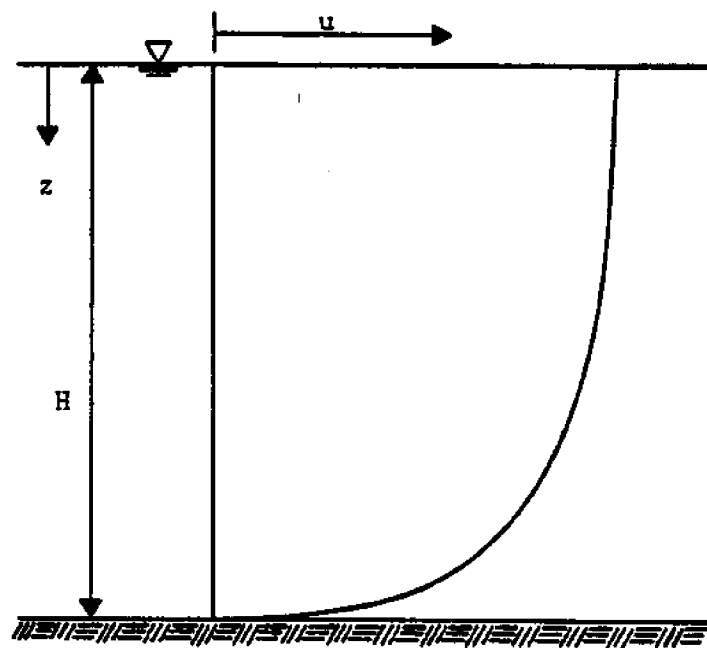


Figure 1.1 One-Dimensional Velocity Profile

transported back and forth between fluid layers, Suppose that Figure 1.2 represents the average velocity, \bar{u} ($\bar{v}, \bar{w} = 0$; $u', v', w' \neq 0$), it can be seen that a fluid particle at point A carried to point B by turbulent velocities would gain momentum from the higher velocity of the surroundings, whereas a fluid particle moving from B to A loses momentum. Because of this type of transport, fluid in a high velocity region will tend to be retarded, and fluid in a low velocity region will tend to be accelerated. Thus, the existence of a turbulent velocity gradient leads to a transport of momentum across surfaces normal to the gradient. The shear stress exerted on a surface is equal to the rate of momentum transport across that surface. In turbulent motion, the shear stresses in the x-direction are:

$$\frac{\tau_{xx}}{\rho} = \nu \frac{\partial u}{\partial x} - \overline{u'u'}; \quad \frac{\tau_{xz}}{\rho} = \nu \frac{\partial u}{\partial z} - \overline{u'w'}; \quad \frac{\tau_{xy}}{\rho} = \nu \frac{\partial u}{\partial y} - \overline{u'v'} \quad (1.3)$$

in which the bar over the primed variables represents a time average of the product of the two variables, and which is generally not equal to zero (as is the case with the time average of a single primed variable). If momentum transfer into a volume differs from the momentum transfer out of a volume, a frictional force per unit volume results.

The turbulent components of shear stress are termed the Reynolds stresses, and for highly turbulent motion, these stresses are much more important than the laminar stress components (except in the boundary layer), which may now be neglected. By assuming that the form of the turbulent shear stress is analagous to the laminar shear stress; we have:

$$\frac{\tau_{xx}}{\rho} = N_{xx} \frac{\partial u}{\partial x}; \quad \frac{\tau_{xz}}{\rho} = N_{xz} \frac{\partial u}{\partial z}; \quad \frac{\tau_{xy}}{\rho} = N_{xy} \frac{\partial u}{\partial y} \quad (1.4)$$

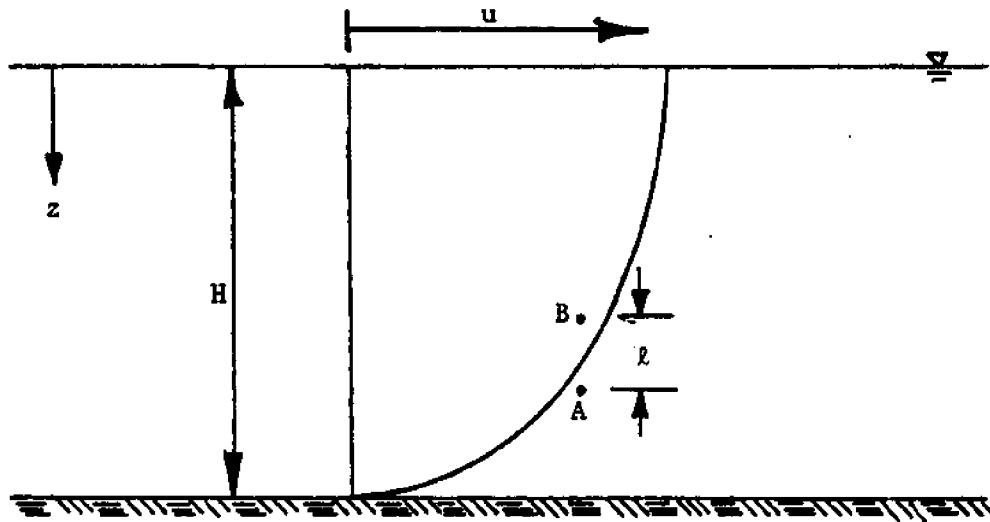


Figure 1.2: Mixing Length Concept

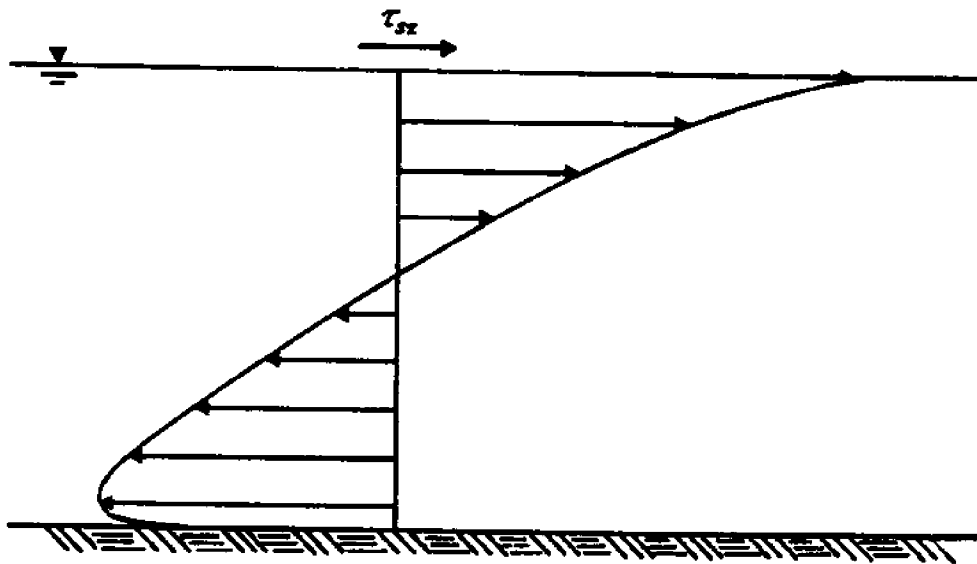


Figure 1.3: Typical Velocity Profile for Case of Wind-Induced Flow in a 1-D Channel of Finite Length

in which N_{xx} , N_{xz} , and N_{xy} are the eddy viscosity coefficients. Note that for laminar flow, N is the kinematic viscosity of the fluid.

There is little theoretical justification for the use of eddy viscosity coefficients. Yet this laminar analogy has been commonly invoked in the past, in part because it is a convenient simplification. In addition, the method has yielded reasonable results for certain applications.

Due to its unsteady nature and lack of strong theoretical foundation, the eddy viscosity parameter has been difficult to quantify. Direct measurement of the eddy viscosity requires instrumentation with fairly rapid response time. The technical problems of obtaining such measurements in an ocean environment are immense. If obtained, these measurements would apply only to the particular point and time at which the data were taken, since the parameter is generally a function of space and time.

Some idea of the magnitude of the eddy viscosity may be obtained using the mixing length hypothesis formulated by Prandtl (1925). Consider two layers of fluid moving in a turbulent environment as shown in Figure 1.2 (recall that the velocity profile represents the average velocity). Assume that at a certain distance from the bottom the average excursion of a fluid particle in the z -direction is l . When a fluid mass at point A travels to point B, it has a momentum deficit of $-\rho l \frac{\partial u}{\partial y}$. The rate of volume transfer from the lower to the upper layer is equal to \bar{w}'_t , which is the time average of the w' values which are greater than zero. The final result for the rate of transfer of (negative) momentum

to the upper layer is

$$\tau = -\rho \ell^2 \left| \frac{\partial u}{\partial z} \right| \frac{\partial u}{\partial z}; \quad (1.5)$$

Comparing this expression to equations (1.4), it is seen that the eddy viscosity coefficients may be interpreted as being equal to the square of the mixing length multiplied by the absolute value of the velocity gradient.

The scale of the mixing length will be inhibited near a solid boundary. The same situation exists at the surface where ℓ will be small, particularly if no waves are breaking. This implies that as the mixing length approaches a value of zero, so does the eddy viscosity. The mixing length and the eddy viscosity must reach a maximum somewhere between the surface and the bottom.

Equation (1.4) and its equivalent in the y-direction could now be substituted into the momentum equations. However, this would amount to replacing five unknowns ($\tau_{xx}, \tau_{xy}, \tau_{xz}, \tau_{yy}, \tau_{yz}$) with six parameters ($N_{xx}, N_{xz}, N_{yy}, N_{yx}, N_{yz}$). Given the uncertain nature of the eddy viscosity coefficients, these six parameters are usually reduced to two: an eddy viscosity coefficient in the horizontal direction, N_H ; and one in the vertical, N_V . Justification for this simplification can be found in Cooper and Pearce (1977).

1.3 Previous Efforts in Circulation Modeling

Many two-dimensional models have been developed which predict

the horizontal variation of the mean flow. These models are typically based on depth-averaged formulations which, although they require reasonable computation time, by the nature of the formulation deliver no information on the vertical velocity profile. Examples of such numerical models include a finite difference model by Leendertse (1967) and a finite element formulation by Wang and Connor (1975).

These models have proven useful in predicting such quantities as mass transport, storm surge and general circulation movement. The depth-averaged formulation will predict the velocities induced by pressure gradients and tides in open waters. However, use of these models to predict wind-induced surface currents is inappropriate. This is clearly seen in the case of one-dimensional flow in a channel of finite length. The velocity predicted by a depth-averaged model is zero. Yet it is known that in such a situation a doubly logarithmic velocity profile similar in form to that shown in Figure 1.3 can be expected.

Ekman (1905) was one of the first to effectively address the problem of modeling the vertical structure of the horizontal velocities. One of his simplest models considers wind-induced drift only and is derived by simplifying the Navier-Stokes equation to include only the effect of the earth's rotation and the frictional force between water layers. This is expressed as:

$$\begin{aligned} -\rho f v &= \frac{\partial}{\partial z} (\tau_{xz}) \\ \rho f u &= \frac{\partial}{\partial z} (\tau_{yz}) \end{aligned} \tag{1.6}$$

f is the Coriolis parameter, equal to $1.44 \times 10^{-4} \sin \phi$ where

ϕ is the latitude

u, v are the time averaged velocity components in the x - and y -directions, respectively

τ_{xz}, τ_{yz} are the horizontal shear stresses induced by the turbulent component of the velocities

A left-handed coordinate system is assumed with z equal to zero at the water surface and pointing positive downward.

Recall that the turbulent shear stresses can be related to the turbulent velocity as discussed in Section 1.2. For the shear stresses under consideration, this relationship is

$$\tau_{xz} = \rho N_v \frac{\partial u}{\partial z}; \quad \tau_{yz} = \rho N_v \frac{\partial v}{\partial z} \quad (1.7)$$

in which N_v is the vertical eddy viscosity coefficient and is considered to be a constant in this case. Equations 1.6 may now be re-written

$$\begin{aligned} fu &= N_v \frac{\partial^2 v}{\partial z^2} \\ -fv &= N_v \frac{\partial^2 u}{\partial z^2} \end{aligned} \quad (1.8)$$

The two boundary conditions necessary to evaluate the constants of integration are:

$$\tau_{sy} = -\rho N_v \left. \frac{du}{dz} \right|_{z=0}; \quad u=v=0 \Big|_{z=\infty} \quad (1.9)$$

where τ_{sy} is the wind shear stress (assuming the wind is blowing in the y -direction only). The solution to equations 1.8 is:

$$\begin{aligned}
 u &= V_0 e^{-(\pi/D)z} \cos \left[\frac{\pi}{4} - \left(\frac{\pi}{D} \right) z \right] \\
 v &= V_0 e^{-(\pi/D)z} \sin \left[\frac{\pi}{4} - \left(\frac{\pi}{D} \right) z \right]
 \end{aligned}
 \tag{1.10}$$

D is the depth of frictional influence, equal to $\pi \sqrt{\frac{2Nv}{f}}$
 V_0 is the magnitude of the surface current, equal to $\frac{\tau_{sy}}{\rho N_v a}$ and
 a is equal to $\sqrt{\frac{f}{N_v}}$

At $z=D$ it is seen from the above expressions that the velocity has been reduced to $1/23$ of V_0 . The result of plotting Equations 1.10 is the classic Ekman "spiral" shown in Figure 1.4. Note that for infinitely deep water the surface current is aligned at 45° to the right of the wind (to the left in the Southern Hemisphere).

For the case of finite depth, Ekman changed the second boundary condition in Equation 1.9 to $u=v=0$ at the bottom, $z=H$. All other assumptions in deriving Equations 1.8 are retained. The resulting solution for the finite depth case is somewhat more complex and will not be shown here. In general, the shallow water solution will yield surface currents of both smaller magnitude and deflection than the infinitely deep case. However, when the water depth is greater than one-half the frictional depth, the surface current no longer feels the effect of the bottom and behaves as if the water were deep.

This Ekman model is inadequate for most real world problems since it does not include: 1) unsteady wind effects, 2) density gradients, 3) lateral boundaries, and 4) variable bathymetry. In part, these inadequacies have since been removed. Neumann (1968) included density effects.

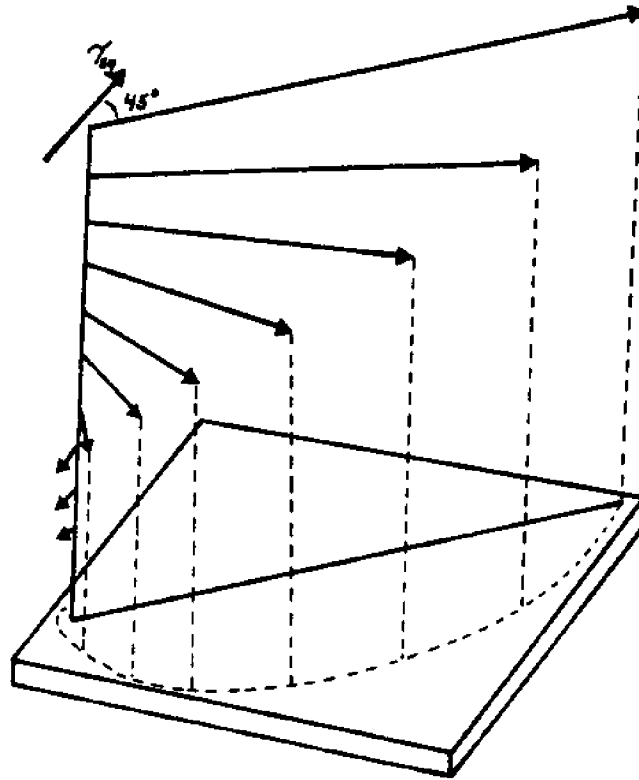


Figure 1.4: Vertical Structure of Pure Drift Current (Figure from Neumann (1968))

Foristall (1974) included unsteady effects and slope currents induced by lateral boundaries by combining an Ekman-type model with a two-dimensional vertically averaged model.

However, there are several characteristics of the Ekman approach which are unrealistic, and are still retained in the improved versions. For example, the Ekman-type solution predicts a deflection angle of 45° in deep water. Yet surface drift experiments (Table 1.1) indicate the deflection angle to be much smaller--of the order 10° . It should be noted that most of these experiments were performed in relatively shallow water and hence one might argue that the surface deflection would have been reduced due to the influence of the bottom. But this does not appear to be the case. Consider the field experiment performed by Teeson et al. (1970). It is possible to establish the extent of bottom influence for these experiments if some value for the vertical eddy viscosity is specified. As was seen in Section 1.2, the value for N_v is not well known. To avoid this problem, it will be assumed that the 3% rule is roughly correct. This assumption allows an approximate evaluation of the vertical eddy viscosity using the expression for V_o in Equation 1.10. Plugging this value for N_v into the expression for the depth of frictional influence D yields a frictional depth of approximately twenty meters for Teeson's experiments. Recall that for water depths greater than half the frictional depth, the surface is no longer affected by the bottom. Hence, for the bottom to have significantly affected the surface current in Teeson's experiments, the water depth would have had to have been less than ten meters. In fact, Teeson's experiments were performed in water depths well above that, in the range

Table 1.1

Summary of Various Experiments Investigating the Effects of Wind on Surface Drift

Name of Investigator	Nature of Experiment	Mean Wind Factor (%)	Standard Dev. (%)	Deflection Angle (degrees)	Standard Dev. (degrees)
Smith (1968)	hindcasting of observed oil slick	3.4	0.17	3.3 right	11.0
Tomczak (1964)	hindcasting of observed oil slick	4.3	N.A.	0.0	N.A.
" "	field experiment with drift cards	4.2	"	"	"
Hughs (1956)	field experiment with drift cards	2.1	0.4	3.5 right	10.7
" "	field experiment with drift cards	2.2	0.4	0.3 left	8.6
Neumann (1966)	field experiment with drift cards	4.2	N.A.	0.0	N.A.
Teeson et al. (1970)	field exper. with plastic sheets	2.8	1.1	13 right	7.0
Smith et al. (1974)	field exper. with drifting oil	0.8	0.7	none	none
Swartzberg (1971)	lab exper. with oil as drift med.	3.7	0.2	N.A.	N.A.
Keulegan (1951)	lab exper. (at high Reynolds #'s)	3.3	none	N.A.	N.A.
Van Dorn (1953)	field experiments in a small basin	3.3	none	N.A.	N.A.
Doebler (1966)	field exper. made off fixed platform using a drifting current pole	1.6	none	5.2 right	none
" "		1.2	none	13.2 right	none
" "		4.3	none	1.9 right	none
" "		5.8	none	4.8 right	none
Wu (1968)	lab experiment	4.1	0.9	N.A.	N.A.

of twenty to thirty meters.

Another possible suspect for creating the deflection angle discrepancy could be unsteady effects. Ekman investigated the length of time necessary for his solution to reach steady state. Figure 1.5 is a hodograph showing the development of the surface current for deep water. The numbers on the spiral are in pendulum hours. Note that after roughly four pendulum hours (five hours real time at 45° latitude) the surface velocity deflection angle never drops below approximately 35° . Most of the field experiments shown in Table 1.1 were performed in open coastal areas where major wind shifts would take place in relatively large time spans.

It is reasonable to conclude that the rather large and consistent discrepancy between the surface deflection angle predicted by Ekman's model and that observed in field experiments is not due to unsteady or shallow water effects. Other factors could conceivably be the cause of the discrepancy, such as currents of other origins (e.g., tidal). However, these other factors would be random in nature implying that one would not expect them to consistently cause the observed deflection angle to be less than that predicted by the Ekman model. Therefore, it is logical to look more closely at the validity of the various assumptions made by the Ekman model in order to find the possible cause for the deflection angle discrepancy.

One of the assumptions made by the Ekman model was that the vertical eddy viscosity was constant throughout the depth. Recall from Section 1.2 that the vertical eddy viscosity arises from the turbulent

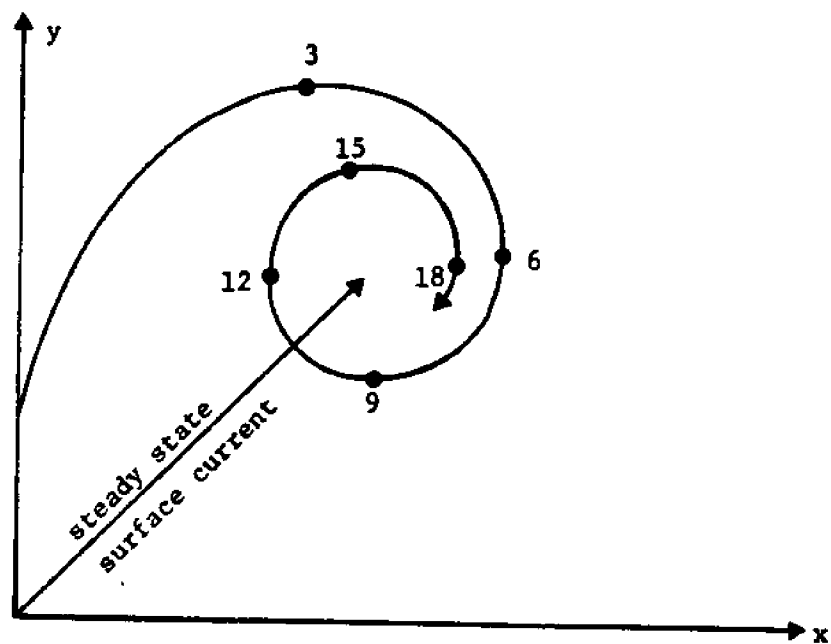


Figure 1.5: Hodograph Showing Development of a Pure Drift Current. The time after wind started to blow with constant speed is given in pendulum hours. (Figure from Neumann (1968))

frictional force between water layers, τ_{xz} and τ_{yz} . Ekman used the laminar analogy to write these stresses as a function of the turbulent eddy viscosity coefficient, N_v , which can also be written in terms of the turbulent velocity components as:

$$\begin{aligned}\tau_{xz} &= -\rho \overline{u'w'} = \rho N_v \frac{\partial u}{\partial z} \\ \tau_{yz} &= -\rho \overline{v'w'} = \rho N_v \frac{\partial v}{\partial z}\end{aligned}\tag{1.11}$$

where u', v', w' are the turbulent components of the velocity in the x-, y-, and z-directions, respectively.

It is clear that w' will be zero near a solid boundary, and since $\frac{\partial u}{\partial z}$ (or $\frac{\partial v}{\partial z}$) will, in general, not be zero near the boundary, then N_v must be zero near that boundary in order to satisfy the right hand side of the equivalence in Equations (1.11). If waves are not breaking at the surface, then the above argument implies that N_v must be near zero at the surface. Thus it is concluded that a realistic variation for N_v would be a shape with N_v near zero at the surface and the bottom, and a maximum somewhere in between. We conclude that a constant vertical eddy viscosity has no real-world analog.

The above argument can be partially substantiated when one examines the effect of including a varying vertical eddy viscosity in the Ekman-type formulation. Madsen (1977) solved the unsteady form of Equation 1.6 using the boundary conditions in Equations 1.9. He assumed the vertical eddy viscosity to be zero at the surface and to increase linearly with depth. For steady state, his results indicate a deflection angle of approximately 10° at the surface--a value consistent with the field observations in Table 1.1. Other aspects of Madsen's model remain

comparatively similar to Ekman's model including the magnitude of the surface current and the total mass flux.

Another situation in which a vertical variation of the eddy viscosity results in more realistic flow patterns is for the case of flow in an infinitely long channel of finite depth with the wind blowing in the axial direction (i.e., one dimensional flow). For this situation, an analytic solution assuming a constant vertical eddy viscosity yields a linear velocity profile.

If instead, it is assumed that N_v varies parabolically (zero at the surface and at the bottom) then the solution for the velocity is a logarithmic profile near the surface and the bottom. Intuitively, this latter solution seems much more correct, since one would expect the velocity to exhibit a logarithmic profile near the surface and the bottom. This intuition is substantiated in laboratory experiments performed by Shemdin (1972).

Thus it is finally concluded that in order to realistically model the velocity profile, a vertical variation in the vertical eddy viscosity should be incorporated into the model. In addition to Madsen, several other modelers have included a vertical variation in N_v .

Thomas (1975) developed an analytical solution for the problem of steady wind-driven currents in a shallow homogeneous water body with a variable vertical eddy viscosity. The functional form was assumed to be linear, being zero at the bottom and reaching a maximum at the surface. As previously mentioned, this formulation is physically realistic as far as the eddy viscosity variation near the bottom is concerned. It does, however, result in a finite eddy viscosity at the free surface. This

result is contrary to the result obtained by Reichardt (1959) and does not produce the experimentally observed logarithmic velocity profile (Shemdin, 1972) near the surface for the one-dimensional case, but rather a linear relation. The deflection angle for the two-dimensional case for this linearly varying eddy viscosity is found to be greater than the value predicted based on a constant vertical eddy viscosity assumption, although it approaches the 45° angle calculated by the Ekman model in deep water.

Leendertse (1975) has developed a three-dimensional layered model based on a finite difference formulation. The model includes density effects and assumes the vertical eddy viscosity to be a constant over each of nine horizontal layers. The overriding problem with this type of formulation is the computational requirement. Even for relatively small problems, the computer time requirement is of the order of hours on the fastest machines available.

Heaps (1972), and Heaps (1974) has recently developed numerical models using the Galerkin, weighted residual technique. The outstanding features of these models include: 1) a relatively simple formulation, 2) reasonable computer-time requirements, and 3) a continuous functional form for the velocity profile. However, the models still assume a constant eddy viscosity.

Thus, the modeling approach taken in this report has been to develop a three-dimensional model utilizing the Galerkin technique and incorporating a varying vertical eddy viscosity.

1.4 Initial Formulation of the Galerkin Solution

In the initial formulation of the model using a Galerkin solution, the functions chosen to approximate the true solution for the velocities were: (see Cooper and Pearce (1977))

$$\begin{aligned}\hat{u} &= \frac{-H\tau_{sx}}{\pi\rho N_v} \sin\left(\frac{\pi z}{H}\right) + \sum_{I=1}^{I'} c_I \cos\left(\frac{a_I z}{H}\right) \\ \hat{v} &= \frac{-H\tau_{sy}}{\pi\rho N_v} \sin\left(\frac{\pi z}{H}\right) + \sum_{I=1}^{I'} d_I \cos\left(\frac{a_I z}{H}\right)\end{aligned}\tag{1.12}$$

\hat{u}, \hat{v} are velocities in the x and y directions, respectively,

H is the still water depth,

τ_{sx}, τ_{sy} are surface stresses in the x and y directions, respectively, due to wind shear,

ρ is the water density,

N_v is the vertical eddy viscosity,

c_I, d_I are coefficients of the cosine terms, to be determined in model solution process,

a_I are prescribed constants,

z is the vertical axis, z equals zero at the surface and z equals H at the bottom,

I' is the number of terms needed to reach the required degree of accuracy.

The solutions obtained from the model using these expressions for the velocities were checked against several simple problems for which analytic solutions are available.

1.4.1 One-Dimensional, Infinitely Long Channel with Constant N_v

The case of wind blowing over an infinitely long channel with a constant N_v was examined first. Figure 1.6 shows the various physical characteristics of the idealized channel which was used. The vertical eddy viscosity was taken as $0.5 \text{ ft}^2/\text{sec.}$, and the wind was applied as a step function at time $t=0$ with a magnitude of 66 ft/sec. The effects of the earth's rotation and the lateral shear stresses were neglected and the water density was assumed homogeneous. Figure 1.7 shows the grid network used by the model. Grids of zero depth are cross-hatched. The dimension of each grid is 2000 feet by 2000 feet.

The model was run for two cases, one with three cosine terms in the series expression for the velocities, and one with five cosine terms. A comparison of the velocity profile from the model and the analytic solution is shown in Figure 1.8. The analytic solution is indicated by the solid line. Notice that the solution with three cosine terms is virtually the same as that using five cosine terms. The difference is not large enough to show up on the plot.

1.4.2 One-Dimensional, Closed-Ended Channel with Constant N_v

The model was next tested for a one-dimensional closed ended channel. The physical characteristics were exactly the same as for the channel in Figure 1.7 except that one end of the channel was blocked off. Likewise, the model grid system remained the same as with the previous case, except that the depth of element (6,2) was set equal to zero (i.e. $H_{6,2}=0$).

Again, the model was run for the cases of three cosine terms

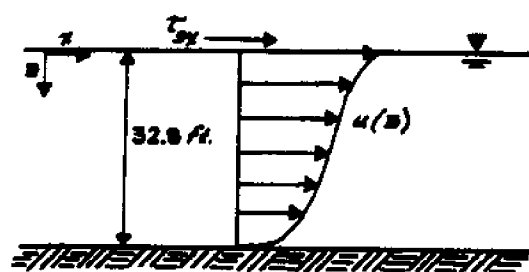


Figure 1.6: Physical Characteristics of the 1-D Channel Used in Model Verification

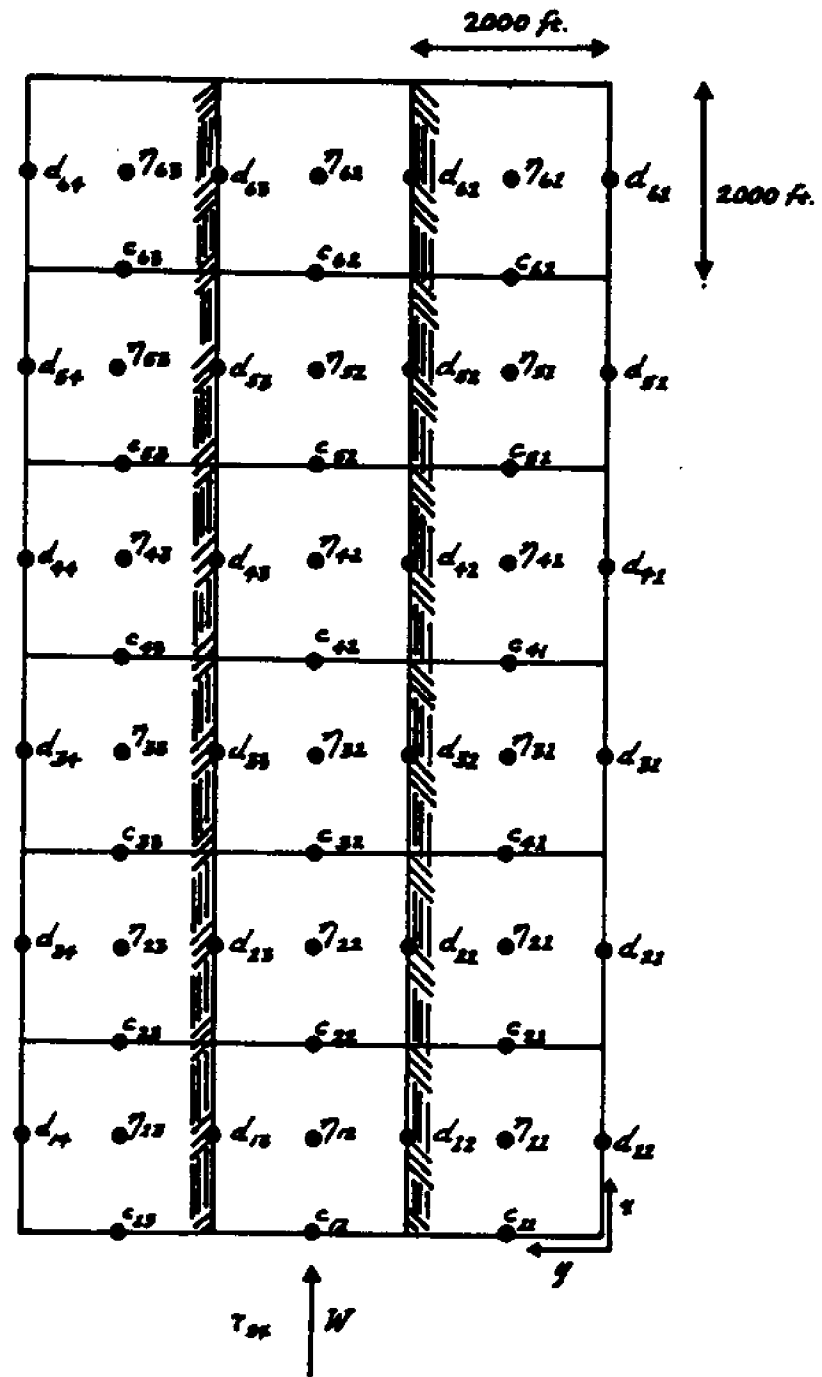


Figure 1.7: Grid Scheme Used for 1-D Channel

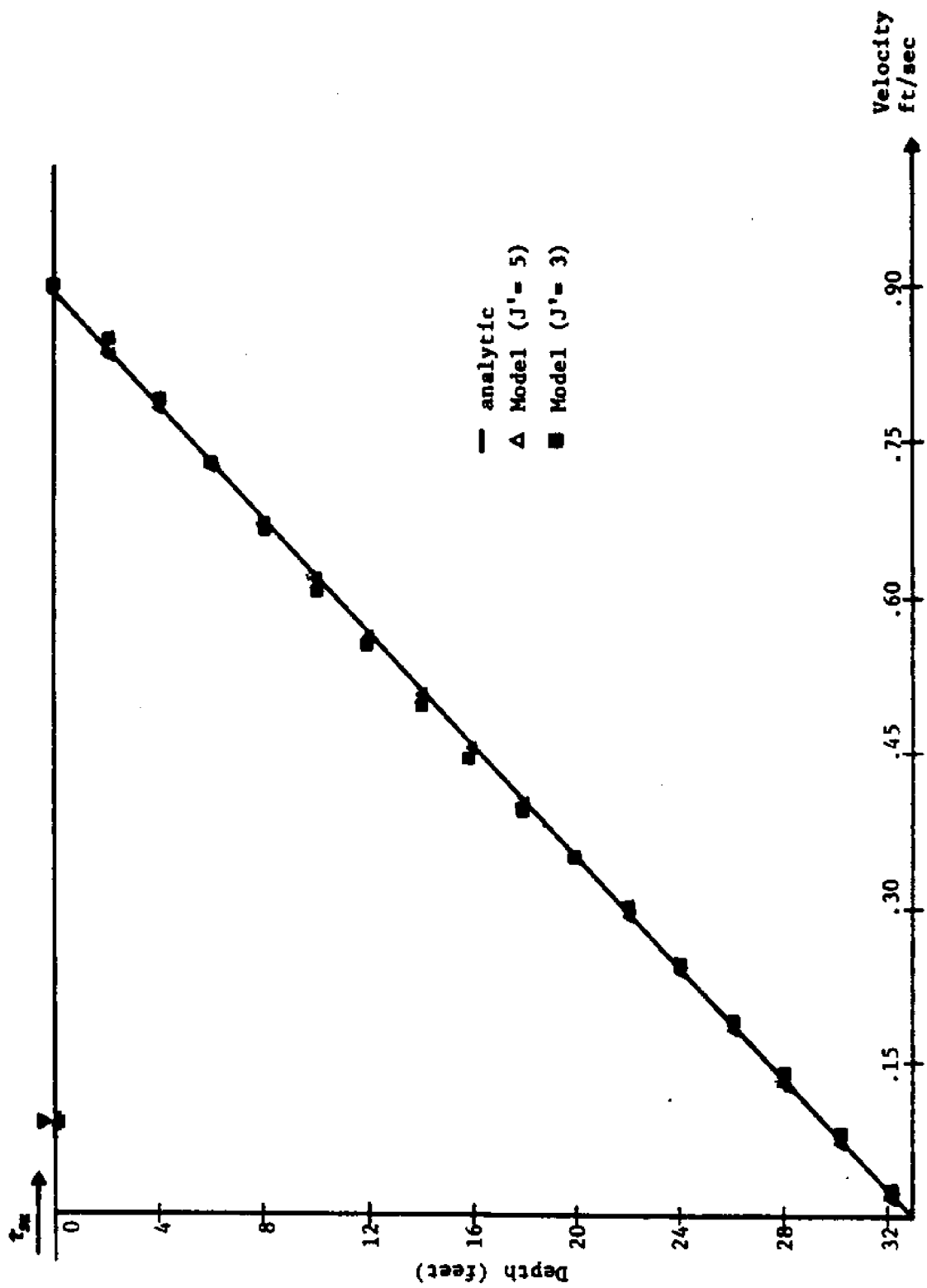


Figure 1.8: Comparison of Steady State Velocity Profile for the Case of a 1-D, Infinitely Long Channel with Constant N_v

and five cosine terms. Steady state results are compared to the analytic solution in Figure 1.9. The upper plot shows set-up η versus distance from the end of the channel. A datum was arbitrarily established at a distance of 9000 feet from the end of the channel. Hence the reason why η is zero at 9000 feet.

The lower plot shows the velocity profile. The model accurately predicts the analytic solution for both surface elevation and the velocity profile. It was found that three terms in the trial function approximated the solution nearly as well as five, the difference being undetectable on the scale used.

1.4.3 One-Dimensional, Infinitely Long Channel with Linear Variation in N_v

The model was next tested for a one-dimensional infinitely long channel identical to that described in Section 1.4.1, except that N_v was no longer considered to be a constant, but rather varied linearly as shown in Figure 1.10.

Because three cosine terms produced accurate results for the previous test cases, the model was run using that number of cosine terms. Figure 1.11 is a comparison of the analytic velocity profile and that predicted by the model. It is seen that the comparison is poor.

Since the analytic solution displays a very steep gradient near the bottom, it was suspected that more cosine terms were needed in order to approximate this steep gradient. Consequently, the number of cosine terms included was increased to eight. Figure 1.11 also includes a comparison of the analytic velocity profile and the velocity profile produced by the model with eight terms in the summation. Though an

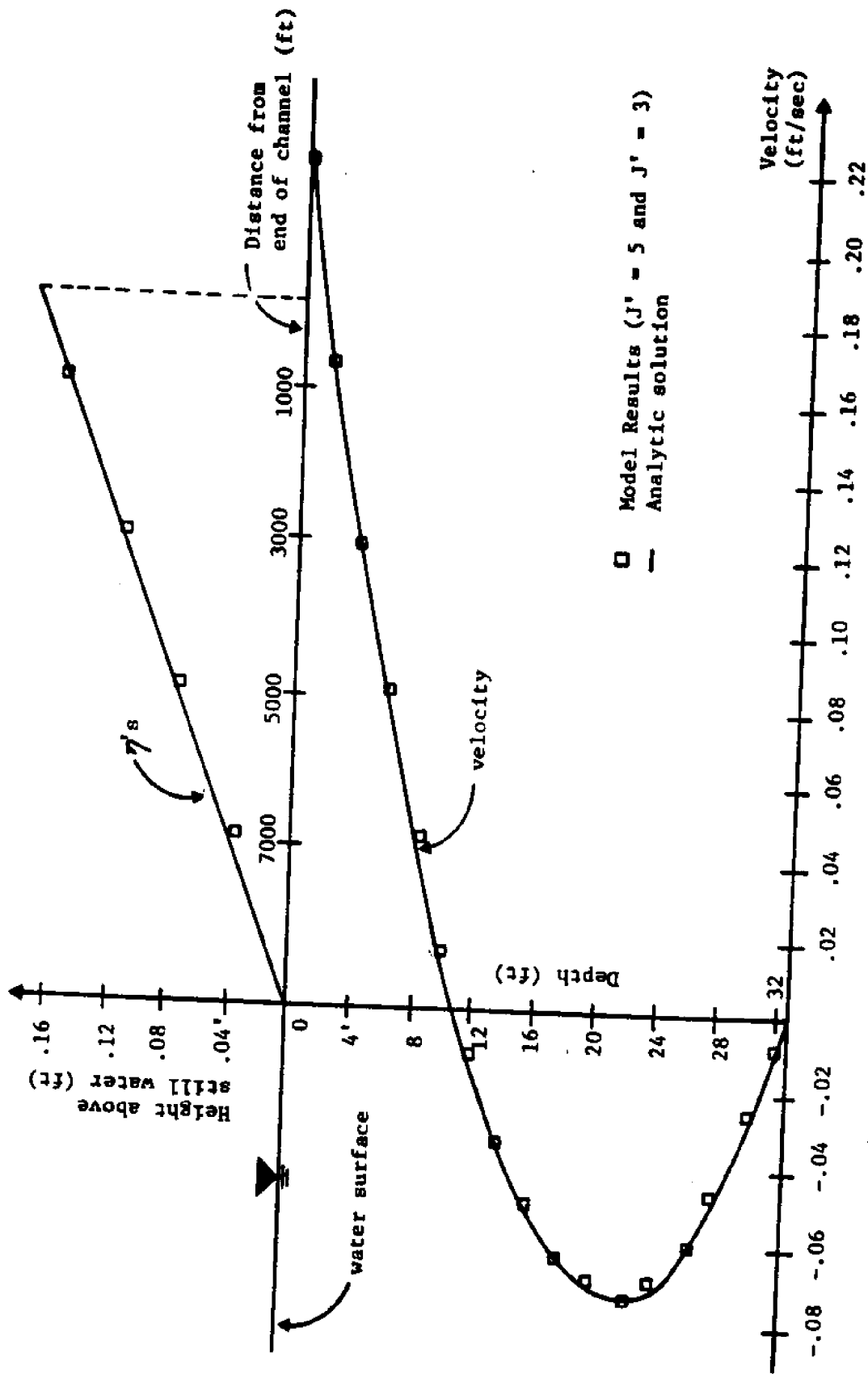


Figure 1.9: Comparison of Galerkin Model to Analytic Solution for 1-D Closed Ended Channel with a Constant Vertical Eddy Viscosity

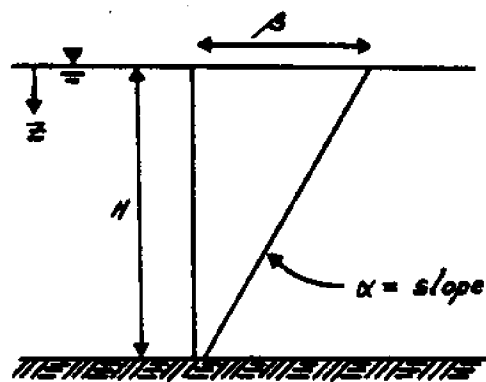


Figure 1.10: Linear Vertical Eddy Viscosity Model

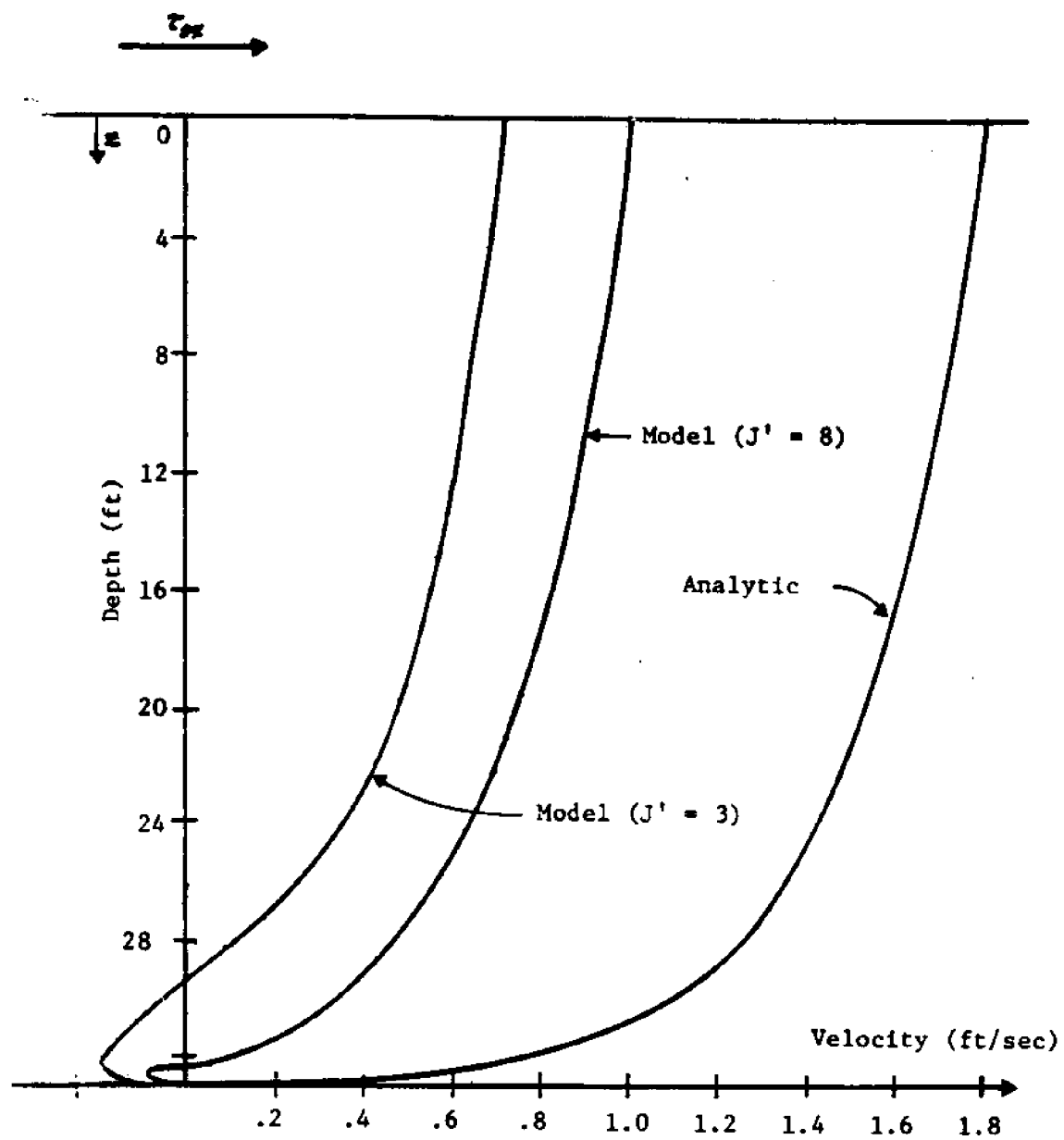


Figure 1.11: Comparison of Velocity Profiles for $\alpha = -0.04639$ ft/sec and $\nu = 1.5246$ ft²/sec

improvement has been made by increasing the number of terms, that improvement is small when compared to the discrepancy which remains between the model and the analytic solution.

1.4.4 Fourier Series Analysis

Further testing of the model indicated that the discrepancy between model and theory became progressively smaller as α was decreased (β held constant). This is not surprising since in the limit as α goes to zero, the problem simply reduces to the constant N_v case. It was shown in Sections 1.4.1 and 1.4.2 that the model yields very good results for this latter case.

Close examination of the components of the velocity trial functions \bar{u} and \bar{v} suggested that the cosine series converged slowly in the case of a linear variation in the vertical eddy viscosity. The truth of this statement can be shown using a Fourier analysis, which is summarized here. A more detailed discussion can be found in Section 3.6 of Cooper and Pearce (1977).

If a function $f(z)$ is specified as

$$f(z) = \sum_1 f_1 \cos \left(\frac{a_1 z}{H} \right) = u_t - u_0 \quad (1.13)$$

f_1 are the coefficients of the cosine series, determined from Fourier series analysis,

u_t is the velocity determined by theory,

u_0 is that part of the velocity trial function not associated with the cosine series, from Equation 1.12, $u_0 = \frac{-H\tau}{\rho N_v} \sin \left(\frac{\pi z}{H} \right)$

then $f(z)$ represents that part of the velocity which must be accounted for by the cosine terms. Figures 1.12 and 1.13 represent the convergence of the cosine series for the velocity calculated at the surface $z = 0$ (i.e., $f(z) = f(0)$), for the constant N_v and the linearly varying N_v cases, respectively. It is seen from Figure 1.12 that the cosine series converges rapidly for the case of constant vertical eddy viscosity -- including only three terms in the cosine series yields very good accuracy. For the case of varying vertical eddy viscosity, $\alpha = 0.04648$ and $\beta = 0.01$, convergence is much slower. Even with twelve cosine terms, the sum of the cosine series is only 90% of the value $f(0)$.

In conclusion, the above analysis indicates that the reason why the model compared so poorly with theory for the case of $\alpha = 0.04648$ and $\beta = 0.01$ is simply because not enough cosine terms were taken. The number of terms needed in the model to approximate this relatively simple one-dimensional profile would be in excess of ten terms. This has dire implications for the real world applicability of the model as formulated. Even if we optimistically assume that the rather complex profiles in a coastal environment could be simulated in the model using only fifteen terms, then for a realistically sized problem with a 20×20 grid system, the computer time requirement would be on the order of hours.

One possible solution to improving convergence of the model is to choose a u_0 term such that $f(z)$ can be more easily approximated by the cosine series. Choosing a u_0 term with this desirable characteristic near the bottom is not generally possible since the velocity and its gradient may be either positive or negative. For example, in the case of

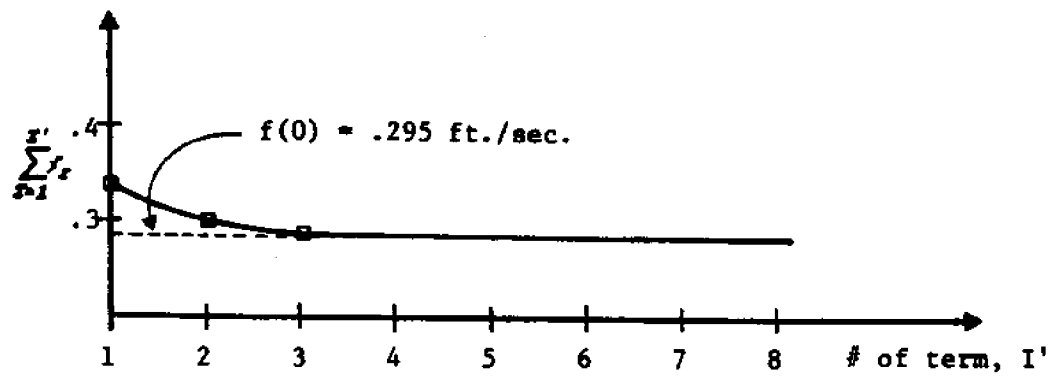


Figure 1.12: Convergence of Fourier Cosine Series for Case of $N_v = 1.5246 \text{ ft}^2/\text{sec}$

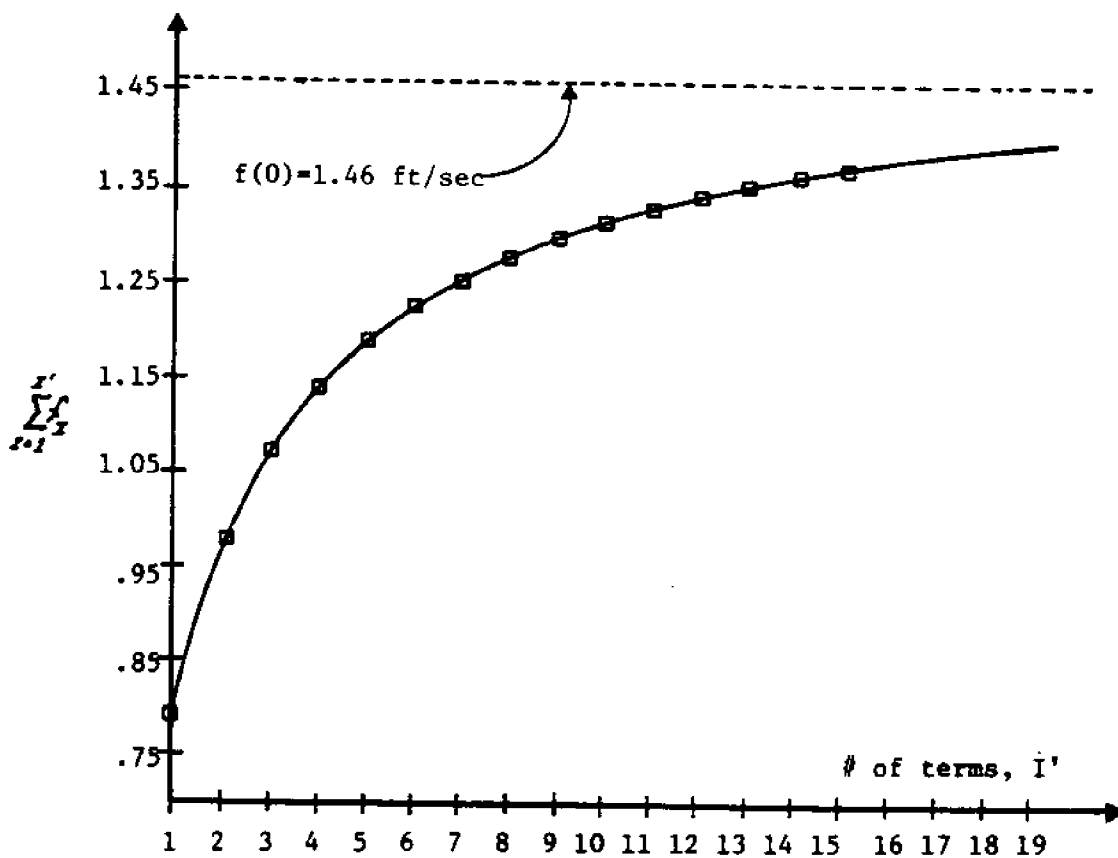


Figure 1.13: Convergence of Fourier Cosine Series for the Case of $\alpha = .04648$ and $\phi = .01$

one-dimensional flow in a channel of finite length, the water velocity near the bottom will be in a negative direction and the velocity gradient will be positive. On the other hand, for the case of one-dimensional flow in a very long channel, the water velocity will be positive and the velocity gradient negative.

An optimal choice of u_0 near the surface is much easier than near the bottom since the velocity gradient and velocity direction will be proportional to the wind velocity. For one-dimensional flow, u_0 can be assumed proportional to τ_{sx} and hence u_0 will always aid in convergence regardless of whether the channel is open or closed. The choice of u_0 may also depend on the form chosen to represent the eddy viscosity.

In the following sections, the Galerkin model is re-formulated for a revised choice of the velocity trial functions, and the results of the model are again compared with simple, analytic solutions.

CHAPTER 2 MODEL FORMULATION

2.1 Governing Equations

For constant density, the turbulent Navier Stokes or Momentum Equations in a left-handed coordinate (z is positive down) system are:

$$\frac{du}{dt} = -g \frac{\rho_s}{\rho} \frac{\partial \eta}{\partial x} + fv + \frac{\partial}{\partial x} \left(\frac{\tau_{xx}}{\rho} \right) + \frac{\partial}{\partial y} \left(\frac{\tau_{xy}}{\rho} \right) + \frac{\partial}{\partial z} \left(\frac{\tau_{xz}}{\rho} \right) - \frac{1}{\rho} \frac{\partial p_a}{\partial x} - \frac{g}{\rho} \int_{-\eta}^z \frac{\partial \rho}{\partial x} d\zeta \quad (2.1)$$

$$\frac{dv}{dt} = -g \frac{\rho_s}{\rho} \frac{\partial \eta}{\partial y} - fu + \frac{\partial}{\partial x} \left(\frac{\tau_{yx}}{\rho} \right) + \frac{\partial}{\partial y} \left(\frac{\tau_{yy}}{\rho} \right) + \frac{\partial}{\partial z} \left(\frac{\tau_{yz}}{\rho} \right) - \frac{1}{\rho} \frac{\partial p_a}{\partial y} - \frac{g}{\rho} \int_{-\eta}^z \frac{\partial \rho}{\partial y} d\zeta$$

where

u, v are the velocities in the x and y directions respectively

η is the water depth relative to some datum (in this case, will be taken relative to mean low water)

g is gravity

f is the Coriolis parameter = $2\omega \sin \phi$; ϕ = latitude

p_a is atmospheric pressure

τ_{ij} is the shear stress acting in the i direction on a plane which has a normal in the j -direction.

An examination of Figure 2.1 may clarify the definitions of the variables.

In most sea and lake circulation problems of practical importance, the vertical velocity component and its gradient are considerably smaller than the horizontal velocities and gradients and are hence neglected.

With this assumption the z -momentum equation simply reduces to an expression of the hydrostatic pressure distribution.

The left-hand-side of Equations (2.1) represent a combination of the unsteady and convective terms as shown below:

$$\frac{du}{dt} = \frac{\partial u}{\partial t} + u \frac{\partial u}{\partial x} + v \frac{\partial u}{\partial y}; \quad \frac{dv}{dt} = \frac{\partial v}{\partial t} + u \frac{\partial v}{\partial x} + v \frac{\partial v}{\partial y} \quad (2.2)$$

The first and second terms on the right-hand side of the equality in Eqns. (2.1) are the surface slope term and the Coriolis force term, respectively. The last term on the right-hand side is the atmospheric pressure gradient term.

Recall from Section 1.2 that shear stresses in turbulent flow can be expressed in terms of the eddy viscosity coefficients. The shear stresses in the x-direction are:

$$\tau_{xx} = \rho N_H \frac{\partial u}{\partial x}; \quad \tau_{xy} = \rho N_H \frac{\partial u}{\partial y}; \quad \tau_{xz} = \rho N_v \frac{\partial u}{\partial z} \quad (2.3)$$

Substituting the expressions for shear stress into the momentum equations yields:

$$\begin{aligned} \frac{du}{dt} = & -g \frac{\rho_s}{\rho} \frac{\partial \eta}{\partial x} + fv + \frac{\partial}{\partial x} (N_H \frac{\partial u}{\partial x}) + \frac{\partial}{\partial y} (N_H \frac{\partial u}{\partial y}) + \frac{\partial}{\partial z} (N_v \frac{\partial u}{\partial z}) - \frac{1}{\rho} \frac{\partial p_a}{\partial x} - \frac{g}{\rho} \int_{-\eta}^z \frac{\partial \rho}{\partial x} d\zeta \\ \frac{dv}{dt} = & -g \frac{\rho_s}{\rho} \frac{\partial \eta}{\partial y} - fu + \frac{\partial}{\partial x} (N_H \frac{\partial v}{\partial x}) + \frac{\partial}{\partial y} (N_H \frac{\partial v}{\partial y}) + \frac{\partial}{\partial z} (N_v \frac{\partial v}{\partial z}) - \frac{1}{\rho} \frac{\partial p_a}{\partial y} - \frac{g}{\rho} \int_{-\eta}^z \frac{\partial \rho}{\partial y} d\zeta \end{aligned} \quad (2.4)$$

Note that if the unsteady, convective, surface slope, atmospheric density and horizontal shear stress terms are neglected, Equations (2.4) reduce to Ekman's formulation.

Conservation of mass yields an additional governing equation. The appropriate form of the continuity equation for an incompressible

fluid is

$$\frac{\partial \bar{u}}{\partial x} + \frac{\partial \bar{v}}{\partial y} = \frac{\partial \eta}{\partial t} \quad (2.5)$$

where \bar{u} and \bar{v} are the mass fluxes per unit length in the x and y directions, respectively, or

$$\bar{u} = \int_{-\eta}^H u dz; \quad \bar{v} = \int_{-\eta}^H v dz$$

Surface Boundary Condition:

The surface boundary condition is:

$$\tau_{sx} \Big|_{z=-\eta} = -\rho_s N_v \frac{\partial u}{\partial z} \Big|_{z=-\eta}; \quad \tau_{sy} \Big|_{z=-\eta} = -\rho_s N_v \frac{\partial v}{\partial z} \Big|_{z=-\eta} \quad (2.6)$$

ρ_s is the density of water at the surface

τ_{sx}, τ_{sy} are the surface shear stresses induced by the wind in the x-and y-directions, respectively

The shear stress can be written as:

$$\tau_{sx} = \rho_s K \cos \theta |W|W; \quad \tau_{sy} = \rho_s K \sin \theta |W|W \quad (2.7)$$

W is the wind velocity

θ is the angle measured between W and the x-axis (positive counterclockwise)

K is a drag coefficient which is a function of the wind speed.

This latter functional relationship has been the topic of many investigations. Van Dorn (1953) published a classic work which included a functional form for K based upon experiments on a small pond. Van Dorn's relationship

has more or less been the standard in the past for determining the drag coefficient.

More recently, Wu (1969) has compiled data from various experiments measuring the wind shear stress including Van Dorn's work. This data displays a large amount of scatter indicating among other things, that the drag coefficient is not simply a function of wind speed but is probably dependent on other factors such as wave height, water and air temperature and fetch. Nevertheless, making the best of available results, Wu suggested a relationship:

$$\begin{aligned} K &= 0.4 * 10^{-6} W^{1/2} & W < 31 \text{ mph} \\ K &= 3.1 * 10^{-6} & W > 31 \text{ mph} \end{aligned} \quad (2.8)$$

The results of this expression can yield values for K which differ by nearly a factor of two from values derived using Van Dorn's functional form. Despite this, Wu's relationship is used in the model because his results are based upon data of a more general nature and because Wu used a relatively large amount of data, which should tend to minimize such factors as experimental error. In any case, it should be remembered that given the current state of knowledge concerning the drag coefficient, calculation of the wind shear stress is only approximate at best.

Bottom Boundary Condition

The shear stresses at the bottom boundary can be expressed as (referring to Eqns. 2.3):

$$\tau_{bx} = - \rho N_v \frac{\partial u}{\partial z} \Big|_{z=H} ; \quad \tau_{by} = - \rho N_v \frac{\partial v}{\partial z} \Big|_{z=H} \quad (2.9)$$

where τ_{bx}, τ_{by} denote the components of bottom friction in the x and y directions, respectively. If it is assumed that bottom friction varies linearly with bottom current as follows:

$$\tau_{bx} = c_b \rho_b u_b; \quad \tau_{by} = c_b \rho_b v_b \quad (2.10)$$

where c_b is a constant, ρ_b is the density at the bottom, and u_b and v_b are the bottom velocities, a comparison of (2.9) and (2.10) results in the expressions:

$$-\rho N \left. \frac{\partial u}{\partial z} \right|_{z=H} = c_b \rho_b u_b; \quad -\rho N \left. \frac{\partial v}{\partial z} \right|_{z=H} = c_b \rho_b v_b \quad (2.11)$$

The bottom boundary condition is:

$$\frac{\partial u}{\partial z} = \frac{-c_b u_b}{N_b}; \quad \frac{\partial v}{\partial z} = \frac{-c_b v_b}{N_b} \quad \text{at } z=H \quad (2.12)$$

where N_b is the eddy viscosity coefficient at the bottom. This is the bottom boundary condition formulated by Heaps (1972).

The effect of bottom roughness in the proposed model can be included by varying N_b and C_b . For the case of an ideally smooth bottom, N_v will theoretically approach the value of the kinematic viscosity near the bottom. As bottom roughness increases, the value for N_v at the bottom can be expected to rise.

Thus, a set of governing differential equations (2.4 and 2.5) and boundary conditions in the vertical (2.7 and 2.12) has been derived. The horizontal boundary conditions about the perimeter of the water body need not be introduced quite yet.

The momentum equations (2.4) are second order, non-linear partial differential equations and cannot be solved analytically. Therefore, a

numerical approach is taken. A variety of methods could be employed, but for the reasons expressed in Chapter 1, the Galerkin method is applied. Application of this technique will transform the two momentum equations into a set of linear, first-order partial differential equations, which can be easily solved using a variety of methods.

2.2 Application of Galerkin Technique

Application of a weighted residual technique begins by assuming a generalized functional relationship to approximate the true solution, or:

$$\hat{u} = u_0 + \sum_{I=1}^{I'} c_I \Omega_I; \quad \hat{v} = v_0 + \sum_{I=1}^{I''} d_I \Omega_I \quad (2.13)$$

where \hat{u} and \hat{v} are the "trial functions," Ω_I 's are prescribed functions, c_I and d_I are coefficients of the prescribed functions which are determined in the solution process, and I' and I'' are the number of terms needed to reach the required degree of accuracy.

In theory, the only restriction in choosing the Ω_I 's is that they must satisfy the vertical boundary conditions when combined with the leading terms, u_0 and v_0 . In practice, however, they are chosen so as to approximate the true solution with as few terms as possible. This implies that if it was known beforehand that the true solution was for example logarithmic, then it would be reasonable to take the prescribed functions to be logarithms.

The leading terms, u_0 and v_0 , are also somewhat arbitrary and may not have the same functional form as that assumed for the prescribed functions. These terms, however, when combined with the summation terms, must meet the necessary vertical boundary conditions.

Heaps chose cosines for the prescribed function. This function has many desirable characteristics, including:

1. it is well defined for all angles,
2. it is well-behaved when differentiated or integrated,
3. it is able to approximate complex functions when combined together in a series, and
4. it is orthogonal with respect to other cosine terms.

Using cosines, the trial functions can be written:

$$\bar{u} = u_0 + \sum_{I=1}^{I'} c_I \cos\left(\frac{a_I z}{H}\right); \quad \bar{v} = v_0 + \sum_{I=1}^{I''} d_I \cos\left(\frac{a_I z}{H}\right) \quad (2.14)$$

where a_I are prescribed constants.

To evaluate u_0, v_0 , and the a_I 's the boundary conditions at the surface and bottom are utilized. Using the surface boundary condition (Equation 2.6) and taking the derivative of the trial function implies that:

$$\left. \frac{\partial u_0}{\partial z} \right|_{z=0} = \frac{-\tau_{sx}}{\rho_s N_v}, \quad \left. \frac{\partial v_0}{\partial z} \right|_{z=0} = \frac{-\tau_{sy}}{\rho_s N_v} \quad (2.15)$$

The summation part of the trial function drops out since the derivative of the cosine series is simply a sine series, which when evaluated at $z=0$ will be zero for any value of a_I .

The surface boundary condition has been evaluated at $z=0$ instead of $z=-\eta$. The necessity for this approximation will become evident later when the Galerkin technique is applied. Note that this approximation is good only when η is much smaller than the still water depth, H . This restriction is easily verified by expanding the velocity gradient by

means of a Taylor series. For simplicity, consider only the x-direction:

$$\left. \frac{\partial u}{\partial z} \right|_{z=-\eta} = \left. \frac{\partial u}{\partial z} \right|_{z=0} - \left. \frac{\partial^2 u}{\partial z^2} \right|_{z=0} \eta + \text{higher order terms} \quad (2.16)$$

To ensure that the velocity gradient evaluated at η be well approximated when evaluated at $z=0$ implies that:

$$\left. \frac{\partial u}{\partial z} \right|_{z=0} \gg \left. \frac{\partial^2 u}{\partial z^2} \right|_{z=0} \eta \quad (2.17)$$

Introducing characteristic scales for the velocity, time and length in this expression yields $\eta \ll H$.

For a linear variation in vertical eddy viscosity, i.e.,

$N_v = \alpha z + \beta$ one possible form of u_o is:

$$u_o = \frac{\tau_{sx} z^2 (z-H)}{\rho H^2 N_b} + \frac{\tau_{sx}}{\rho \alpha} \ln \left(\frac{N_b}{N_v} \right) \quad (2.18)$$

where $N_{vb} = \alpha H + \beta$ is the eddy viscosity at the bottom.

Evaluating the surface boundary condition (in the x-direction):

$$\begin{aligned} \left. \frac{\partial u}{\partial z} \right|_{z=0} = & \left. \frac{2\tau_{sx} z(z-H)}{\rho H^2 N_b} \right|_{z=0} + \left. \frac{\tau_{sx} z^2}{\rho H^2 N_b} \right|_{z=0} - \left. \frac{\tau_{sx}}{\rho(\alpha z + \beta)} \right|_{z=0} \\ & - \sum_{I=1}^{\infty} \frac{c_I a_I}{H} \sin \left(\frac{a_I z}{H} \right) \Big|_{z=0} \end{aligned} \quad (2.19)$$

It is seen that the first, second, and fourth terms of the right-hand side of Equation (2.19) vanish. The remaining expression is:

$$\left. \frac{\partial u}{\partial z} \right|_{z=0} = \frac{-\tau_{sx}}{\rho(\alpha z + \beta)} \Big|_{z=0} \quad (2.20)$$

which is the boundary condition obtained in Equation (2.15).

At the bottom, $z=H$, $N_b = \alpha H + \beta$, and the velocity gradient at the

bottom is expressed by Equation (2.12)

$$\left. \frac{\partial u}{\partial z} \right|_{z=H} = \left. \frac{2\tau_{sx} z(z-H)}{\rho H^2 N_b} \right|_{z=H} + \left. \frac{\tau_{sx} z^2}{\rho H^2 N_b} \right|_{z=H} - \left. \frac{\tau_{sx}}{\rho(\alpha z + \beta)} \right|_{z=H} - \sum_{I=1}^{I'} \frac{c_I a_I}{H} \sin\left(\frac{a_I z}{H}\right) \bigg|_{z=H} \quad (2.21)$$

At $z=H$, the first term of the right-hand side vanishes, the second and third terms cancel, and applying equation (2.12)

$$-\sum \frac{c_I a_I}{H} \sin a_I = -\frac{c_b}{N_b} \sum c_I \cos a_I \quad (2.22)$$

$$\text{or} \quad a_I \tan a_I = \frac{c_b H}{N_b} \quad (2.23)$$

Thus, the coefficients a_I will be dependent on the slip velocity coefficient, c_b . The final form of the trial functions can be written as:

$$\begin{aligned} \hat{u} &= \frac{\tau_{sx} z^2(z-H)}{\rho H^2 N_b} + \frac{\tau_{sx}}{\rho \alpha} \ln\left(\frac{N_b}{N_v}\right) + \sum_{I=1}^{I'} c_I \cos\left(\frac{a_I z}{H}\right) \\ \hat{v} &= \frac{\tau_{sy} z^2(z-H)}{\rho H^2 N_b} + \frac{\tau_{sy}}{\rho \alpha} \ln\left(\frac{N_b}{N_v}\right) + \sum_{I=1}^{I''} d_I \cos\left(\frac{a_I z}{H}\right) \end{aligned} \quad (2.24)$$

where all variables are specified constants except for the undetermined parameters c_I and d_I .

Figure 2.2 is a plot of the first three Ω_I terms. This figure indicates how the Ω_I terms can approximate very complex shapes when weighted by the appropriate amplitude, c_I or d_I .

Now that the trial functions have been specified, they can be substituted into the momentum equations (2.4). In general,

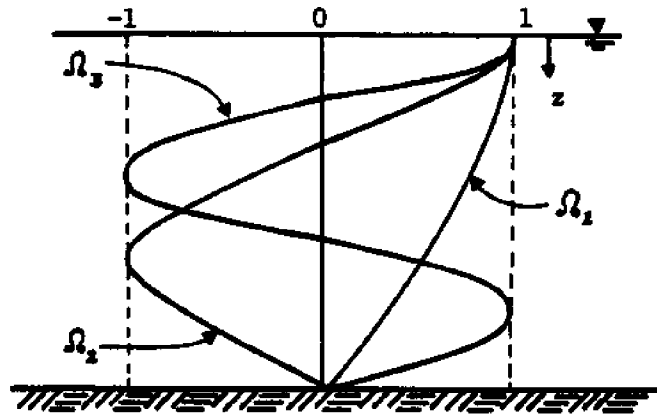


Figure 2.2 Plot of Prescribed Functions,
 Ω_1 vs. Depth.

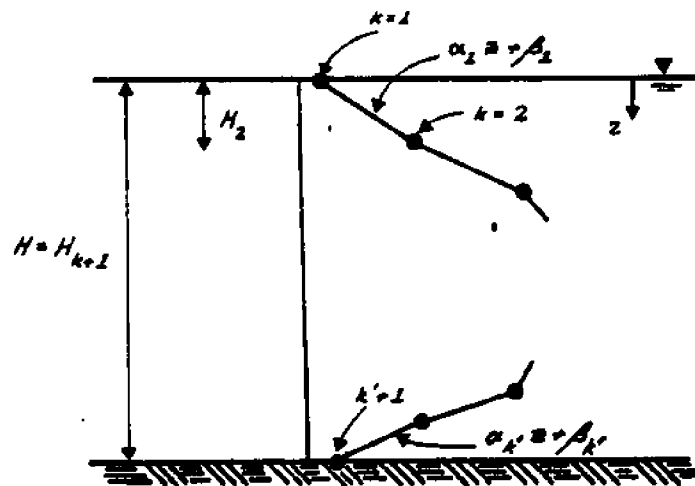


Figure 2.3: The Functional Form for the Vertical Variation
of N_v Used in the Model.

there will be an error associated with this substitution, since the trial functions are not the exact solutions to the momentum equations. This error is commonly referred to as the "residual". Performing this substitution yields:

$$R = \frac{d\hat{u}}{dt} + \frac{\rho_s}{\rho} g \frac{\partial \eta}{\partial x} - \frac{\partial}{\partial x} (N_H \frac{\partial \hat{u}}{\partial x}) - \frac{\partial}{\partial y} (N_H \frac{\partial \hat{u}}{\partial y}) - \frac{\partial}{\partial z} (N_v \frac{\partial \hat{u}}{\partial z}) - f\hat{u} + \frac{1}{\rho} \frac{\partial p_a}{\partial x} + \frac{g}{\rho} \int_{-\eta}^z \frac{\partial \rho}{\partial x} d\zeta \neq 0 \quad (2.25)$$

For the sake of brevity, only the residual in the x-direction is shown.

The error is minimized by specifying that the sum of the residual over a region be zero. For the case of interest, it is convenient to minimize the residual over a water column which yields:

$$\int_{-\eta}^H R dz = 0 \quad (2.26)$$

The residual can also be multiplied by an arbitrary weighting function, W , i.e.,

$$\int_{-\eta}^H RW dz = 0 \quad (2.27)$$

Various names are commonly associated with Equation (2.27), depending on the form of the weighting function, W . For example, if W is taken as R , then the technique is commonly called the Method of Least Squares. If the weighting function W is specified as the prescribed function Ω_I , then the technique is labeled the Galerkin Method.

The use of a weighting factor can significantly simplify the solution of Equation (2.27) over that of Equation (2.26). A well-chosen

weighting function W can ease computational requirements. If W and R form an orthogonal set of functions, then both the complexity of the solution as well as the computational requirement will be reduced.

Noting this last characteristic and observing that the residual R is composed primarily of sinusoidal functions, it is reasonable to utilize the Galerkin technique. W is set to be the prescribed functions Ω_I which consist of cosines. Substituting Ω_I for W in Equation (2.27) and neglecting pressure and density gradient terms yields:

$$\begin{aligned} \int_0^H R \Omega_I dz = & \int_0^H \frac{d\hat{u}}{dt} \Omega_I dz + g \frac{\partial \eta}{\partial x} \int_0^H \Omega_I dz - \int_0^H \left\{ \frac{\partial}{\partial x} (N_H \frac{\partial \hat{u}}{\partial x}) \right. \\ & + \frac{\partial}{\partial y} (N_H \frac{\partial \hat{u}}{\partial y}) \left. \right\} \Omega_I dz - \int_0^H \left(\frac{\partial N_v}{\partial z} \frac{\partial \hat{u}}{\partial z} \right) \Omega_I dz - \int_0^H N_v \frac{\partial^2 \hat{u}}{\partial z^2} \Omega_I dz \\ & - f \int_0^H \hat{u} \Omega_I dz = 0 \end{aligned} \quad (2.28)$$

where the N_v term has been differentiated and conveniently separated. There is an equivalent Galerkin statement for the y -direction.

Observe that the lower limit on the integration in Equation (2.28) has been moved from $z = -\eta$ to $z = 0$. As discussed earlier, η must be much less than the still water depth H for this approximation to be valid. The reason for neglecting the time variation of water depth should now be evident. If this assumption was not made, then the integrals in Equation (2.28) would have to be continually re-evaluated in time, since η is a function of time. This re-evaluation would be computationally prohibitive.

In order to evaluate the integrals, a functional form for the vertical variation of the vertical eddy viscosity must be specified. This is done by approximating N_v with a series of linear segments as shown in Figure 2.3. The slope α_k , the intercept β_k , and the number of segments k' must be supplied by the model user.*

This linear approximation scheme has several obvious advantages. It is fairly simple to integrate, and it can approximate very complex functional forms.

2.3 Evaluation of the Galerkin Statement

2.3.1 Unsteady Term

Term (1) consists of an unsteady term and convective terms. Upon substitution of the trial function and the prescribed function, the unsteady portion of the first term becomes:

$$\int_0^H \frac{\partial u}{\partial t} \Omega_I dz = \int_0^H \frac{\partial}{\partial t} \left\{ \frac{\tau_{sx} z^2 (z-H)}{\rho H^2 N_b} + \frac{\tau_{sx}}{\rho \alpha_1} \ln \left(\frac{N_b}{N_1} \right) + \sum_{I=1}^{I'} c_I \cos \left(\frac{a_I z}{H} \right) \right\} \cos \left(\frac{a_J z}{H} \right) dz \quad (2.29)$$

where $N_1 = \alpha_1 z + \beta_1$

The time step used in the model will be of the order 1 minute, which is short compared to the anticipated time change of τ_s , ρ and N_v . Hence it is reasonable to neglect the time derivative of the u_0 term.

As for the summation term, it is greatly simplified by using the orthogonality property of cosines. The integral of the summation term will be non-zero only when $I = J$ and in this case yields:

*Note that when more than one linear segment is used (i.e. $k' \geq 2$) then N_b in equations 2.23 & 2.24 should be replaced by $N'_b = \alpha_{k'} H + \beta_{k'}$, and N_v in equations 2.24 should be replaced by $N_1 = \alpha_1 z + \beta_1$.

$$\int_0^H \cos^2 \left(\frac{a_J z}{H} \right) dz = \frac{H}{2} \quad (2.30)$$

Thus, the unsteady portion of term 1 reduces to:

$$\int_0^H \frac{\partial \hat{u}}{\partial t} \Omega_J dz = \frac{H}{2} \frac{\partial c_J}{\partial t} \quad (2.31)$$

The convective terms are not so easily dealt with. The terms can be somewhat simplified if the wind and vertical eddy viscosity are assumed to vary slowly with respect to the spatial discretization in the horizontal. This assumption is reasonable for many situations since the typical grid element is of the order one mile in length and spatial gradients of N_v and τ_s should be relatively small over such length scales. With this approximation, the first convective term becomes:

$$\int_0^H \hat{u} \frac{\partial \hat{u}}{\partial x} \Omega_J dz = \int_0^H \left[\frac{\tau_{sx} z^2 (z-H)}{\rho H^2 N_b} + \frac{\tau_{sx}}{\rho \alpha_1} \ln \left(\frac{N_b}{N_1} \right) + \sum_{I=1}^{I'} c_I \cos \left(\frac{a_I z}{H} \right) \right] \frac{\partial \hat{u}}{\partial x} \cos \left(\frac{a_I z}{H} \right) dz \quad (2.32)$$

where $\frac{\partial \hat{u}}{\partial x}$ can be a very complex term, depending on the variables which are considered to be functions of x .

Cooper and Pearce (1977) show that the convective terms may be neglected if

$$u^* \frac{U^2}{L} \frac{\partial u^*}{\partial x^*} \ll f v^* V \quad (2.34)$$

where $u = U u^*$ $v = V v^*$ $x = L x^*$

which implies that

$$U \ll fL \quad (2.35)$$

This can be literally interpreted to imply that if the horizontal grid length for a particular problem is 1 mile, for example, model accuracy may become questionable in regions where the velocity difference between adjacent grid nodes is greater than roughly 1 ft/sec.

2.3.2 Surface Slope Term

Substituting the prescribed function, term (2) becomes

$$g \frac{\partial \eta}{\partial x} \int_0^H \Omega_J dz = g \frac{\partial \eta}{\partial x} \int_0^H \cos \frac{a_J z}{H} dz \quad (2.36)$$

For the purpose of the model formulation, it will be assumed that the density is constant over the depth. Integrating Equation 2.36

$$\begin{aligned} g \frac{\partial \eta}{\partial x} \int_0^H \cos \left(\frac{a_J z}{H} \right) dz &= g \frac{\partial \eta}{\partial x} \frac{H}{a_J} \sin \frac{a_J z}{H} \Big|_{z=0}^H \\ &= g \frac{\partial \eta}{\partial x} \frac{H}{a_J} \sin a_J \end{aligned} \quad (2.37)$$

2.3.3 Horizontal Shear Stress Terms

First consider the $\frac{\partial}{\partial x}$ term which can be conveniently broken into two parts:

$$\int_0^H \frac{\partial}{\partial x} \left(N_H \frac{\partial \hat{u}}{\partial x} \right) \Omega_J dz = \int_0^H \frac{\partial N_H}{\partial x} \frac{\partial \hat{u}}{\partial x} \Omega_J dz + \int_0^H N_H \frac{\partial^2 \hat{u}}{\partial x^2} \Omega_J dz \quad (2.38)$$

Note that the second integral involves the second derivative of the trial function. Recalling the form of the integral for the convective terms, it is seen that this integral will be complicated and difficult.

As in the case of the convective terms, the problem is sometimes avoided by arguing that the terms involving the horizontal eddy viscosity are small relative to the other terms in the momentum equations. This argument is best advanced by comparing the order of magnitude of the lateral shear stresses (τ_{xx} and τ_{xy}) from which the terms involving N_H originated, to the vertical shear stress (τ_{xz}) from which the term involving N_v originated. It follows that terms involving N_H can be neglected if

$$\frac{\partial \tau_{xy}}{\partial y} \ll \frac{\partial \tau_{xz}}{\partial z}; \quad \frac{\partial \tau_{xx}}{\partial x} \ll \frac{\partial \tau_{xz}}{\partial z} \quad (2.39)$$

Using the definition of Reynolds stresses, Equation (2.39) implies

$$\frac{\partial (\overline{u'v'})}{\partial y} \ll \frac{\partial (\overline{u'w'})}{\partial z}; \quad \frac{\partial (\overline{u'u'})}{\partial x} \ll \frac{\partial (\overline{u'w'})}{\partial z} \quad (2.40)$$

Inserting the characteristic horizontal and vertical length scales, L and H' respectively, and the characteristic horizontal and vertical velocity fluctuations, u' and w' , respectively, yields:

$$\frac{\overline{u'^2}}{L} \ll \frac{\overline{u'w'}}{H'} \quad (2.41)$$

The time increment over which the turbulent fluctuations are time averaged is the same order as the model time step in the case of a numerical model. A typical time step will be of the order one minute and for such short time scales it is reasonable to assume that the characteristic velocity fluctuation in the vertical will be of the same order as those in the horizontal. This assumption is substantiated by

laboratory experiments performed by Schubauer (1954) who found the turbulent component of the velocities inside a pipe to be nearly homogeneous except very near the wall. With this assumption of homogeneous turbulence, Equation 2.41 indicates that the lateral shear stresses are smaller than the vertical since L is generally much larger than H .

It is easier to see the implications of neglecting the lateral stresses by considering several specific examples. First consider the case of flow near a lateral boundary as pictured in Figure 2.4. Clearly a model without lateral shear stresses cannot predict the boundary layer that will occur in real world flow. Hence, velocity information within the boundary layer which is derived from such a model would be invalid. These regions could not generally be modeled anyway, simply because the cost of running a model with sufficiently small enough grids would be prohibitive.

Another example of the limitations imposed on a model by neglecting the lateral shear stresses can be seen by considering an idealized case of a permanent current passing by a bay. This situation is pictured in Figure 2.5. For the sake of clarity, neglect other forcing mechanisms such as tides, wind or Coriolis effect. In the real world the permanent current would induce complex gyres and eddies in the bay which would be characterized by a net counter-clockwise circulation.

Now assume that a model is applied with the discretization scheme shown in the figure and that the current is entered as a tangential flow at the boundary. If the model is based on a formulation which neglects lateral shear stresses, then clearly the model will simply

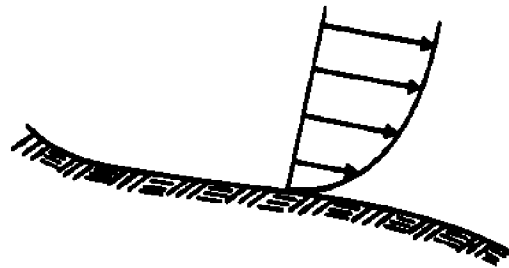


Figure 2.4: Horizontal Velocity Profile (at $z = \text{constant}$)
Near a Coastline

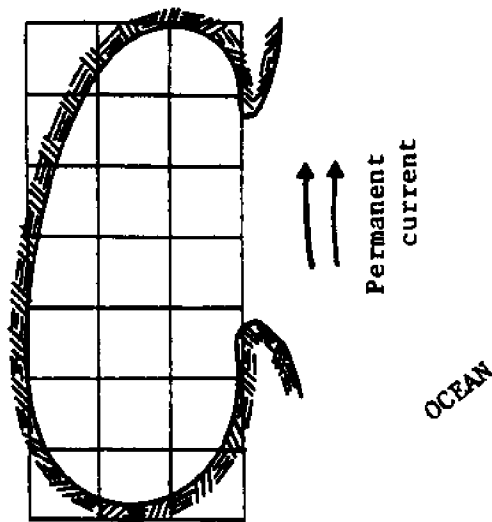


Figure 2.5: Circulation Induced in a Bay Due to a
Tangential Permanent Current.

indicate a stagnate bay. There would be no mechanism in the model to transfer the shearing motion induced by the permanent current. Similar inaccuracies can be anticipated in the modeling of circulation induced by large river flows into a bay.

Heaps no doubt recognized the inadequacies of completely ignoring the lateral shear stresses. He included the lateral shear stress by assuming a linearized approximation of the form

$$\frac{\partial}{\partial x} (N_H \frac{\partial u}{\partial x}) + \frac{\partial}{\partial y} (N_H \frac{\partial u}{\partial y}) = \epsilon u \quad (2.42)$$

The term ϵ is sometimes referred to as the geostrophic coefficient. This parameter is a complicated function of x and y and little is known about the nature of that variation.

Using Equation 2.42, term 3 can be re-written:

$$\begin{aligned} & - \int_0^H \frac{\partial}{\partial x} (N_H \frac{\partial \hat{u}}{\partial x}) \Omega_J dz - \int_0^H \frac{\partial}{\partial y} (N_H \frac{\partial \hat{u}}{\partial y}) dz = -\epsilon \int_0^H \hat{u} \Omega_J dz \\ & = -\epsilon \int_0^H \left(\frac{\tau_{sx} z^2 (z-H)}{\rho H^2 N_b} + \frac{\tau_{sx}}{\rho \alpha_1} \ln \left(\frac{N_b}{N_1} \right) + \sum_{I=1}^{I'} c_I \cos \frac{a_I z}{H} \right) \cos \frac{a_J z}{H} dz \end{aligned} \quad (2.43)$$

After integration, the horizontal eddy viscosity term can be expressed as:

$$-\epsilon H \left[\frac{\tau_{sx}}{N_1 \rho} (\psi_J - \gamma_J) + \frac{\tau_{sx}}{\rho} \Gamma_J + \frac{c_J}{2} \right] \quad (2.44)$$

where

$$\psi_J = \frac{\sin \frac{a_J}{a_J}}{a_J} + \frac{3}{a_J^2} \cos a_J - \frac{6}{a_J^2} \phi_J$$

$$\phi_J = \frac{\cos a_J}{a_J^2} + \frac{\sin a_J}{a_J} - \frac{1}{a_J^2}$$

$$\gamma_J = \frac{2}{a_J^2} \cos a_J + \left(\frac{1}{a_J} - \frac{2}{a_J^3}\right) \sin a_J$$

$$\Gamma_J = \frac{1}{a_J} \int_0^H \frac{\sin\left(\frac{a_J z}{H}\right)}{N_1}$$

The mechanics of integrating term 3 are included in Appendix A.

Note that Γ_J has no closed solution and must be integrated numerically. A simple trapezoidal numerical integration scheme was employed to obtain a value of Γ_J . This scheme approximates the integrand of Γ_J with a series of rectangles of equal width, Δx , as indicated in Figure 2.6. The height of the rectangle is taken as the value of the integrand at the middle of the element. The integral Γ_J is simply the sum of the areas of the rectangles.

The number of rectangles used to approximate Γ_J is specified by the model user. Since the numerator of the integrand is periodic, the number of terms needed for a given accuracy will increase as a_J increases.

2.3.4 Vertical Eddy Viscosity Term - Part One

Inserting the trial function, the prescribed function Ω_J , and the linear segment model for N_v , term 4 can be written:

$$\begin{aligned} - \int_0^H \frac{\partial N_v}{\partial z} \frac{\partial \Omega}{\partial z} \Omega_J dz = & - \sum_{K=1}^{K'} \alpha_K \int_{H_{K-1}}^{H_K} \left\{ \frac{2\tau_{sx} z(z-H)}{\rho H^2 N_b} + \frac{\tau_{sx} z^2}{\rho H^2 N_b} - \frac{\tau_{sx}}{\rho(\alpha_1 z + \beta_1)} \right. \\ & \left. - \frac{\sum_{I=1}^{C_I} a_I}{H} \sin\left(\frac{a_I z}{H}\right) \right\} \cos \frac{a_J z}{H} dz \end{aligned} \quad (2.45)$$

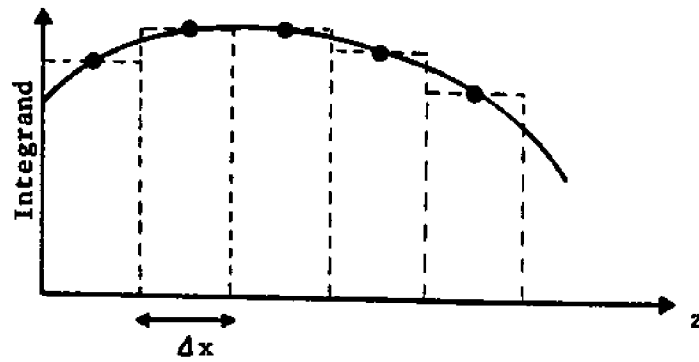


Figure 2.6: Discrete-Area Numerical Integration Scheme Used in the Model

Integrating and simplifying Equation 2.45 yields:

$$\frac{\tau_{ax}}{\rho N_b} \left[\sum_{K=1}^{K'} \alpha_K (2\phi_{KJ} - 3\gamma_{KJ}) \right] + \frac{1}{\rho} v_J - \sum_I c_I \delta_{IJ} \quad (2.46)$$

in which $\phi_{KJ} = \frac{1}{a_J} [\cos a_J \zeta_K + a_J \zeta_K \sin a_J \zeta_K - \cos a_J \zeta_{K-1} - a_J \zeta_{K-1} \sin a_J \zeta_K]; \quad \zeta_K = \frac{H_K}{H}$

$$\gamma_{KJ} = \frac{2\zeta_K \cos a_J \zeta_K}{a_J^2} + \left(\frac{a_J^2 \zeta_K^2 - 2}{a_J^3} \right) \sin a_J \zeta_K - \frac{2\zeta_{K-1} \cos a_J \zeta_{K-1}}{a_J^2} - \frac{(a_J^2 \zeta_{K-1}^2 - 2)}{a_J^3} \sin a_J \zeta_{K-1}$$

$$v_J = \sum_{K=1}^{K'} \alpha_K \int_{H_{K-1}}^{H_K} \frac{\cos \frac{a_J z}{H}}{a_1 z + \beta_1} dz$$

$$\sum_{I=1}^{I'} c_I \delta_{IJ} = \sum_{I=1}^{I'} \frac{a_I}{2} c_I \sum_{K=1}^{K'} \alpha_K \lambda_{KIJ}$$

where λ_{KIJ} can be expressed as:

$$\lambda_{KIJ} = \left[\frac{\cos(\theta_{IJ} \zeta_K) - \cos(\theta_{IJ} \zeta_{K-1})}{\theta_{IJ}} + \frac{\cos(\theta'_{IJ} \zeta_K) - \cos(\theta'_{IJ} \zeta_{K-1})}{\theta'_{IJ}} \right]$$

if $I \neq J$,

$$\theta_{IJ} = a_I - a_J$$

$$\theta'_{IJ} = a_I + a_J,$$

or

$$\lambda_{KIJ} = \frac{1}{a_I} [\cos^2(a_I \zeta_K) - \cos^2(a_I \zeta_{K-1})] \quad \text{if } I = J.$$

The integral v_J does not have a closed form solution, and must also be evaluated numerically using the trapezoidal scheme described in Section 2.3.3.

2.3.5 Vertical Eddy Viscosity Term-Part Two

Substituting the trial function, the prescribed function, and the linear segment model for N_v into term 5 yields:

$$\begin{aligned}
 -\int_0^H N_v \frac{\partial^2 \hat{u}}{\partial z^2} \Omega_J dz = & -\sum_{K=1}^{K'} \int_{H_{K-1}}^{H_K} (\alpha_K z + \beta_K) \left(\frac{6\tau_{sx} z}{\rho H^2 N_b} - \frac{2\tau_{sx}}{\rho H N_b} + \frac{\tau_{sx} \alpha_1}{(\alpha_1 z + \beta_1)^2} \right. \\
 & \left. - \sum_{I=1}^I \frac{c_I a_I^2}{H^2} \cos\left(\frac{a_I z}{H}\right) \right) \Omega_J dz
 \end{aligned} \tag{2.47}$$

Simplifying results in the following expression for term 5:

$$\begin{aligned}
 \frac{-6\tau_{sx}}{\rho N_b} \left[H \sum_{K=1}^{K'} \alpha_K \gamma_{KJ} + \sum_{K=1}^{K'} \beta_K \phi_{KJ} \right] + \frac{2\tau_{sx}}{\rho N_b} \left[H \sum_{K=1}^{K'} \alpha_K \phi_{KJ} + \sum_{K=1}^{K'} \beta_K S_{KJ} \right] \\
 - \frac{\tau_{sx} v_J'}{\rho} + \sum_{I=1}^I c_I \sigma_{IJ}
 \end{aligned} \tag{2.48}$$

where ϕ_{KJ} and γ_{KJ} are defined as in Section 2.3.4, and

$$\begin{aligned}
 v_J' &= \alpha_1 \sum_{K=1}^{K'} \int_{H_{K-1}}^{H_K} (\alpha_K z + \beta_K) \frac{\cos \frac{a_J z}{H}}{(\alpha_1 z + \beta_1)^2} dz \\
 S_{KJ} &= \frac{\sin(\zeta_K a_J) - \sin(\zeta_{K-1} a_J)}{a_J} \\
 \sigma_{IJ} &= \frac{a_I^2}{2} \sum_{K=1}^{K'} \left[\alpha_K \xi_{KIJ} + \frac{\beta_K}{H} \lambda_{KIJ}^* \right]
 \end{aligned}$$

If $I \neq J$,

$$\theta_{IJ} = a_I - a_J; \quad \theta'_{IJ} = a_I + a_J$$

$$\xi_{KIJ} = \frac{\cos(\theta_{IJ}\zeta_K) - \cos(\theta_{IJ}\zeta_{K-1})}{\theta_{IJ}^2} + \frac{\cos(\theta'_{IJ}\zeta_K) - \cos(\theta'_{IJ}\zeta_{K-1})}{\theta_{IJ}'^2}$$

$$+ \frac{\zeta_K \sin(\theta_{IJ}\zeta_K) - \zeta_{K-1} \sin(\theta_{IJ}\zeta_{K-1})}{\theta_{IJ}}$$

$$+ \frac{\zeta_K \sin(\theta'_{IJ}\zeta_K) - \zeta_{K-1} \sin(\theta'_{IJ}\zeta_{K-1})}{\theta'_{IJ}}$$

$$\lambda^*_{KIJ} = \frac{\sin(\theta_{IJ}\zeta_K) - \sin(\theta_{IJ}\zeta_{K-1})}{\theta_{IJ}} + \frac{\sin(\theta'_{IJ}\zeta_K) - \sin(\theta'_{IJ}\zeta_{K-1})}{\theta'_{IJ}}$$

and when $I = J$

$$\xi_{KII} = \frac{\zeta_K^2 - \zeta_{K-1}^2}{2} + \frac{\cos(2a_I\zeta_K) - \cos(2a_I\zeta_{K-1})}{4a_I^2}$$

$$+ \frac{\zeta_K \sin(2a_I\zeta_K) - \zeta_{K-1} \sin(2a_I\zeta_{K-1})}{2a_I}$$

$$\lambda^*_{KII} = \zeta_K - \zeta_{K-1} + \frac{\sin(2a_I\zeta_K) - \sin(2a_I\zeta_{K-1})}{2a_I}$$

Note that v_J' must be integrated numerically in addition to Γ_J and v_J .

Section 2.3.6 Coriolis Term

Term 6 can be expressed as:

$$-f \int_0^H \varpi \Omega_J dz = -f \int_0^H \left[\frac{\tau_{sy} z^2 (z-H)}{\rho H^2 N_b} + \frac{\tau_{sy}}{\rho \alpha_1} \ln \left(\frac{N_b}{N_1} \right) + \sum_{I=1}^{I'} d_I \cos \left(\frac{a_I z}{H} \right) \right] \cos \frac{a_J z}{H} dz \quad (2.49)$$

or, performing the integrations and simplifying

$$= -fH \left[\frac{\tau_{sy}^H}{N_b} (\psi_J - \gamma_J) + \frac{\tau_{sy}}{\rho} \Gamma_J + \frac{d_J}{2} \right] \quad (2.50)$$

where ψ_J , Γ_J and γ_J are the same as in term 3.

Substituting all the terms back into the original Galerkin statement (Equation 2.27) yields for the x-direction:

$$\begin{aligned} \int_0^H R \Omega_J dz &= \frac{H}{2} \frac{\partial c_J}{\partial t} + \frac{gH}{a_J} \sin a_J \frac{\partial \eta}{\partial x} - \epsilon H \left[\frac{\tau_{sx}^H}{\rho N_b} (\psi_J - \gamma_J) + \frac{\tau_{sx}}{\rho} \Gamma_J + \frac{c_J}{2} \right] \\ &+ \frac{\tau_{sx}^H}{\rho N_b} \left[\sum_{K=1}^{K'} \alpha_K (2\phi_{KJ} - 3\gamma_{KJ}) \right] + \frac{\tau_{sx}}{\rho} v_J - \sum_{I=1}^{I'} c_J \delta_{IJ} \\ &- \frac{6\tau_{sx}}{\rho N_b} \left[H \sum_{K=1}^{K'} \alpha_K \gamma_{KJ} + \sum_{K=1}^{K'} \beta_K \phi_{KJ} \right] + \frac{2\tau_{sx}}{\rho N_b} \left[H \sum_{K=1}^{K'} \alpha_K \phi_{KJ} + \sum_{K=1}^{K'} \beta_K S_{KJ} \right] \\ &- \frac{\tau_{sx}}{\rho} v_J' + \sum_{I=1}^{I'} c_I \sigma_{IJ} - fH \left[\frac{\tau_{sy}^H}{\rho N_b} (\psi_J - \gamma_J) + \frac{\tau_{sy}}{\rho} \Gamma_J + \frac{d_J}{2} \right] = 0 \end{aligned} \quad (2.51)$$

which can be organized more compactly as:

$$\frac{\partial c_J}{\partial t} = -2B_J \frac{\partial \eta}{\partial x} + \epsilon c_J + f d_J + \frac{2}{H} \sum_{I=1}^{I'} c_I \overline{\delta \sigma}_{IJ} + 2 \frac{\tau_{sx}}{\rho} D_J' + 2f \frac{\tau_{sy}}{\rho} E_J' \quad (2.52)$$

where $E_J' = \frac{H}{N_b} (\psi_J - \gamma_J) + \Gamma_J$

$$B_J = \frac{g}{a_J} \sin a_J$$

$$\overline{\delta \sigma}_{IJ} = \delta_{IJ} - \sigma_{IJ}$$

$$D_J' = \epsilon E_J' + \frac{A_J}{H}$$

$$A_J = \frac{1}{N_b} \left[\sum_{K=1}^{K'} H \alpha_K (9\gamma_{KJ} - 4\phi_{KJ}) + \beta_K (6\phi_{KJ} - 2S_{KJ}) \right] + v_J' - v_J$$

A similar expression may be derived for the y-momentum equation:

$$\frac{\partial d_J}{\partial t} = -2B_J \frac{\partial \eta}{\partial y} + \epsilon d_J - f c_J + \frac{2}{H} \sum_{I=1}^{I'} d_I \bar{\delta \sigma}_{IJ} + \frac{2\tau_{sy}}{\rho} D_J' - 2f \frac{\tau_{sx}}{\rho} E_J' \quad (2.53)$$

The summation term in Equation 2.53 is taken from $I=1$ to I' , not I'' as indicated in the formula for the velocity trial functions, Equation 2.13. Since it will not generally be known before model execution whether more cosine terms will be needed to approximate the velocity in the y direction or in the x-direction, it is reasonable to simplify the model by taking the same number of cosine terms in the x- and y-directions.

Equations 2.52 and 2.53 can be conveniently thought of as the governing Momentum Equations for a water column. All parameters are specified except the unknowns c_J , d_J , and η . Equations 2.52 and 2.53 represent a set of $2 \cdot I'$ equations with $2 \cdot I' + 1$ unknowns. To solve for the unknowns, one more equation linking the c_J 's and d_J 's to η must be specified. This equation is the Continuity Equation.

2.4 Continuity

The continuity equation was obtained in Section 2.1

$$\frac{\partial \bar{u}}{\partial x} + \frac{\partial \bar{v}}{\partial y} = \frac{\partial \eta}{\partial t} \quad (2.54)$$

The mass fluxes, represented by \bar{u} & \bar{v} , can be written in terms of the undetermined parameters. This expression is, for the x-direction:

$$\bar{u} = \int_0^H \hat{u} dz = \int_0^H \left\{ \frac{\tau_{sx} z^2 (z-H)}{\rho H^2 N_b} + \frac{\tau_{sx}}{\rho \alpha_1} \ln \left(\frac{N_b}{N_1} \right) + \sum_{I=1}^{I'} c_I \cos \frac{a_I z}{H} \right\} dz \quad (2.55)$$

After performing the integrations and simplifying, Equation 2.55 can be written as:

$$\bar{u} = F_x + H \sum_{I=1}^{I'} c_I S_{1I} \quad (2.56)$$

where

$$F_x = - \frac{H^2 \tau_{sx}}{12 N_b \rho} + G \frac{\tau_{sx}}{\rho}$$

$$G = \frac{1}{\alpha_1} [H \ln N_b - \frac{1}{\alpha_1} (N_b \ln N_b - N_b) + \frac{1}{\alpha_1} (\beta_1 \ln \beta_1 - \beta_1)]$$

$$S_{1I} = \frac{\sin \left(\frac{a_I}{H} \right)}{a_I}$$

and in the y-direction:

$$\bar{v} = F_y + H \sum_{I=1}^{I'} d_I S_{1I} \quad (2.57)$$

where

$$F_y = - \frac{H^2 \tau_{sy}}{12 N_b \rho} + G \frac{\tau_{sy}}{\rho}$$

Detailed derivation of this form of the continuity equation can be found in Appendix A.

The result of this formulation is that the original second order, non linear, momentum equations, together with the nonhomogeneous vertical boundary conditions have been reduced to a set of $2 \cdot J$ equations (Equations 2.52 and 2.53) which are linear, first order partial differential

equations. These equations are coupled with the continuity equation (2.54) and the boundary conditions about the horizontal perimeter of the water body, thus yielding a set of equations with a unique solution for the unknown variables c_J , d_J , and η . Once the c_J 's and d_J 's are determined, the velocities \hat{u} and \hat{v} are found using Equations 2.24.

2.5 Model Discretization Scheme

The method chosen to solve the momentum and continuity equations is the "split-time", finite difference scheme used by modelers such as Pearce (1972) and Reid et al. (1968). A detailed discussion of finite difference models will not be included here, however, it is important to be aware of the advantages and disadvantages of such a scheme.

The split-time, finite difference scheme has several prominent deficiencies. Because it is an explicit scheme, the method requires a smaller time step to maintain stability than might an implicit scheme. Additionally, it is impractical to use a grid system other than one composed of squares of equal size, due to the nature of the finite difference method. Such a grid system may produce unrealistic or time-consuming results for water bodies which are long, narrow and contorted.

There are several advantages supporting the choice of a finite difference scheme, including that the scheme:

1. has second order accuracy in both space and time,
2. yields an explicit solution for the "new" c_J 's, d_J 's and η 's,
3. requires relatively simple computer programming logic to implement,

4. requires minimal computer storage requirements, and
5. was implemented by Heaps (1972 and 1974) proving that the scheme is stable and convergent for the constant N_v case.

It was felt that if the model formulation proved successful using a simple finite difference scheme, then other, more sophisticated schemes could be implemented later.

To apply the method, the water body is discretized in the manner shown in Figure 2.7 where the variables c_J, d_J, n, H, \bar{u} , and \bar{v} are associated with the spatial points as indicated in Figure 2.7b. The subscripts ℓ and m are spatial location counters associated with the x and y directions, respectively. The time counter is n . There will be ℓ' grids in the x -direction, m' grids in the y -direction, and n' total number of time steps. So, for example, $\bar{u}_{1,2,3}$ would be the mass flux in the x -direction associated with element 1,2 at time $3\Delta t$, where Δt is the time increment.

Applying the discretization scheme to the governing differential equations (2.52, 2.53, 2.54) yields:

$$\begin{aligned}
 c_J(\ell, m, n+1) = & \varepsilon'(\ell, m, n) * c_J(\ell, m, n) - B_J'(\ell, m, n) * \bar{n}_x(\ell, m, n+1/2) + \\
 & c_2 * \bar{d}_J(\ell, m, n) + c_3(\ell, m) * \sum_{I=1}^{I'} c_I(\ell, m, n) * \bar{\delta\sigma}_{IJ}(\ell, m, n) + \\
 & \bar{\tau}_{xJ}(\ell, m, n)
 \end{aligned} \tag{2.58}$$

$$\begin{aligned}
 d_J(\ell, m, n+1) = & \varepsilon'(\ell, m, n) + d_J(\ell, m, n) - B_J'(\ell, m, n) * \bar{n}_y(\ell, m, n+1/2) - \\
 & c_2 * \bar{c}_J(\ell, m, n) + c_3(\ell, m) * \sum_{I=1}^{I'} d_J(\ell, m, n) * \bar{\delta\sigma}_{IJ}(\ell, m, n) + \\
 & \bar{\tau}_{yJ}(\ell, m, n)
 \end{aligned} \tag{2.59}$$

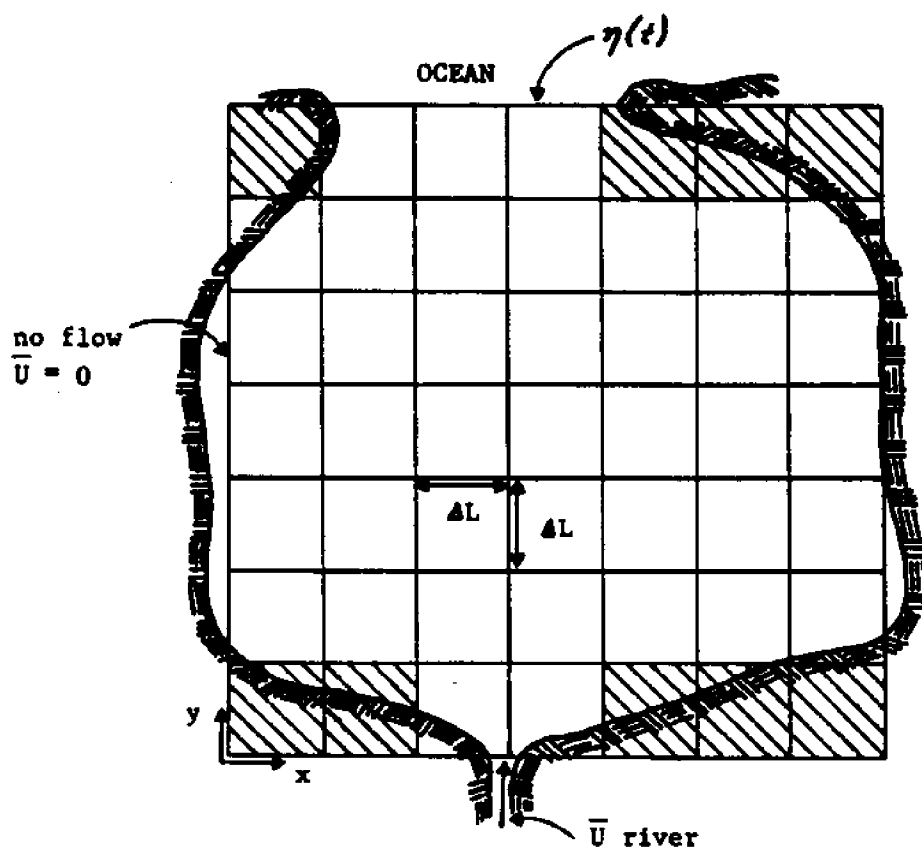


Figure 2.7a: Finite Difference Discretization Scheme

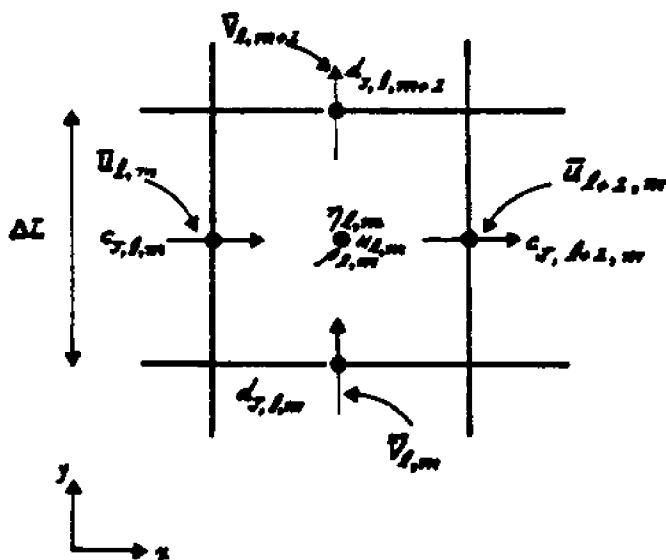


Figure 2.7b: Location of Critical Parameters

in which

$$\epsilon'(\ell, m, n) = 1 + \Delta t * \epsilon(\ell, m, n)$$

$$c_2 = 0.25 f \Delta t$$

$$c_3(\ell, m) = \frac{2\Delta t}{H}$$

$$\bar{c}_J(\ell, m, n) = c_J(\ell, m, n) + c_J(\ell+1, m, n) + c_J(\ell, m-1, n) + c_J(\ell+1, m-1, n)$$

$$\bar{d}_J(\ell, m, n) = d_J(\ell, m+1, n) + d_J(\ell, m, n) + d_J(\ell-1, m+1, n) + d_J(\ell-1, m, n)$$

$$B'_J = \frac{2\Delta t}{\Delta L} * B_J(\ell, m, n)$$

$$\bar{\tau}_{xJ}(\ell, m, n) = D_J(\ell, m, n) \frac{\tau_{sx}}{\rho} + E_J(\ell, m, n) \frac{\tau_{sy}}{\rho}$$

$$\bar{\tau}_{yJ}(\ell, m, n) = D_J(\ell, m, n) \frac{\tau_{sy}}{\rho} - E_J(\ell, m, n) \frac{\tau_{sx}}{\rho}$$

$$D_J = 2\Delta t D'_J; \quad E_J = 2\Delta t f E'_J$$

$$\bar{\eta}_x(\ell, m, n+1/2) = \eta(\ell, m, n+1/2) - \eta(\ell-1, m, n+1/2)$$

$$\bar{\eta}_y(\ell, m, n+1/2) = \eta(\ell, m, n+1/2) - \eta(\ell, m-1, n+1/2)$$

$$\eta(\ell, m, n+3/2) = \eta(\ell, m, n+1/2) + \frac{\Delta t}{\Delta L} \{ \bar{u}(\ell, m, n+1) - \bar{u}(\ell+1, m, n+1) + \bar{v}(\ell, m, n+1) - \bar{v}(\ell, m+1, n+1) \} \quad (2.60)$$

$$\bar{u}(\ell, m, n+1) = F_x(\ell, m, n) + H(\ell, m) * \sum_{I=1}^{I'} c_I(\ell, m, n+1) * S_{1I}(\ell, m, n+1)$$

$$\bar{v}(\ell, m, n+1) = F_y(\ell, m, n) + H(\ell, m) * \sum_{I=1}^{I'} d_I(\ell, m, n+1) * S_{1I}(\ell, m, n+1)$$

Equation 2.58 explicitly expresses the new c_J at time $(n+1)$ in terms of the old c_J 's at time n . The "old" η 's are evaluated at time $n+1/2$ instead of time n . This characteristic is the basis for the name "split-time" scheme. From Figure 2.7, it can be seen that the term \bar{d}_J is simply an

average of the d_J 's at the four locations nearest $c_J(\ell, m)$. Additionally, the spatial gradients $\frac{\partial \eta}{\partial x}$, $\frac{\partial \eta}{\partial y}$, $\partial \bar{u}/\partial x$, and $\partial \bar{v}/\partial y$ are easily defined using the proposed scheme.

The last segment of this section consists of a brief analysis of the model, including its solution scheme, computer space and time requirements, and stability criteria.

2.6 Special Considerations

Model Solution Strategy. The model first calculates all variables and arrays which are not time-dependent. At time $t=0$, all parameters are specified, and initial values are supplied for the c_J 's and d_J 's. Initial values for the η 's are supplied for time $1/2 \Delta t$. The new c_J 's and d_J 's are calculated at time Δt using Equations 2.58 and 2.59, and these new values are incorporated into the continuity equation (2.60) to yield the updated values for η , now at time $3/2 \Delta t$. The new η 's are substituted into 2.58 and 2.59 to solve for c_J 's and d_J 's at $3\Delta t$, and so on until the solution converges. If, at any time step, the velocities are required, Equations 2.24 must be solved. However, if the velocities are not desired for that particular time step, the additional calculations needed to solve Equations 2.24 can be avoided.

Computer Time and Storage Requirements. As previously mentioned, several numerical three-dimensional models developed in the past have been severely limited in scope, simply because their computer time and storage requirements were too large for problems of practical interest. One of the major objectives of this research was to develop

a three-dimensional model which could be applied to real-world problems. Therefore, it was essential to estimate the computer time and storage requirements of the Model before it was coded for computer runs. If the time and storage requirements did not seem reasonable, the model would have to be reformulated.

Cooper and Pearce (1977) have made an analysis of computer requirements of such a model, and concluded that a coastal area which is modeled with a 20 x 20 grid with each grid 1 square mile and with a minimum depth of fifty feet would require one minute of cpu time to run one tidal cycle (on an IBM 370/168 machine). Storage requirement for the model is approximately 300K.

Stability. The split-time finite difference scheme is an explicit scheme and is usually conditionally stable. For the case of one-dimensional flow, it was found that the time increment must be the minimum of:

$$\Delta t < \frac{2}{[a_I^2 \frac{N_{va}}{H^2}]_{\max}} \quad (2.61)$$

or

$$\Delta t < \frac{\Delta L}{\sqrt{gH}} \quad (2.62)$$

where N_{va} is the geometric average of the vertical eddy viscosity distribution. In other words, if the vertical variation of N_v is linear then N_{va} would be

$$\frac{|N_s - N_b|}{2} \quad (2.63)$$

where N_s is the value of the vertical eddy viscosity at the surface and N_b is the value of N_v at the bottom.

Equation 2.62 is the Courant Condition for stability. Note that in this equation, the maximum water depth will determine the minimum time step whereas in the case of Equation 2.61 the minimum water depth will govern.

Also observe that as the number of terms in the trial function increases, (i.e. I' increases), the allowable time step indicated by Equation 2.61 goes down in proportion to I'^2 . If Equation 2.61 governs then the computational requirements of the Model become proportional to I'^4 .

Order of magnitude arguments can be used to determine whether Equation 2.75 or 2.76 govern for most real-world problems. Assume that the minimum and maximum depth are of the order 5 feet and 500 feet, respectively, and that N_{va} is of the order $1 \text{ ft}^2/\text{sec}$. A typical grid spacing will be of the order 10^3 ft . The Courant Condition (Equation 2.62) indicates a permissible time step of about 10 seconds. This implies that if $a_I^2 > 5$, then Equation 2.61 will govern.

CHAPTER 3

MODEL VERIFICATION

Model verification is perhaps the most important step in the modeling process. In this section, model solutions for four cases are compared against analytic solutions to check for model convergence and accuracy. Cases 1, 2, and 4 use the grid layout and wind speed described in Section 1.4.1.

3.1 Test Case 1. Flow in an Infinite Channel

The form of the vertical eddy viscosity is shown in Figure 3.1. Values of α and β were chosen to be 0.04648 ft/sec. and 0.01 ft/sec., respectively. The following assumptions are made in the derivation of the analytic solution for this test case:

- (1) flow is one-dimensional, steady, and uniform (i.e. $v = 0$ where v is velocity in the lateral direction in the channel),
- (2) the Coriolis term does not contribute significantly,
- (3) atmospheric pressure does not vary spatially
- (4) density is constant throughout the fluid.

If these assumptions are applied to the equations of motion (Equation 2.1),

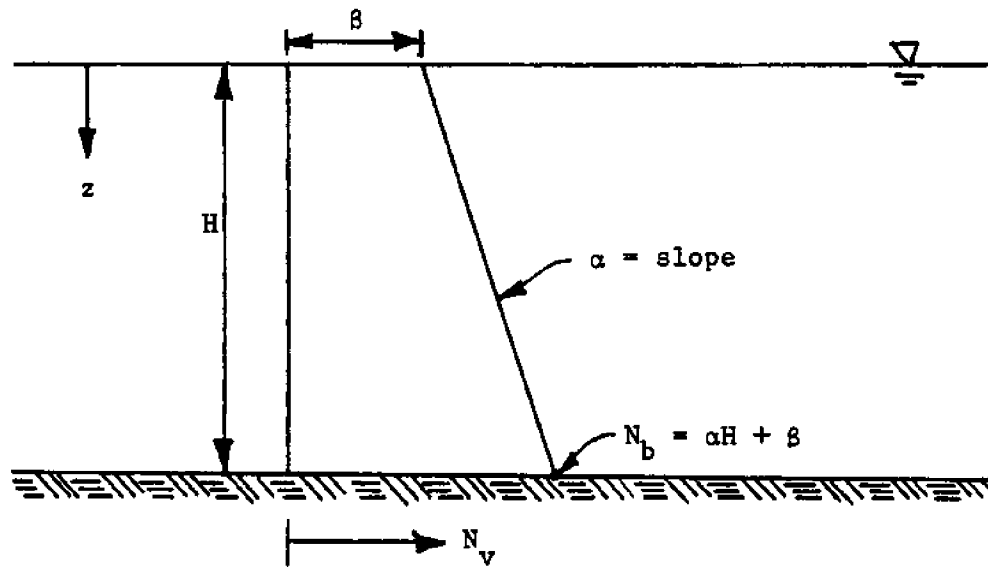


Figure 3.1: Form of Eddy Viscosity Used in Test Cases 1, 2 and 3.

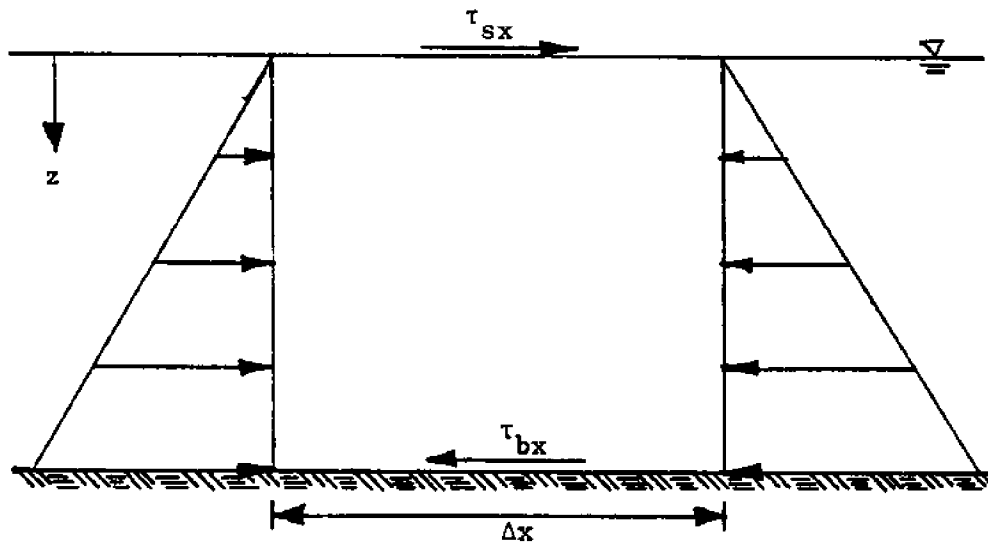


Figure 3.2: Forces Acting on Fluid Section in 1-D Infinite Channel

the governing equation becomes

$$\frac{\partial}{\partial z} \left(N_v \frac{\partial u}{\partial z} \right) = 0 \quad (3.1)$$

Surface Boundary Condition. Wind blowing over a water surface creates a transfer of momentum which, though the mechanism of momentum transfer is not fully understood, results in a shear stress, similar to the stresses developed in a fluid as explained in Section 1.2. The shear stress acting at the water surface can be related to a shear velocity u_* , as in the following expression:

$$\frac{\tau_{sx}}{\rho} = u_*^2 \quad (3.2)$$

where τ_{sx} represents the shear stress at the surface and ρ is the fluid density. Applying Equation 2.6, the surface boundary condition is,

$$u_*^2 = -N_v \left. \frac{\partial u}{\partial z} \right|_{z=0} \quad (3.3)$$

Bottom Boundary Condition. At the bottom boundary, shear stress is assumed to vary linearly with velocity, or:

$$\tau_{bx} = \rho u_b c_b \quad (3.4)$$

τ_{bx} = bottom shear stress

u_b = fluid velocity at bottom

c_b = constant of proportionality

Examining the forces acting on the water column as shown in Figure 3.2, it is seen that only hydrostatic forces and shear forces on the surface and bottom (assuming side shears are negligible) exist. Hydrostatic pressure forces are equal and opposite, implying that the surface shear stress and the bottom shear stress must also be equal and opposite, e.g., $\tau_s = \tau_b$. From Equations 3.2 and 3.4,

$$u_*^2 = u_b c_b$$

or

$$u_b = \frac{u_*^2}{c_b} \quad (3.6)$$

To determine the analytic solution, the governing equation (Equation 3.1) is first integrated over the depth. The result is the following expression:

$$N_v \frac{\partial u}{\partial z} = c \quad (3.7)$$

where c is a constant. Invoking the surface boundary condition, Equation 3.3, implies

$$c = -u_*^2 \quad (3.8)$$

Re-writing Equation 3.7 and integrating again over the depth:

$$\int \frac{\partial u}{\partial z} dz = - \int \frac{u_*^2}{N_v} dz \quad (3.9)$$

$$u + c = \frac{-u_*^2}{\alpha} \ln N_v; \quad c = \text{constant} \quad (3.10)$$

Applying the bottom boundary condition expressed in Equation 3.6,

$$u_b + c = \frac{-u_*^2}{\alpha} \ln N_b \quad (3.11)$$

and

$$c = \frac{u_*^2}{\alpha} \ln N_b - u_b$$

or

$$c = \frac{u_*^2}{\alpha} \ln N_b - \frac{u_*^2}{c_b} \quad (3.12)$$

Thus the analytic solution for the velocity in an infinitely long channel with one dimensional flow is

$$u = \frac{u_*^2}{\alpha} \ln \frac{N_b}{N_v} + \frac{u_*^2}{c_b} \quad (3.13)$$

A comparison of the model and analytic solutions is shown in Figure 3.3 for a depth of 32.8 feet and bottom friction coefficient of 0.05. The model results were obtained using three terms of the cosine series and running the model to steady state -- approximately 6000 seconds -- for the grid shown in Figure 1.7. As is seen in Figure 3.3, the difference between the two solutions is indistinguishable on the scale used.

3.2 Test Case 2. Flow in a Closed-Ended Channel

The grid used in this test case is exactly the same as that used in Test Case 1 but with the channel closed off at one end. This is accomplished by setting the depth in grid (6,2) of Figure 1.7 equal to zero and applying a no-flow boundary condition into that grid.

The assumptions made in this test case are similar to Test Case 1 except that $\partial\eta/\partial x$ no longer equals zero. The governing equation for flow in a closed-ended channel is

$$g \frac{\partial\eta}{\partial x} = \frac{\partial}{\partial z} \left(N_v \frac{\partial u}{\partial z} \right) \quad (3.14)$$

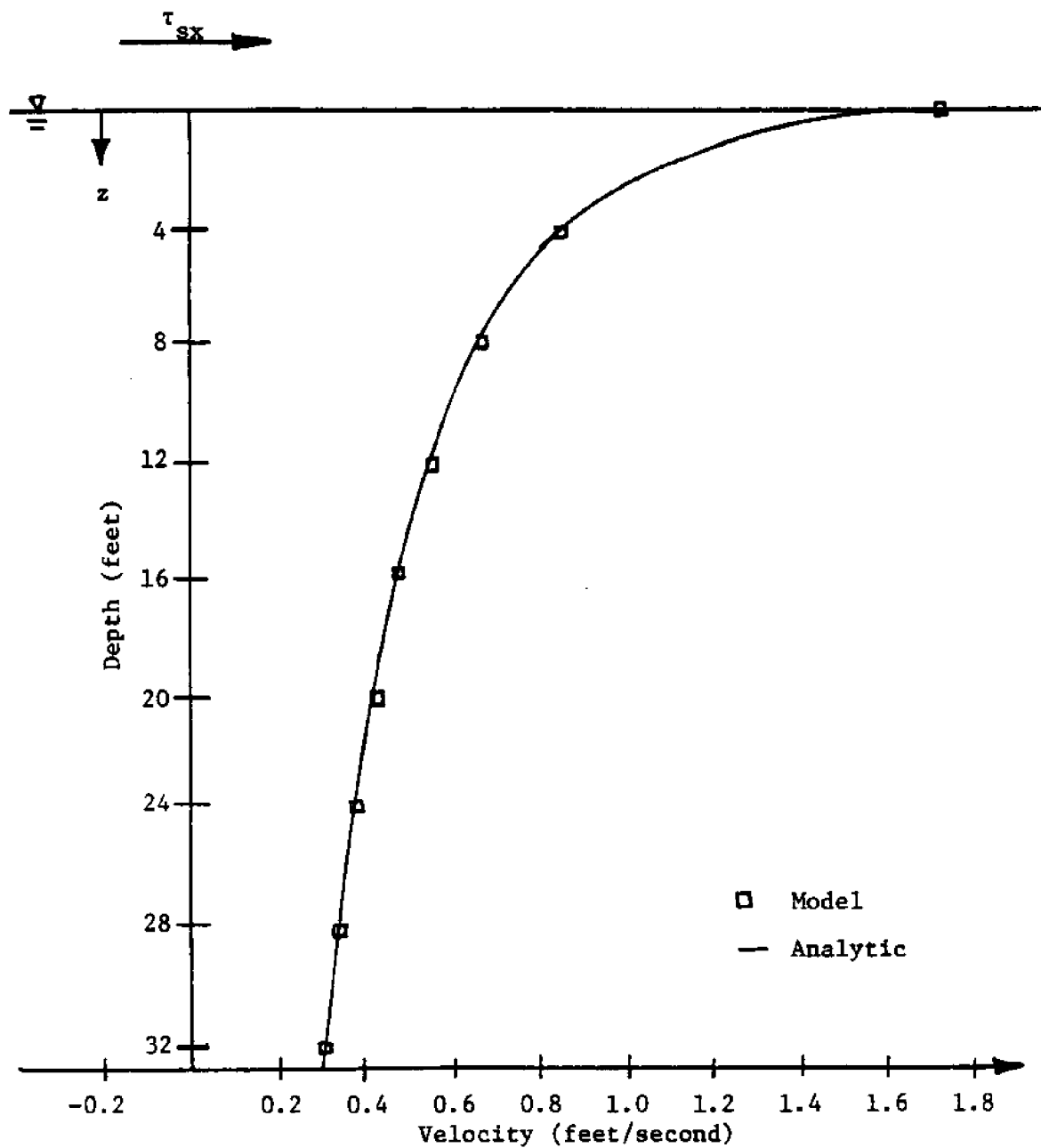


Figure 3.3: Comparison of Steady State Velocity Profile from Model and Analytic Solution for 1-D Channel of Infinite Length with $\alpha = 0.04648$, $\beta = 0.01$, Bottom Friction Coefficient = 0.05 ft/sec.

The surface and bottom boundary conditions are given by Equations 3.2 and 3.4 respectively. Following the solution process outlined in Section 3.1, the governing equation is first integrated with respect to depth. Performing the integration yields:

$$g \frac{\partial \eta}{\partial x} z = N_v \frac{\partial u}{\partial z} + c \quad (3.15)$$

The constant c is determined using the surface boundary condition, which is applied at $z = 0$:

$$0 = -u_*^2 + c$$

or

$$c = u_*^2 \quad (3.16)$$

which results in:

$$g \frac{\partial \eta}{\partial x} z = N_v \frac{\partial u}{\partial z} + u_*^2 \quad (3.17)$$

Dividing both sides of Equation 3.17 by N_v and integrating again over the depth:

$$g \frac{\partial \eta}{\partial x} \left[\frac{z}{\alpha} - \frac{\beta}{\alpha^2} \ln N_v \right] = u + \frac{u_*^2}{\alpha} \ln N_v + c \quad (3.18)$$

Combining Equations 3.4 and 3.18

$$g \frac{\partial \eta}{\partial x} \left[\frac{H}{\alpha} - \frac{\beta}{\alpha^2} \ln N_b \right] = u_b + \frac{u_*^2}{\alpha} \ln N_b + c$$

or

$$c = g \frac{\partial \eta}{\partial x} \left[\frac{H}{\alpha} - \frac{\beta}{\alpha^2} \ln N_b \right] - u_b - \frac{u_*^2}{\alpha} \ln N_b \quad (3.19)$$

Thus, the governing equation becomes:

$$u = \frac{g}{\alpha} \frac{\partial \eta}{\partial x} \left[z - H + \frac{\beta}{\alpha} \ln \frac{N_b}{N_v} \right] + u_b + \frac{u_*^2}{\alpha} \ln \frac{N_b}{N_v} \quad (3.20)$$

Some information about the surface slope can be obtained from an examination of forces acting on a section of fluid under steady

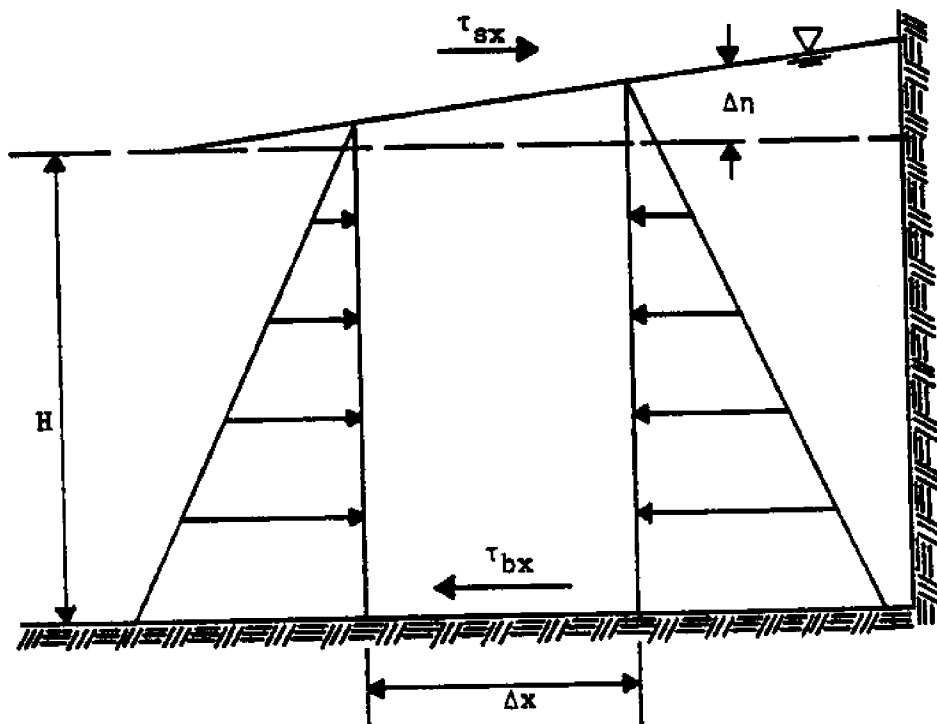


Figure 3.4 Forces Acting on Section of Water in Closed Channel at Steady State

state conditions in a closed-ended channel, as shown in Figure 3.4. For steady state to exist, the sum of the forces acting on the fluid section must be equal to zero. Consideration of force balance in the x-direction results in the following relation:

$$\frac{\partial \eta}{\partial x} = \frac{(\tau_s - \tau_b)}{\rho g H} \quad (3.21)$$

Substituting values of τ_s and τ_b from the boundary condition expressions:

$$\frac{\partial \eta}{\partial x} = \frac{1}{g H} (u_*^2 - u_b c_b) \quad (3.22)$$

which can be rearranged to obtain an expression for u_b :

$$u_b = -\frac{g H}{c_b} \frac{\partial \eta}{\partial x} + \frac{u_*^2}{c_b} \quad (3.23)$$

Combining this equation with Equation 3.20 yields

$$u = \frac{g}{\alpha} \frac{\partial \eta}{\partial x} \left[z - H + \frac{\beta}{\alpha} \ln \frac{N_b}{N_v} \right] - \frac{g H}{c_b} \frac{\partial \eta}{\partial x} + \frac{u_*^2}{c_b} + \frac{u_*^2}{\alpha} \ln \frac{N_b}{N_v} \quad (3.24)$$

One other fact which is known about the steady state condition for flow in a closed-ended channel is that the integral of the velocity over the depth must be equal to zero. Integrating Equation 3.24 with respect to depth and setting the result equal to zero yields a solution for $\partial \eta / \partial x$:

$$\frac{\partial \eta}{\partial x} = \frac{\frac{\alpha}{g} u_*^2 \left[-\frac{H}{c_b} - \frac{H}{\alpha} \ln N_b + \frac{N_b}{\alpha^2} (\ln N_b - 1) - \frac{\beta}{\alpha^2} (\ln \beta - 1) \right]}{\frac{H^2}{2} + \frac{\beta H}{\alpha} \ln N_b - \frac{\beta N_b}{\alpha^2} (\ln N_b - 1) + \frac{\beta^2}{\alpha^2} (\ln \beta - 1) - \frac{\alpha}{c_b} H^2} \quad (3.25)$$

The velocity profile is obtained by first solving Equation 3.25 for $\partial \eta / \partial x$, and substituting this result into Equation 3.24, which is re-written here as:

$$u = \frac{g}{\alpha} \frac{\partial \eta}{\partial x} \left[z - H + \frac{\beta}{\alpha} \ln \frac{N_b}{N_v} - \frac{H}{c_b} \right] + u_*^2 \left[\frac{1}{c_b} + \frac{1}{\alpha} \ln \frac{N_b}{N_v} \right] \quad (3.26)$$

The model was run for a channel depth of 32.8 feet, a linearly varying eddy viscosity of $\alpha = 0.04648$ ft/sec. and $\beta = 0.01$ ft/sec., and with a bottom friction coefficient $c_b = 0.05$ ft/sec. Model results are compared with the analytic solution in Figure 3.5.

3.3 Test Case 3: 3-D Analytical Model Comparison

This verification model is for a sea with an infinite lateral extent, with a linearly varying N_v and with a slip velocity at the bottom. For the governing equations we have as in the Ekman formulation,

$$-f \cdot v = \frac{\partial}{\partial z} \left(N_v \frac{\partial u}{\partial z} \right)$$

$$f \cdot u = \frac{\partial}{\partial z} \left(N_v \frac{\partial v}{\partial z} \right)$$

$$\text{with } u_*^2 = -N_v \frac{\partial u}{\partial z}; \quad v_*^2 = -N_v \frac{\partial v}{\partial z} \quad @ \quad z = 0$$

$$\text{and with } u = u_b = \frac{-N_b}{c_b} \frac{\partial u}{\partial z} \quad v = v_b = -\frac{N_b}{c_b} \frac{\partial v}{\partial z} \quad @ \quad z = H$$

Letting $w = u + iv$, multiplying the y-momentum equation by i and adding to the x-momentum equation yields:

$$f (iu - v) = \frac{\partial}{\partial z} \left(N_v \frac{\partial}{\partial z} \{u + iv\} \right)$$

or

$$fiw = \frac{\partial}{\partial z} \left\{ N_v \frac{\partial w}{\partial z} \right\}$$

$$\text{where } N_v = \alpha z + \beta$$

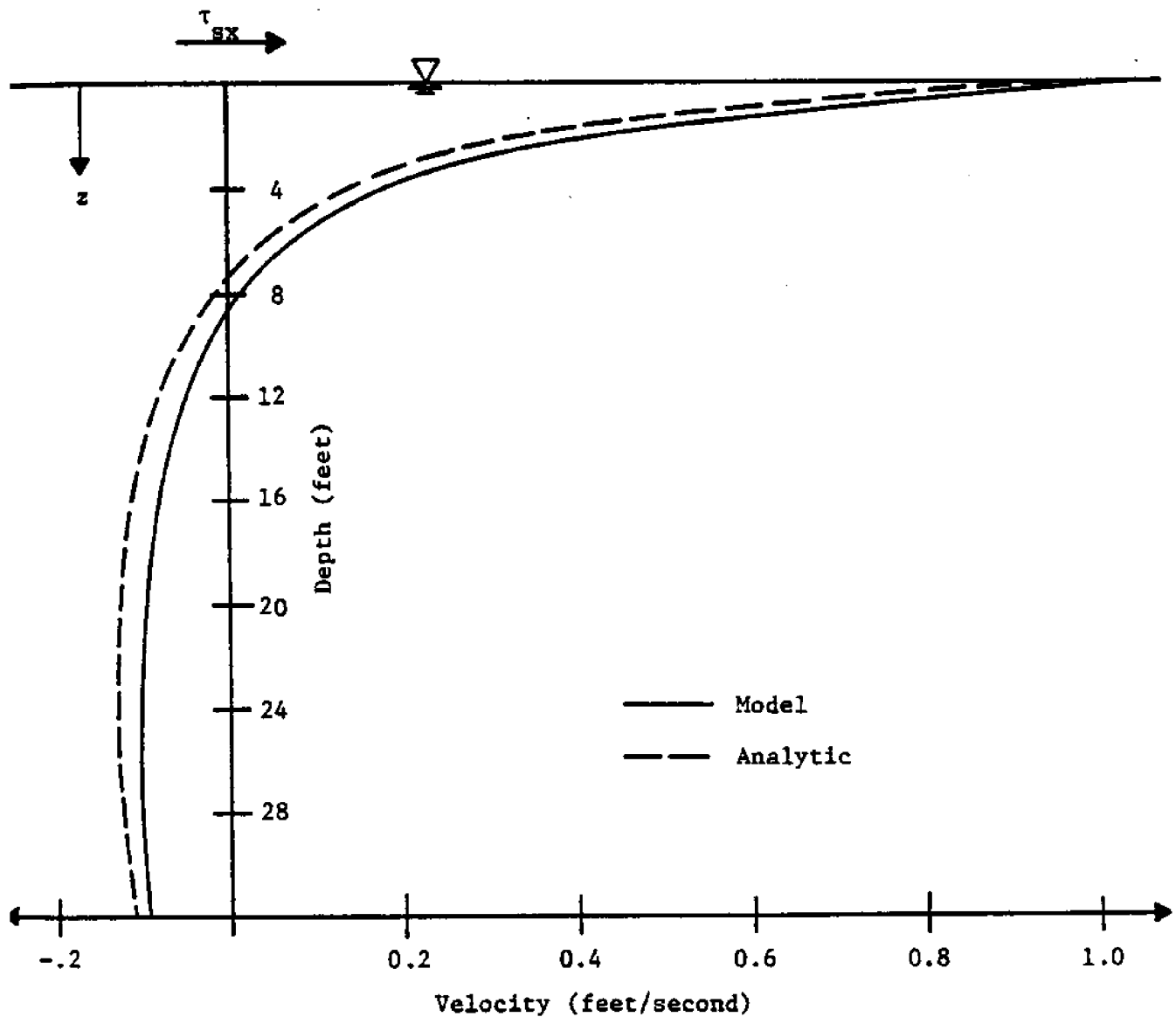


Figure 3.5. Comparison of Steady State Velocity Profile from Model and Analytic Solution for 1-D Channel of Finite Length with $\alpha = 0.04648$, $\beta = 0.01$ and Bottom Friction Coefficient = 0.05.

For the surface boundary condition:

$$u_*^2 + i v_*^2 = -N_s \frac{\partial}{\partial z} (u + iv) \quad @ \quad z=0 \quad N_s = \beta$$

or

$$w_* \bar{w}_* = -N_s \frac{\partial w}{\partial z} \quad @ \quad z=0$$

For the bottom boundary condition:

$$w_b = u_b + i v_b$$

or

$$w_b = -\frac{N_b}{c_b} \frac{\partial w}{\partial z} \quad @ \quad z=H$$

To summarize, the equations of motion and necessary boundary conditions are:

$$(\alpha z + \beta) \frac{\partial^2 w}{\partial z^2} + \alpha \frac{\partial w}{\partial z} - ifw = 0 \quad (3.27)$$

$$w_*^2 = -N_s \frac{\partial w}{\partial z} \Big|_{z=0} \quad (3.28)$$

$$w_b = -\frac{N_b}{c_b} \frac{\partial w}{\partial z} \Big|_{z=H} \quad (3.29)$$

Equation (3.27) can be placed into the following general form, Hildebrand (1963)

$$x^2 y'' + xy' - (k^2 x^2) y = 0$$

by making a dimensionless transformation

$$\zeta = \left[4 \frac{f}{\alpha^2} (\alpha z + \beta) \right]^{1/2},$$

or

$$\frac{\alpha \zeta^2}{4f} - \frac{\beta}{\alpha} = z \quad + \quad \frac{\partial z}{\partial \zeta} = \frac{2\alpha \zeta}{4f} = \frac{\alpha \zeta}{2f}$$

Introducing this transformation into equation (3.27) produces:

$$\frac{\partial^2 w}{\partial \zeta^2} + \frac{1}{\zeta} \frac{\partial w}{\partial \zeta} - iw = 0 \quad (3.30)$$

The surface boundary condition (3.28) becomes:

$$w_s' = -N_s \frac{\partial w}{\partial z} = -N_s \frac{2f}{\alpha \zeta} \frac{\partial w}{\partial \zeta} \Big|_{\zeta=\zeta_s} = -\frac{1}{e_s} \frac{\partial w}{\partial \zeta} \Big|_{\zeta=\zeta_s} \quad (3.31)$$

where $\zeta_s = \zeta \Big|_{z=0}$ or $\zeta_s = \frac{2}{\alpha} \sqrt{fN_s}$
 $\beta = N_s$
 $e_s = \frac{\alpha \zeta_s}{2fN_s} = \frac{1}{\sqrt{fN_s}}$

The bottom boundary condition becomes:

$$w_b' = -\frac{N_b}{c_b} \frac{2f}{\alpha \zeta_b} \frac{\partial w}{\partial \zeta} \Big|_{\zeta=\zeta_b} = -\frac{1}{c_b e_b} \frac{\partial w}{\partial \zeta} \quad (3.32)$$

where $\zeta_b = \zeta \Big|_{z=0}$
 $\zeta_b = \frac{2}{\alpha} \sqrt{fN_b}$
 $e_b = \frac{\alpha \zeta_b}{2fN_b} = \frac{1}{\sqrt{fN_b}}$

The solution to Equation (3.30) is given by Hildebrand (1963), Section 4.11

as

$$w = Z_0 (i^{3/2} \zeta)$$

or

$$w = c_1 \text{ber}_0 \zeta + c_2 \text{ker}_0 \zeta + i[c_1 \text{bei}_0 \zeta + c_2 \text{kei}_0 \zeta] \quad (3.33)$$

To evaluate the constants it is necessary to find the derivative

$\frac{\partial w}{\partial \zeta}$. This is most conveniently done by rewriting the Kelvin functions in terms of modified Bessel functions or

$$w = z_0 (i^{3/2} \zeta) = c_1 J_0(i^{3/2} \zeta) + c_2 K_0(i^{1/2} \zeta)$$

For the derivative, see Hildebrand (1963), Eq. 114,

$$\frac{\partial w}{\partial \zeta} = -i^{3/2} c_1 J_1(i^{3/2} \zeta) - i^{1/2} c_2 K_1(i^{1/2} \zeta)$$

$$\frac{\partial w}{\partial \zeta} = -i^{1/2} [ic_1 J_1(i^{3/2} \zeta) + c_2 K_1(i^{1/2} \zeta)]$$

Applying the surface boundary condition leads to:

$$-e_s w_*^2 = -i^{1/2} \{c_1 i J_1(i^{3/2} \zeta_s) + c_2 K_1(i^{1/2} \zeta_s)\}$$

$$c_1 = \frac{e_s w_*^2}{i^{3/2} J_1(i^{3/2} \zeta_s)} - \frac{c_2 K_1(i^{1/2} \zeta_s)}{i J_1(i^{3/2} \zeta_s)}$$

$$c_1 = \frac{ic_2 K_1(i^{1/2} \zeta_s) - i^{1/2} e_s w_*^2}{J_1(i^{3/2} \zeta_s)} \quad (3.34)$$

Applying the bottom boundary conditions leads to:

$$c_1 J_0(i^{3/2} \zeta_b) + c_2 K_0(i^{1/2} \zeta_b) = \frac{i^{1/2}}{c_b e_b} \{c_1 i J_1(i^{3/2} \zeta_b) + c_2 K_1(i^{1/2} \zeta_b)\}$$

$$c_1 J_0(i^{3/2} \zeta_b) - \frac{i^{3/2}}{c_b e_b} c_1 J_1(i^{3/2} \zeta_b) = c_2 [-K_0(i^{1/2} \zeta_b) + \frac{i^{1/2}}{c_b e_b} K_1(i^{1/2} \zeta_b)]$$

$$c_1 = c_2 \frac{\left[\frac{i^{1/2} K_1(i^{1/2} \zeta_b)}{c_b e_b} - K_0(i^{1/2} \zeta_b) \right]}{\left[J_0(i^{3/2} \zeta_b) - \frac{i^{3/2} c_1 J_1(i^{3/2} \zeta_b)}{c_b e_b} \right]}$$

$$= c_2 \frac{\left[\frac{iK_1(i^{1/2}\zeta_b)}{c_b e_b} - i^{1/2}K_0(i^{1/2}\zeta_b) \right]}{i^{1/2}J_0(i^{3/2}\zeta_b) + \frac{J_1(i^{3/2}\zeta_b)}{c_b e_b}} = M c_2 \quad (3.35)$$

Equating equations (3.34). and (3.35) yields:

$$\frac{ic_2 K_1(i^{1/2}\zeta_s) - i^{1/2}e_s w_*^2}{J_1(i^{3/2}\zeta_s)} = M c_2$$

therefore:

$$\frac{-i^{1/2}e_s w_*^2}{J_1(i^{3/2}\zeta_s)} = c_2 M - \frac{ic_2 K_1(i^{1/2}\zeta_s)}{J_1(i^{3/2}\zeta_s)}$$

or

$$c_2 = \frac{-i^{1/2}e_s w_*^2}{J_1(i^{3/2}\zeta_s)} [M - \frac{iK_1(i^{1/2}\zeta_s)}{J_1(i^{3/2}\zeta_s)}]^{-1}$$

$$c_2 = -i^{1/2}e_s w_*^2 / \{J_1(i^{3/2}\zeta_s)M - iK_1(i^{1/2}\zeta_s)\} \quad (3.36)$$

Substituting (3.36) into (3.35) yields

$$c_1 = -i^{1/2}e_s w_*^2 M / \{J_1(i^{3/2}\zeta_s)M - iK_1(i^{1/2}\zeta_s)\} \quad (3.37)$$

It is to be noted that M has two values depending upon which root of $i^{1/2}$ is taken. For simplicity we first looked at the case where $c_b = \infty$, as noted before this is equivalent to the condition of no slip or $u=v=0$ at $z=0$. Letting $c_b = \infty$ produces:

$$M = -\frac{K_0(i^{1/2}\zeta_b)}{J_0(i^{3/2}\zeta_b)} ; \quad c_1 = M c_2$$

Substituting this value for M into equations 3.36 and 3.37 provides for c_1 and c_2 :

$$c_2 = \frac{i^{1/2} e_s w_*^2 J_0(i^{3/2} \zeta_b)}{J_1(i^{3/2} \zeta_b) K_0(i^{1/2} \zeta_b) + i K_1(i^{1/2} \zeta_b) J_0(i^{3/2} \zeta_b)}$$

$$c_1 = \frac{-i^{1/2} e_s w_*^2 K_0(i^{3/2} \zeta_b)}{J_1(i^{3/2} \zeta_b) K_0(i^{1/2} \zeta_b) + i K_1(i^{1/2} \zeta_b) J_0(i^{3/2} \zeta_b)}$$

Figure 3.6 shows a comparison between the numerical, Galerkin model and the analytic model presented above for the case of linearly varying eddy viscosity. The parameters of interest are:

Wind stress $u_*^2 = 0.0135 \text{ ft}^2/\text{sec}^2$

Coriolis $f = 10^{-4} \text{ sec}^{-1}$

Bottom Friction Coefficient $c_b = 9000 \text{ ft/sec} = \infty$

Slope of $N_v = .02 \text{ ft/sec}$

Intercept of $N_v = .01 \text{ ft}^2/\text{sec}$

The comparison between the analytic and numerical models is quite good.

Figure 3.7 shows a comparison for the case of constant eddy viscosity. The analytic model is the Ekman solution for a sea of infinite horizontal extent and finite depth. The comparison is not as good as in the previous figure. The reason for this is because in the case of constant N_v , the second term of the trial function (u_0) becomes linear, reaching a maximum at the surface. This term, when added with the first term in the trial function forms a function which is quite difficult to simulate with cosine terms.

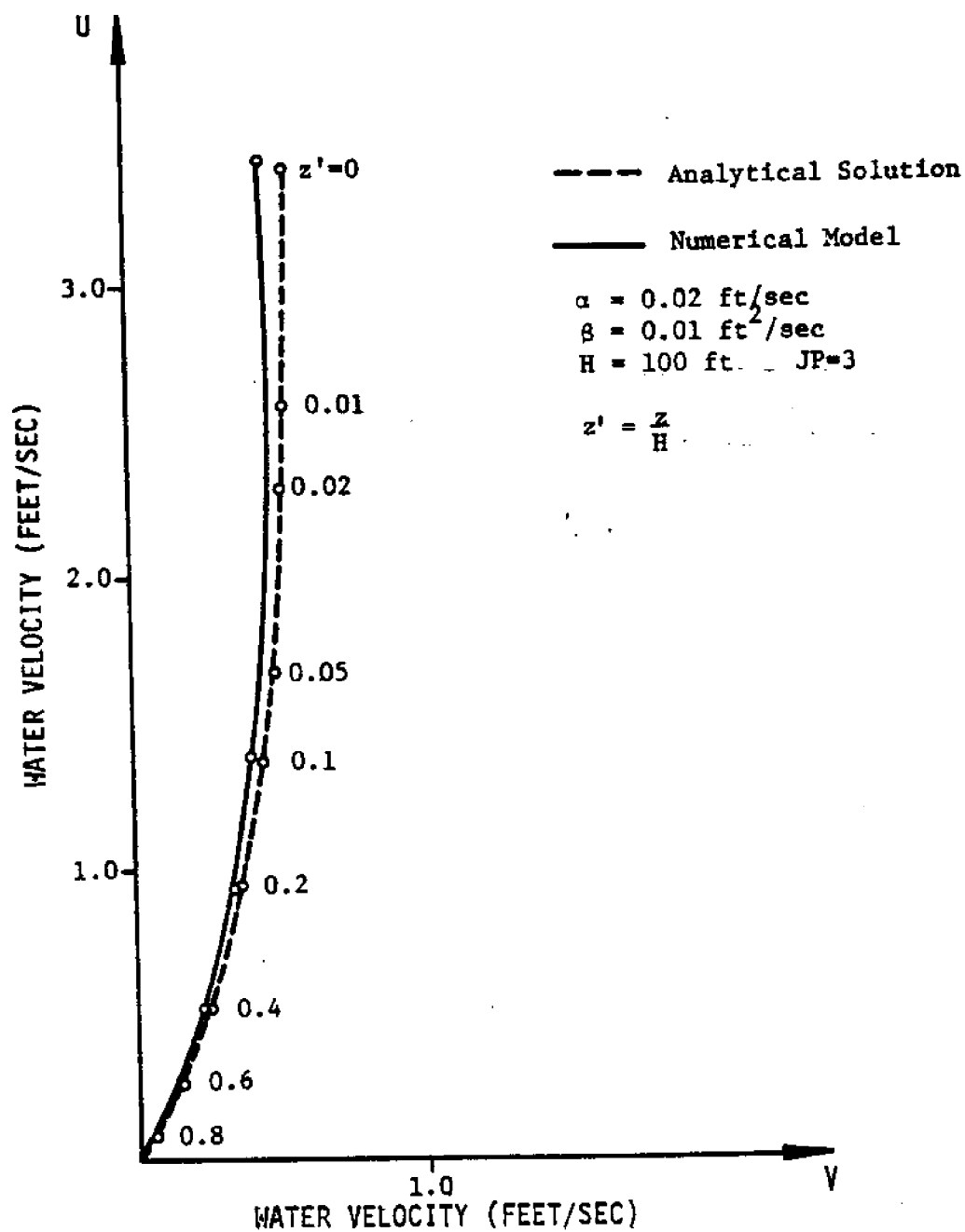


Figure 3.6: Comparison of 3-D Solution for Numerical and Analytical Models for Variable Eddy Viscosity

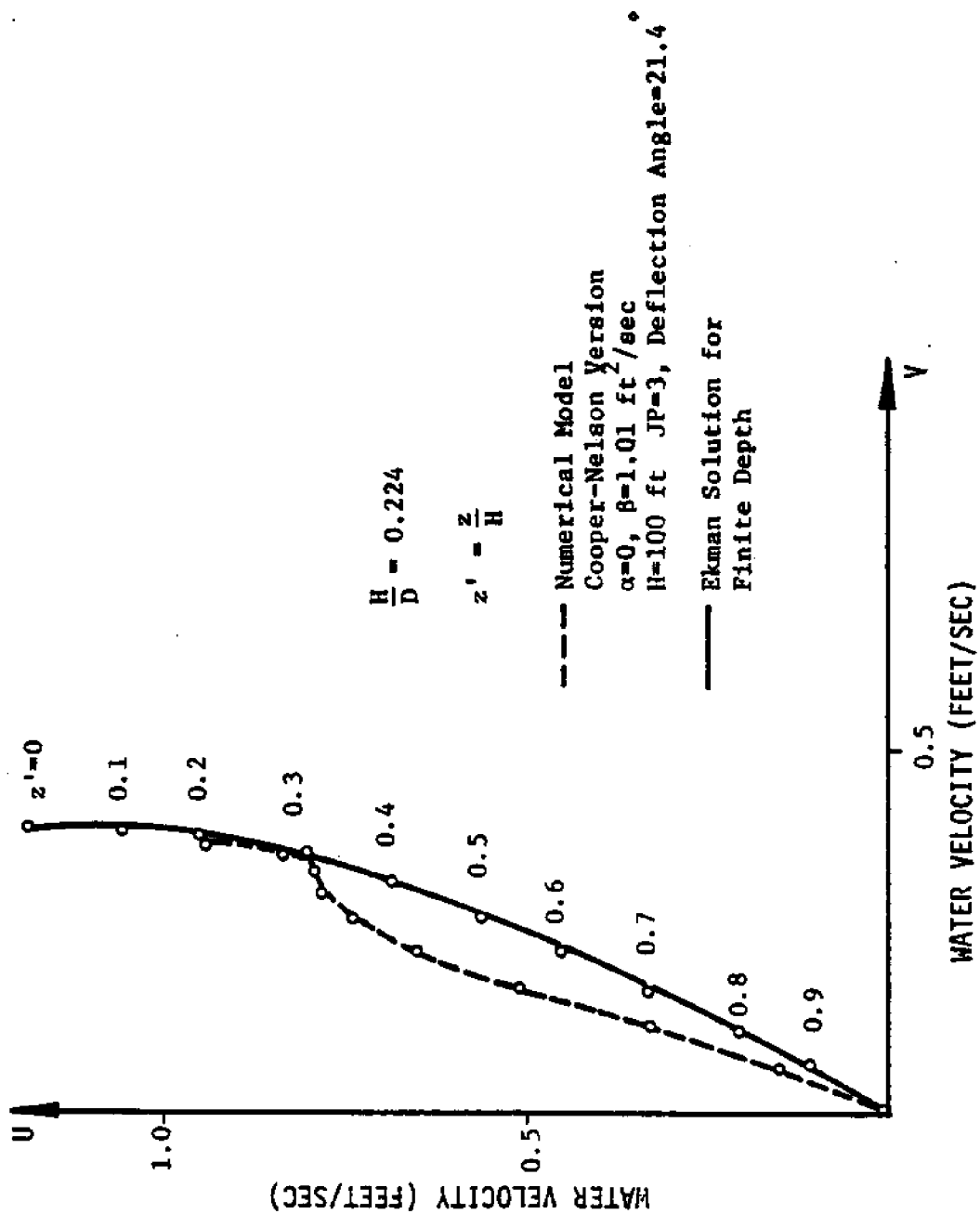


Figure 3.7: Comparison of 3-D Solution for Numerical and Analytical Models for Constant Eddy Viscosity

The comparison for the constant N_v case can no doubt be improved by taking more cosine terms (only 3 cosine terms were used in the results shown in Figure 3.7). In any event, it must be remembered that the new formulation does fit the varying N_v case, which is more physically realistic than the constant N_v case.

3.4 Test Case 4: Flow in an Infinite Channel with a Multi-Linear Variation in the Eddy Viscosity

Section 1.2 indicated that a reasonable variation in the eddy viscosity would be one where N_v was a minimum near an interface and reached a maximum somewhere in between.

Therefore, it follows that for real-world problems in well mixed water bodies a bilinear variation such as that shown in Figure 3.8 might be plausible. To test the model coding and to gain insight into the response of the model to such a variation in N_v , a simple analytic solution was derived for the infinite channel of constant depth.

The governing equation for this case and the surface and bottom b.c.'s are the same as for Test Case 1 (i.e. equations 3.1, 3.3 and 3.4). However, the problem must now be considered in two parts: $0 \leq z \leq H_1$ and $H_1 \leq z \leq H$. An additional b.c. is available at the interface (i.e. $z=H_1$) by specifying the velocities to be equal or:

$$u = u_I @ z = H_1 \tag{3.38}$$

To derive the analytic solution, 3.1 is integrated twice using the surface b.c. (equation 3.3) and interface b.c. (equation 3.38) to evaluate the constants of integration. This yields:

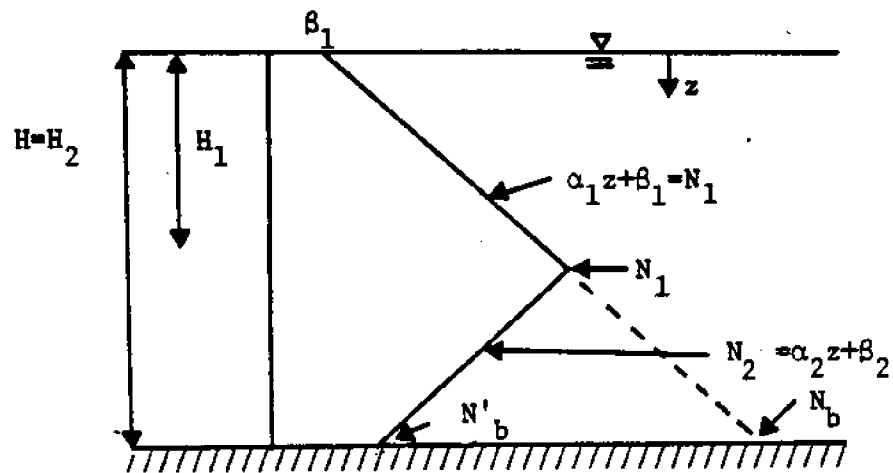


Figure 3.8: Variation of N_v used in Test Case 4.

$$u = \frac{u_*^2}{\alpha_1} \ln \left(\frac{N_I}{N_1} \right) + u_I \quad 0 \leq z \leq H_1 \quad (3.39)$$

where $N_I = \alpha_1 H_1 + \beta_1 = \alpha_2 H_1 + \beta_2$ and $N_1 = \alpha_1 z + \beta_1$

Now, for the lower layer, equation 3.1 can be integrated once which yields

$$N_2 \frac{\partial u}{\partial z} = c \quad (3.40)$$

where $N_2 = \alpha_2 z + \beta_2$

To evaluate c requires use of the bottom b.c. which can be written as:

$$\left. \frac{\partial u}{\partial z} \right|_{z=H} = \frac{-\tau_b}{\rho N'_b}$$

where $N'_b = \alpha_2 H + \beta_2$. Recall from Case 1 that equilibrium requires that $\tau_s = \tau_b$ implying that:

$$\left. \frac{\partial u}{\partial z} \right|_{z=H} = \frac{-\tau_s}{\rho N'_b} = \frac{-u_*^2}{N'_b} \quad (3.41)$$

Equation 3.41 can be used to evaluate c and equation 3.40 becomes:

$$N_2 \frac{\partial u}{\partial z} = -u_*^2$$

Integrating this equation again and applying the b.c. at the interface to evaluate the constant of integration gives:

$$u = \frac{u_*^2}{\alpha_2} \ln \left(\frac{N_I}{N_2} \right) + u_I \quad H_1 \leq z \leq H \quad (3.42)$$

Equations 3.39 and 3.42 give the velocity profile over the entire depth. However, u_I still is undefined. This problem is solved by first using the expression for the slip velocity, u_b , derived in Section 3.1 or equation 3.6.

$$u_b = \frac{u_*^2}{c_b} \quad (3.6)$$

With u_b expressed in terms of known parameters, u_I can be found by evaluating equation 3.42 @ $z=H$ or

$$u_I = u_b - \frac{u_*^2}{\alpha_2} \ln \left(\frac{N_I}{N'_b} \right) \quad (3.43)$$

Finally, this expression for u_I can be substituted into equations 3.42 and 3.39 to get expressions for the velocity profile. After some algebraic manipulations, the velocity profile can be written as:

$$\begin{aligned} 0 \leq z \leq H_1 \quad u &= \frac{u_*^2}{\alpha_1} \ln \left(\frac{N_I}{N_1} \right) + \frac{u_*^2}{c_b} - \frac{u_*^2}{\alpha_2} \ln \left(\frac{N_I}{N'_b} \right) \\ H_1 \leq z \leq H \quad u &= \frac{u_*^2}{\alpha_2} \ln \left(\frac{N'_b}{N_2} \right) + \frac{u_*^2}{c_b} \end{aligned} \quad (3.44)$$

Figure 3.9 shows a comparison between GAL and the analytic solution for the 1-D Channel described in Section 3.1. The eddy viscosity variation is bilinear with a moderate slope near the bottom (i.e. $\frac{N_I}{N'_b} \approx 1$). The important constants are:

$N_s = 0.01 \text{ ft}^2/\text{sec.}$	$H_1 = 16.4 \text{ ft.}$
$N_I = 1.0 \text{ ft}^2/\text{sec.}$	$H = 32.8 \text{ ft.}$
$N'_b = 0.8 \text{ ft}^2/\text{sec.}$	$c_b = \infty \text{ (no slip)}$
$J' = 3$	$u_*^2 = .0135 \text{ ft}^2/\text{sec}^2$

The comparison between GAL and the analytic solution is excellent.

Another comparison was made with the same constants except that $N'_b = .01 \text{ ft}^2/\text{sec.}$, making the slope of the eddy viscosity near the bottom much higher (i.e. $\frac{N_I}{N'_b} = 100$). Figure 3.10 shows the results and indicates that the comparison is not particularly good for the case of $J' = 3$ and is only marginally improved for the case of $J' = 5$.

To understand the basis of the problem, first note that above a depth of roughly 25 feet, the slope of the analytic solution and numeric solution compares quite well. Second note that the analytic solution displays the strong logarithmic profile near the bottom which occurs whenever N_v has a strong negative gradient near the bottom. Recall that there is no logarithmic term in the trial function of the numeric solution near the bottom and therefore the cosine terms (i.e. $\sum_{J=1}^{J'} \cos \frac{a_J z}{H}$) in the trial function must simulate the logarithmic variation alone. In Section 1.4.4 it was shown that cosine terms are extremely slow to converge in approximating a logarithmic function. Hence, the reason GAL does not compare well

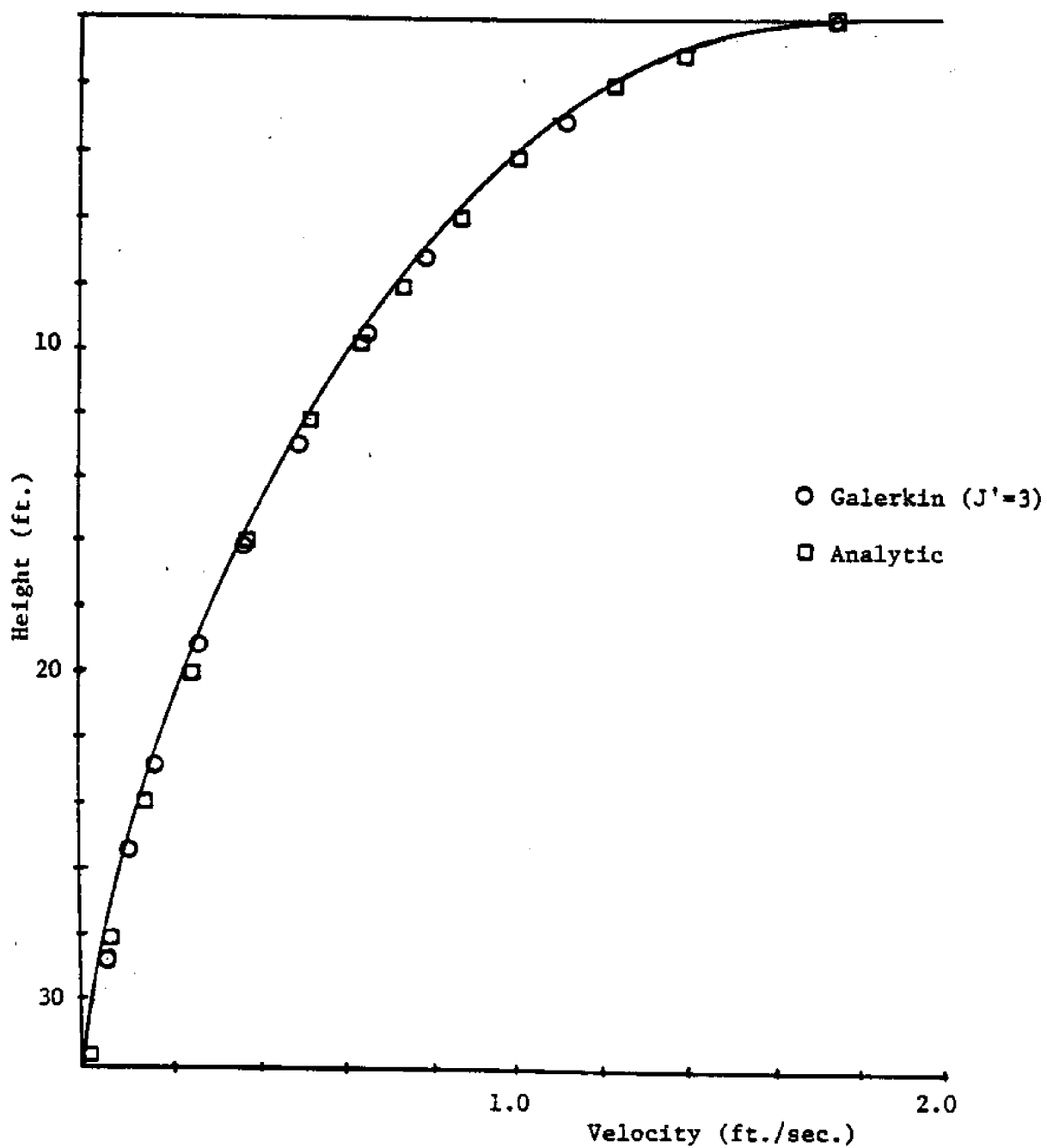


Figure 3.9: Comparison of the Model to the Analytic Solution for the Case of a Bilinear Variation in N_v ($N_I/N'_b=1$)

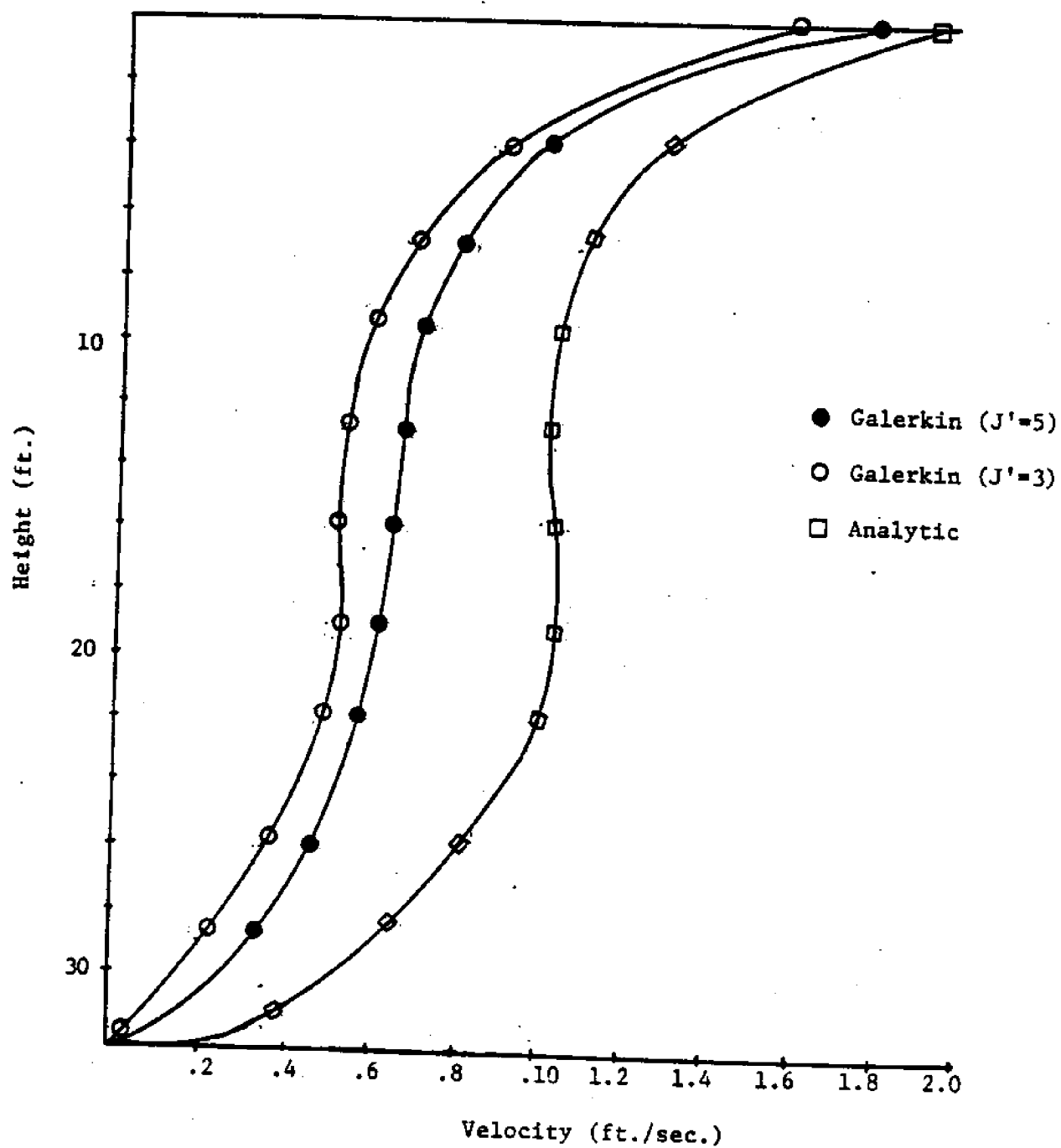


Figure 3.10: Comparison of the Model to the Analytic Solution for the Case of a Bilinear Variation in N_v ($N_I/N'_b=100$)

to the analytic solution is simply because of the slow convergence of the trial function near the bottom.

One solution to improve convergence would be to include a u_0 term which would contain a logarithmic component near the bottom. A similar approach was taken near the surface to improve the initial formulation of GAL. But as discussed in Section 1.4.4, this approach is not generally possible near the bottom since the direction of flow cannot usually be predetermined for most real-world problems.

Thus it is concluded that GAL will not yield exact results in the case where N_v near the bottom has a strong negative slope. This in turn means that velocity structure within the bottom boundary layer cannot be modeled by GAL. However, as Cooper and Pearce (1977) pointed out, this aspect of GAL is not restrictive since the thickness of the bottom boundary layer typically constitutes a very small percentage of the total depth and its influence on the waters lying above can be effectively simulated through the use of the slip coefficient, c_b , which is included in the formulation of GAL.

CHAPTER 4 SUMMARY AND DESCRIPTION OF FURTHER WORK

The purpose of the research presented in this report has been to develop a model which will predict the variation of the horizontal velocities in both the horizontal and vertical directions, following the basic solution procedure used by Heaps. Most previous efforts at three-dimensional circulation modeling have assumed a constant vertical eddy viscosity term. These models essentially follow Ekman's solution for circulation in deep water, which predicts a surface deflection angle of 45° between the flow direction and the wind direction. This value does not compare well to values of the deflection angle obtained in measurements of wind-generated currents. The reason for this discrepancy has been traced to the assumption of constant eddy viscosity. Measurement of this parameter has shown that it is not constant with depth and thus use of a constant vertical eddy viscosity has no real world analog.

The model developed here is similar to the Galerkin models previously developed but incorporates a varying vertical eddy viscosity which is represented by a series of linear segments over the depth. The model is based on the horizontal momentum equations and the continuity equation. The momentum equations are simplified by neglecting the convective terms and the vertical velocities, linearizing the horizontal shear stress terms, and by assuming constant density throughout the fluid. The velocities are assumed to be approximated by a series of cosines of undetermined amplitudes. These trial functions are substituted into the momentum equations, and the error resulting from replacement

of the unknown "true" solution for the velocity by the approximate solution is minimized over the vertical domain using the Galerkin Method. A set of $2I'$ linear partial differential equations is obtained involving a set of $2I'$ undetermined amplitudes, where I' represents the number of cosine terms which have been taken. This set of equations applies to a water column. The water body is discretized in the horizontal plane and in time using a split-time, finite difference scheme. The water columns are linked to one another using the continuity equation.

The initial model formulation was tested against several simple cases for which analytic solutions were available. While the model performed well in predicting velocities for cases of constant vertical eddy viscosity, it was found to compare very poorly with the analytic solution utilizing a linearly varying vertical eddy viscosity. A Fourier cosine series analysis was used to verify that the reason for poor model performance was due to slow convergence of the trial function. It was estimated that for reasonable values of the vertical eddy viscosity, the number of cosine terms needed in the model to achieve an acceptable approximation of the velocity profile would be an unreasonable number of terms. It would be impossible to apply this formulation to any field situation, since computer time and storage requirements would be prohibitive.

One possible means of improving convergence is to choose a u_0 term in the velocity trial function which will allow the cosine series to more easily approximate the velocity over the depth. Since the analytic solution for the velocity in a one-dimensional, infinitely long

channel is known to be a logarithmic function, the model was reformulated to include a logarithmic term in the u_0 part of the velocity trial function. This second formulation resulted in a good comparison between the analytical and numerical solution for the 1-D open and closed ended case with linearly varying eddy viscosity. An acceptable comparison was also found for the 3-D sea with an infinite horizontal extent with linearly varying N_v but the comparison was not as good for the 3-D case with constant N_v . The discrepancy is not considered important because the model compares well to the cases with linear variation which is closer to reality than the constant eddy viscosity case.

The improvement gained in convergence by implementing the new trial function appears to make the model very economical in terms of computer costs. The most interesting and useful work can begin now that an operational model has been obtained.

REFERENCES

1. Cooper, C.K., B.R. Pearce (1977), "A Three-Dimensional Numerical Model to Calculate Currents in Coastal Waters Utilizing a Depth Varying Vertical Eddy Viscosity," Ralph M. Parsons Lab. for Water Resources and Hydrodynamics, M.I.T., Technical Report No. 226.
2. Ekman, V.W. (1905), "On the Influence of the Earth's Rotation on Ocean Currents," *Ark. Mat. Astron. Fys.*, 2, 1-53.
3. Forristall, G.Z. (1974), "Three-Dimensional Structure of Storm-Generated Currents," *Journal of Geophysical Research*, 79, 2721-1187.
4. Heaps, N.S. (1972), "On the Numerical Solution of the Three-Dimensional Hydrodynamic Equations for Tides and Storm Surges," *Mem. Soc. R. Sci. Liege*, 6(2), 143-180.
5. Heaps, N.S. (1974), "Development of a Three-Dimensional Model of the Irish Sea," *Rapp. P.-V. Reun. Cons. Int. Explor. Mer.*, Dec. 1974, 147-162.
6. Hildebrand, F.B. (1963), Advanced Calculus for Applications, Prentice Hall, New Jersey.
7. Leendertse, J.J. (1967), "Aspects of Computational Model for Long-Period Water Wave Propagation," Memorandum Rm-5294 PR, Rand Corporation.
8. Leendertse, J.J. and S.K. Liu (1975), "Modeling of Three-Dimensional Flows in Estuaries," *Symposium on Modeling Techniques, ASCE*, Vol. 1, 625-642.
9. Madsen, O.S. (1977), "A Realistic Model of the Wind-Induced Ekman Boundary Layer," *Journal of Physical Oceanography*.
10. Neumann, G. (1968), Ocean Currents, Elsevier Oceanography Series, Elsevier Scientific Publishing Company, New York.
11. Pearce, B. R. (1972), "Numerical Calculation of the Response of Coastal Waters to Storm Systems", Coastal & Oceanographic Engineering Lab., U. of Florida, Technical Report No. 12.
12. Prandtl, L. (1952), Essentials of Fluid Dynamics, Hafner Publishing Co., New York.
13. Reichardt, H. (1959), "Gesetzmässigkeiten der geradlinigen turbulenten Couette-Strömung," *Mitteilungen aus Max-Planck-Institut für Strömungsforschung und der Aerodynamischen Versuchsanstalt*, No. 22 Göttingen, 1-45.
14. Reid, R. O., & B. R. Bodine (1968), "Numerical Model for Storm Surges in Galveston Bay", *Journal of the Waterways and Harbors Division, ASCE*, 94, WW1.

15. Schubauer, G.B. (1954), "Turbulent Processes Observed in Boundary Layers and Pipes," J. Appl. Phys., 25, 2.
16. Shemdin, O.H. (1972), "Wind Generated Current and Phase Speed of Wind Waves," Journal of Physical Oceanography, 2, 411-419.
17. Stolzenbach, K.D., O.S. Madsen, E.E. Adams, A.M. Pollack, and C.K. Cooper (1977), "A Review and Evaluation of Basic Techniques for Predicting the Behavior of Surface Oil Slicks," Ralph M. Parsons Lab. for Water Resources and Hydrodynamics, M.I.T., Technical Report No. 222.
18. Sverdrup, H.V., M.W. Johnson, and R.H. Fleming (1942), The Oceans, Prentice-Hall, Inc., Englewood Cliffs, New Jersey.
19. Teeson, D., F.M. White and A. Schenck (1970), "Studies of the Simulation of Drifting Oil by Polyethelene Sheets," Ocean Engineering, 2, 1-11, Pergamon Press.
20. Thomas, J.H. (1975), "A Theory of Steady Wind-Driven Currents in Shallow Water with Variable Eddy Viscosity," Journal of Physical Oceanography, 5, 136-142.
21. Van Dorn, W.G. (1953), "Wind Stress on an Artificial Pond," Journal of Marine Research, 12(3), 219-275.
22. Wang, J.D. and J.J. Connor (1975), "Mathematical Modeling of Near Coastal Circulation," Ralph M. Parsons Lab. for Water Resources and Hydrodynamics, M.I.T., Technical Report No. 200.
23. Wu, J. (1969), "Wind Stress and Surface Roughness at the Air-Sea Interface," Journal of Geophysical Research, 74, 444-445.

Appendix A

Detailed Integration of the Terms of the Residual Equation

A.1. Unsteady Term

If the convective portion of the unsteady term is neglected, integration of the unsteady term yields:

$$\int_0^H \frac{\partial \hat{u}}{\partial t} \Omega_J dz = \int_0^H \frac{\partial}{\partial t} (u_0 + \sum_I c_I \cos \frac{a_I z}{H}) \cos \frac{a_J z}{H} dz \quad (A.1)$$

It is assumed that the time scale of variation in wind shear and vertical eddy viscosity is much larger than the scale of the time step. Due to the orthogonality property of cosines, the only non-zero term in the summation will be when $I = J$. Performing the integration:

$$\int_0^H \frac{\partial \hat{u}}{\partial t} \Omega_J dz = \frac{H}{2} \frac{\partial c_J}{\partial t} \quad (A.2)$$

A.2. Surface Slope Term

Integration of the surface slope term is straight forward and appears below:

$$\begin{aligned} g \frac{\partial \eta}{\partial x} \int_0^H \Omega_J dz &= g \frac{\partial \eta}{\partial x} \int_0^H \cos \frac{a_J z}{H} dz \\ &= g \frac{\partial \eta}{\partial x} \frac{H}{a_J} \sin \frac{a_J z}{H} \Big|_{z=0}^{z=H} = g \frac{\partial \eta}{\partial x} \frac{H}{a_J} \sin a_J \end{aligned} \quad (A.3)$$

A.3. Horizontal Shear Stress Term

After substitution of the linear form for the horizontal eddy viscosity term in Equation 2.28:

$$-\epsilon \int_0^H \omega \Omega_J dz = -\epsilon \int_0^H \left[\frac{u_*^2 z^2 (z-H)}{H^2 N_b} + \frac{u_*^2}{\alpha_1} \ln \frac{N_b}{N_1} + \frac{\epsilon c_I}{I} \cos \frac{a_I z}{H} \right] \cos \frac{a_J z}{H} dz \quad (A.4)$$

Examining each term separately, and breaking the first term into two parts:

$$-\epsilon \int_0^H \frac{u_*^2 z^2 (z-H)}{H^2 N_b} \Omega_J dz = -\frac{\epsilon u_*^2}{H^2 N_b} \left[\int_0^H z^3 \cos \frac{a_J z}{H} dz + \int_0^H -z^2 H \cos \frac{a_J z}{H} dz \right] \quad (A.5)$$

Considering the first term of Equation A.5:

$$\begin{aligned} \int_0^H z^3 \cos \frac{a_J z}{H} dz &= \frac{H}{a_J} z^3 \sin \frac{a_J z}{H} \Big|_{z=0}^H - \frac{3H}{a_J} \int_0^H z^2 \sin \frac{a_J z}{H} dz \\ &= \frac{H^4}{a_J} \sin a_J - \frac{3H}{a_J} \left[-\frac{H}{a_J} z^2 \cos \frac{a_J z}{H} \Big|_{z=0}^H + \frac{2H}{a_J} \int_0^H z \cos \frac{a_J z}{H} dz \right] \\ &= \frac{H^4}{a_J} \sin a_J + \frac{3H^4}{a_J^2} \cos a_J - \frac{6H^2}{a_J^2} \left[\frac{H^2}{a_J^2} \cos a_J + \frac{H^2}{a_J} \sin a_J - \frac{H^2}{a_J^2} \right] \\ &= H^4 \left[\frac{\sin a_J}{a_J} + \frac{3}{a_J^2} \cos a_J - \frac{6}{a_J^2} \phi_J \right] = H^4 \psi_J \end{aligned} \quad (A.6)$$

Taking a $-H$ outside of the integral sign and integrating the second part:

$$\begin{aligned} \int_0^H z^2 \cos \frac{a_J z}{H} dz &= \frac{2z \cos \frac{a_J z}{H}}{a_J^2/H^2} + \left(\frac{a_J^2 z^2}{H^2} - 2 \right) \sin \frac{a_J z}{H} \Big|_{z=0}^H \\ &= \frac{2H^3}{a_J^2} \cos a_J + \left(\frac{H^3}{a_J^2} - \frac{2H^3}{a_J^2} \right) \sin a_J = H^3 \gamma_J \end{aligned} \quad (A.7)$$

Finally, the first term of Equation A.4 becomes

$$-\frac{\epsilon u_*^2}{H^2 N_b} [H^4 \psi_J - H(H^3 \gamma_J)] = -\frac{\epsilon u_*^2 H^2}{N_b} (\psi_J - \gamma_J) \quad (A.8)$$

The integration of the second part of the horizontal shear stress term is performed using integration by parts:

$$- \frac{\epsilon u_*^2}{\alpha_1} \int_0^H \ln\left(\frac{N_b}{N_1}\right) \cos \frac{a_J z}{H} dz$$

Let $U = \ln \frac{N_b}{N_1}$ and $dV = \cos \frac{a_J z}{H}$. This implies $dU = -\frac{\alpha_1}{N_1} dz$ and

$$V = \frac{H}{a_J} \sin \left(\frac{a_J z}{H} \right).$$

$$\int_0^H \ln \left(\frac{N_b}{N_1} \right) \cos \frac{a_J z}{H} dz = \ln \left(\frac{N_b}{N_1} \right) \frac{H}{a_J} \sin \frac{a_J z}{H} \Big|_{z=0}^H + \frac{\alpha_1 H}{a_J} \int_0^H \frac{\sin \frac{a_J z}{H}}{N_1} dz \quad (A.9)$$

The first term vanishes at both boundaries, and the second term must be integrated numerically. This second term will be represented as follows:

$$\frac{\alpha_1 H}{a_J} \int_0^H \frac{\sin \frac{a_J z}{H}}{N_{v_1}} dz = \alpha_1 H \Gamma_J \quad (A.10)$$

and the second part of the horizontal shear stress term becomes:

$$- \frac{\epsilon u_*^2}{\alpha_1} \alpha_1 H \Gamma_J = -\epsilon u_*^2 H \Gamma_J \quad (A.11)$$

The orthogonality property of cosines can be used to simplify the integral for the third part of the horizontal shear stress term.

$$-\epsilon \int_0^H \sum_I c_I \cos \frac{a_I z}{H} \cos \frac{a_J z}{H} dz = -\epsilon H \frac{c_J}{2} \quad (A.12)$$

Combining Equations A.8, A.11, and A.12 yields the horizontal shear stress term:

$$-\epsilon H \left[\frac{u_*^2 H}{N_b} (\psi_J - \gamma_J) + u_*^2 \Gamma_J + \frac{c_J}{2} \right] \quad (\text{A.13})$$

A.4. Vertical Eddy Viscosity Term - Part One

The first part of the vertical eddy viscosity term is also examined term by term:

$$-\int_0^H \frac{\partial N}{\partial z} \frac{\partial \Omega}{\partial z} \Omega_J dz = -\sum_{K=1}^{K'} \alpha_K \int_{H_{K-1}}^{H_K} \left[\frac{3u_*^2 z^2}{H^2 N_b} - \frac{2u_*^2 z}{HN_b} - \frac{u_*^2}{\alpha_1 z + \beta_1} \right. \\ \left. - \sum_I \frac{c_I a_I}{H} \sin \frac{a_I z}{H} \right] \cos \frac{a_J z}{H} dz \quad (\text{A.14})$$

Integrating the first term:

$$-\sum_{K=1}^{K'} \alpha_K \int_{H_{K-1}}^{H_K} \frac{3u_*^2 z^2}{H^2 N_b} \cos \frac{a_J z}{H} dz = -\frac{3u_*^2}{H^2 N_b} \sum_{K=1}^{K'} \alpha_K \left[\frac{2z \cos \frac{a_J z}{H}}{a_J^2 / H^2} \right. \\ \left. + \frac{\frac{a_J^2}{H^2} z^2 - 2}{a_J^3 / H^3} \sin \frac{a_J z}{H} \right] \Big|_{H_{K-1}}^{H_K} = \frac{-3u_*^2}{H^2 N_b} \sum_{K=1}^{K'} \alpha_K H^3 \left[\frac{2 \frac{z}{H} \cos \frac{a_J z}{H}}{a_J^2} \right. \\ \left. + \left(\frac{\frac{a_J^2}{H^2} \frac{z^2}{H^2} - 2}{a_J^3} \right) \sin \frac{a_J z}{H} \right] \Big|_{H_{K-1}}^{H_K} = \frac{-3u_*^2}{H^2 N_b} \sum_{K=1}^{K'} K^H^3 \left[\frac{2 \frac{H_K}{H} \cos \frac{a_J H_K}{H}}{a_J^2} \right. \\ \left. + \left(\frac{\frac{a_J^2}{H^2} \frac{H_K^2}{H^2} - 2}{a_J^3} \right) \sin a_J \frac{H_K}{H} - \frac{2 \frac{H_{K-1}}{H}}{a_J^2} \cos \frac{a_J H_{K-1}}{H_K} - \left(\frac{\frac{a_J^2}{H^2} \frac{H_{K-1}^2}{H^2} - 2}{a_J^3} \right) \right. \\ \left. \sin \frac{a_J H_{K-1}}{H} \right] \quad (\text{A.15})$$

Equation A.15 can be simplified by incorporating a nondimensionalized height $\zeta_K = H_K/H$.

As a result, Equation A.15 can be rewritten:

$$\frac{-3u_*^2 H}{N_b} \sum_{K=1}^{K'} \alpha_K \gamma_{KJ}$$

where $\gamma_{KJ} = \frac{2\zeta_K \cos a_J \zeta_K}{a_J^2} + \left(\frac{a_J^2 \zeta_K^2 - 2}{a_J^3} \right) \sin a_J \zeta_K$

$$- \frac{2\zeta_{K-1} \cos a_J \zeta_{K-1}}{a_J^2} - \left(\frac{a_J^2 \zeta_{K-1}^2 - 2}{a_J^3} \right) \sin a_J \zeta_{K-1} \quad (A.16)$$

Looking at the second term on the right hand side of Equation

A.14:

$$\frac{2u_*^2}{HN_b} \sum_{K=1}^{K'} \alpha_K \int_{H_{K-1}}^{H_K} z \cos \frac{a_J z}{H} dz$$

$$= \frac{2u_*^2}{HN_b} \sum_{K=1}^{K'} \alpha_K \left[\frac{H^2}{a_J^2} \cos \frac{a_J z}{H} + \frac{H}{a_J} z \sin \frac{a_J z}{H} \right] \Big|_{H_{K-1}}^{H_K}$$

$$= \frac{2u_*^2 H}{N_b} \sum_{K=1}^{K'} \alpha_K \phi_{KJ} \quad (A.17)$$

where $\phi_{KJ} = \frac{1}{2} \left[\cos a_J \zeta_K + a_J \zeta_K \sin a_J \zeta_K - \cos a_J \zeta_{K-1} - a_J \zeta_{K-1} \sin a_J \zeta_{K-1} \right]$

Here again, the substitution $\zeta_K = \frac{H_K}{H}$ is incorporated.

The third term of Equation A.14 has no closed solution, and must be integrated numerically. This term is expressed as:

$$u_*^2 \sum_{K=1}^{K'} \alpha_K \int_0^H \frac{\cos \frac{a_J z}{H}}{\alpha_1 z + \beta_1} dz = u_*^2 v_J \quad (A.18)$$

The last term on the right hand side of Equation A.14 is integrated by first moving all terms not functions of z outside the integral sign.

$$\sum_{K=1}^{K'} \alpha_K \int_{H_{K-1}}^{H_K} \sum_I \frac{c_I a_I}{H} \sin \frac{a_I z}{H} \cos \frac{a_J z}{H} dz = \sum_K \alpha_K \sum_I \frac{c_I a_I}{H} \int_{H_{K-1}}^{H_K} \sin \frac{a_I z}{H} \cos \frac{a_J z}{H} dz \quad (A.19)$$

Performing the integration:

$$\begin{aligned} & - \sum_K \alpha_K \sum_I \frac{c_I a_I}{H} \frac{H}{2} \left[\frac{\cos(\theta_{IJ} \zeta_K) - \cos(\theta_{IJ} \zeta_{K-1})}{\theta_{IJ}} + \frac{\cos(\theta'_{IJ} \zeta_K) - \cos(\theta'_{IJ} \zeta_{K-1})}{\theta'_{IJ}} \right] \\ & = - \frac{1}{2} \sum_I c_I a_I \sum_K \alpha_K \lambda_{KIJ} \end{aligned} \quad (A.20)$$

with $\theta_{IJ} = a_I - a_J$ and $\theta'_{IJ} = a_I + a_J$.

The first term of A.20 will be singular when $I = J$, and the integral must be re-evaluated for this case:

$$\begin{aligned} & - \frac{1}{2} \sum_K \alpha_K \sum_I c_I a_I \frac{1}{a_I} [\cos^2(a_I \zeta_K) - \cos^2(a_I \zeta_{K-1})] = \\ & = \frac{1}{2} \sum_K \alpha_K \sum_I c_I a_I \lambda_{KII} \end{aligned} \quad (A.21)$$

Letting

$$\delta_{IJ} = \frac{a_I}{2} \sum_{K=1}^{K'} \alpha_K \gamma_{KIJ}$$

this term becomes

$$- \sum_I c_I \delta_{IJ} \quad (A.22)$$

Combining Equations A.16, A.17, and A.22 yields the final form for the first part of the vertical eddy viscosity term:

$$- \int_0^H \frac{\partial N_v}{\partial z} \frac{\partial \hat{u}}{\partial z} \Omega_J dz = \frac{u_*^2 H}{N_b} \left[\sum_K \alpha_K (2\phi_{KJ} - 3\gamma_{KJ}) \right] + u_*^2 v_J - \sum_I c_I \delta_{IJ} \quad (A.23)$$

A.5. Vertical Eddy Viscosity Term - Part Two

$$\begin{aligned} - \int_0^H N_v \frac{\partial^2 u}{\partial z^2} \Omega_J dz &= - \sum_{K=1}^{K'} \int_{H_{K-1}}^{H_K} (\alpha_K z + \beta_K) \left[\frac{6u_*^2 z}{H^2 N_b} - \frac{2u_*^2}{HN_b} + \frac{u_*^2 \alpha_1}{(\alpha_1 z + \beta_1)^2} \right. \\ &\quad \left. - \sum_I \frac{c_I a_I^2}{H^2} \cos \frac{a_I z}{H} \right] \Omega_J dz \quad (A.24) \end{aligned}$$

Considering the right hand side of Equation A.24 term by term, the first term is split into two parts:

$$\begin{aligned} - \frac{6u_*^2}{H^2 N_b} \sum_{K=1}^{K'} \int_{H_{K-1}}^{H_K} (\alpha_K z + \beta_K) z \cos \frac{a_J z}{H} dz &= - \frac{6u_*^2}{H^2 N_b} \sum_{K=1}^{K'} \left[\alpha_K \int_{H_{K-1}}^{H_K} z^2 \cos \frac{a_J z}{H} dz + \beta_K \int_{H_{K-1}}^{H_K} z \cos \frac{a_J z}{H} dz \right] \quad (A.25) \end{aligned}$$

The first term in brackets is very similar to the first term on the right hand side of Equation A.14 and the second term in brackets is very similar to the term integrated in Equation A.16. Equation A.25 can be rewritten as

$$\frac{-6u_*^2}{N_b} \left[H \sum_K \alpha_K \gamma_{KJ} + \sum_K \beta_K \phi_{KJ} \right] \quad (A.26)$$

The second term on the right hand side of Equation A.24 is integrated as follows:

$$\begin{aligned} & \frac{2u_*^2}{HN_b} \sum_K \int_{H_{K-1}}^{H_K} (\alpha_K z + \beta_K) \cos \frac{a_J z}{H} dz \\ &= \frac{2u_*^2}{HN_b} \left[\sum_K \alpha_K \int_{H_{K-1}}^{H_K} z \cos \frac{a_J z}{H} dz + \sum_K \beta_K \int_{H_{K-1}}^{H_K} \cos \frac{a_J z}{H} dz \right] \\ &= \frac{2u_*^2}{HN_b} \left[\sum_K \alpha_K H^2 \phi_{KJ} + \sum_K \beta_K \frac{H}{a_J} (\sin \zeta_K a_J - \sin \zeta_{K-1} a_J) \right] \\ &= \frac{2u_*^2}{N_b} \left[H \sum_K \alpha_K \phi_{KJ} + \sum_K \beta_K S_{KJ} \right] \end{aligned} \quad (A.27)$$

where

$$S_{KJ} = \frac{\sin(\zeta_K a_J) - \sin(\zeta_{K-1} a_J)}{a_J}$$

The third term is similar to the third term of Equation A.14 and must be integrated numerically. This term is expressed as:

$$-u_*^2 \alpha_1 \sum_K \int_{H_{K-1}}^{H_K} \frac{(\alpha_K z + \beta_K) \cos \frac{a_J z}{H}}{(\alpha_1 z + \beta_1)^2} dz = -u_*^2 v_J, \quad (A.28)$$

and that $v_J' = v_J$ for the case of $K=2$.

The fourth term in Equation A.24 can be rearranged as:

$$\begin{aligned}
& \sum_K \int_{H_{K-1}}^{H_K} (\alpha_K z + \beta_K) \sum_I \frac{c_I a_I^2}{H^2} \cos \frac{a_I z}{H} \cos \frac{a_J z}{H} dz \\
&= \frac{1}{H^2} \sum_K \sum_I c_I a_I^2 \left[\int_{H_{K-1}}^{H_K} \alpha_K z \cos \frac{a_I z}{H} \cos \frac{a_J z}{H} dz \right. \\
&\quad \left. + \beta_K \int_{H_{K-1}}^{H_K} \cos \frac{a_I z}{H} \cos \frac{a_J z}{H} dz \right] \\
&= \frac{1}{2} \sum_K \sum_I c_I a_I^2 \left[\alpha_K \left\{ \frac{\cos(\theta_{IJ} \zeta_K) - \cos(\theta_{IJ} \zeta_{K-1})}{\theta_{IJ}^2} \right. \right. \\
&\quad + \frac{\cos(\theta'_{IJ} \zeta_K) - \cos(\theta'_{IJ} \zeta_{K-1})}{\theta_{IJ}'^2} + \frac{\zeta_K \sin(\theta_{IJ} \zeta_K) - \zeta_{K-1} \sin(\theta_{IJ} \zeta_{K-1})}{\theta_{IJ}} \\
&\quad \left. \left. + \frac{\zeta_K \sin(\theta'_{IJ} \zeta_K) - \zeta_{K-1} \sin(\theta'_{IJ} \zeta_{K-1})}{\theta_{IJ}'} \right\} + \right. \\
&\quad \left. \frac{\beta_K}{H} \left\{ \frac{\sin(\theta_{IJ} \zeta_K) - \sin(\theta_{IJ} \zeta_{K-1})}{\theta_{IJ}} + \frac{\sin(\theta'_{IJ} \zeta_K) - \sin(\theta'_{IJ} \zeta_{K-1})}{\theta_{IJ}'} \right\} \right] \\
&= \frac{1}{2} \sum_K \sum_I c_I a_I^2 \left[\alpha_K \xi_{KIJ} + \frac{\beta_K}{H} \lambda_{KIJ}^* \right] \tag{A.29}
\end{aligned}$$

with $\theta_{IJ} = a_I - a_J$ and $\theta'_{IJ} = a_I + a_J$. For the case of $I=J$, this expression will become singular. Re-evaluating the integral for the case of $I=J$

$$\begin{aligned}
& \frac{1}{H^2} \sum_K \sum_I c_I a_I^2 \int_{H_{K-1}}^{H_K} (\alpha_K z + \beta_K) \cos \frac{a_I z}{H} \cos \frac{a_J z}{H} dz \\
&= \frac{1}{2} \sum_K \sum_I c_I a_I^2 \left[\alpha_K \xi_{KIJ} + \frac{\beta_K}{H} \lambda_{KIJ}^* \right]
\end{aligned} \tag{A.30}$$

in which

$$\begin{aligned}
\xi_{KIJ} &= \frac{\zeta_K^2 - \zeta_{K-1}^2}{2} + \frac{\cos(2a_I \zeta_K) - \cos(2a_I \zeta_{K-1})}{4a_I^2} \\
&+ \frac{\zeta_K \sin(2a_I \zeta_K) - \zeta_{K-1} \sin(2a_I \zeta_{K-1})}{2a_I}
\end{aligned}$$

and

$$\lambda_{KIJ}^* = \zeta_K - \zeta_{K-1} + \frac{\sin(2a_I \zeta_K) - \sin(2a_I \zeta_{K-1})}{2a_I}$$

Defining:

$$\sigma_{IJ} = \frac{a_I^2}{2} \sum_K \left[\alpha_K \xi_{KIJ} + \frac{\beta_K}{H} \lambda_{KIJ}^* \right] \tag{A.31}$$

The fourth term can be expressed in its final form:

$$\sum_K \int_{H_{K-1}}^{H_K} (\alpha_K z + \beta_K) \sum_I \frac{c_I a_I^2}{H^2} \cos \frac{a_I z}{H} \cos \frac{a_J z}{H} dz = \sum_I c_I \sigma_{IJ} \tag{A.32}$$

Summing the parts of the second vertical eddy viscosity term
(Equations A.26, A.27, A.28, A.32):

$$\begin{aligned}
- \int_0^H N_v \frac{\partial^2 \hat{u}}{\partial z^2} \Omega_J dz &= \frac{-6u_*^2}{N_b} [H \sum_K \alpha_K \gamma_{KJ} + \sum_K \beta_K \phi_{KJ}] \\
+ \frac{2u_*^2}{N_b} [H \sum_K \alpha_K \phi_{KJ} + \sum_K \beta_K S_{KJ}] &- u_*^2 v_J^2 + \sum_I c_I \sigma_{IJ}
\end{aligned} \tag{A.33}$$

A.6 Coriolis Term

The Coriolis term is

$$-f \int_0^H \hat{v} \Omega_J dz \tag{A.34}$$

The form of this term is essentially identical to the horizontal shear stress term if the following substitutions are made:

c_J becomes d_J

u_*^2 becomes v_*^2

ϵ becomes f

Performing the integration as in Section A.3:

$$-f \int_0^H \hat{v} \Omega_J dz = -f H \left[\frac{v_*^2}{N_b} (\psi_J - \gamma_J) + v_*^2 \Gamma_J + \frac{d_J}{2} \right] \tag{A.35}$$

Appendix B

Continuity Equation

The continuity equation was given in Equation 2.5:

$$\frac{\partial \bar{u}}{\partial x} + \frac{\partial \bar{v}}{\partial y} = \frac{\partial \eta}{\partial t} \quad (2.5)$$

It is possible to obtain expressions for \bar{u} and \bar{v} using the definition of the mass fluxes (calculated here for the x-direction only):

$$\bar{u} = \int_0^H \hat{u} \, dz = \int_0^H \left[\frac{u_*^2 z^2 (z-H)}{H^2 N_b} + \frac{u_*^2}{\alpha_1} \ln \left(\frac{N_b}{N_1} \right) + \sum_{I=1}^{I'} c_I \cos \frac{a_I z}{H} \right] dz \quad (B.1)$$

Performing the integration for the first term:

$$\frac{u_*^2}{H^2 N_b} \int_0^H (z^3 - z^2 H) \, dz = \frac{u_*^2}{H^2 N_b} \left[\frac{z^4}{4} - \frac{z^3 H}{3} \right] \bigg|_{z=0}^H = -\frac{u_*^2 H^2}{12 N_b} \quad (B.2)$$

Integrating the second term on the right hand side of Equation B.1:

$$\begin{aligned} \frac{u_*^2}{\alpha_1} \int_0^H \ln \left(\frac{N_b}{N_1} \right) \, dz &= \frac{u_*^2}{\alpha_1} \int_0^H (\ln N_b - \ln N_1) \, dz \\ &= \frac{u_*^2}{\alpha_1} \left[z \ln N_b - \frac{1}{\alpha_1} (N_1 \ln N_1 - N_b) \right] \bigg|_{z=0}^H \\ &= \frac{u_*^2}{\alpha_1} \left[H \ln N_b - \frac{1}{\alpha_1} (N_b \ln N_b - N_b) + \frac{1}{\alpha_1} (\beta_1 \ln \beta_1 - \beta_1) \right] = u_*^2 G \end{aligned} \quad (B.3)$$

The third term is integrated to yield:

$$\int_0^H \sum_I c_I \cos \frac{a_I z}{H} \, dz = \sum_I c_I \int_0^H \cos \frac{a_I z}{H} \, dz = H \sum_I c_I \frac{\sin a_I}{a_I} \quad (B.4)$$

Combining B.2, B.3, and B.4:

$$\bar{u} = -\frac{u_*^2 H^2}{12N_b} + u_*^2 G + H \sum_I c_I \frac{\sin a_I}{a_I} \quad (\text{B.5})$$

Similarly, in the y-direction:

$$\bar{v} = -\frac{v_*^2 H^2}{12N_b} + v_*^2 G + H \sum_I d_I \frac{\sin a_I}{a_I} \quad (\text{B.6})$$

These expressions are substituted into Equation 2.5, and Equation 2.5 is discretized as in Equation 2.60 to be used in the model.

National Sea Grant Depository
 Pell Library Building - GSO
 University of Rhode Island
 Narragansett, RI 02882-1197USA